MICROCOPY RESOLUTION TEST CHART

NATIONAL BUREAU OF STANDARDS-1963-A

AFGL-TR-83-0140

AD A138632

ANALYSIS OF SPACECRAFT CHARGING, PARTICLE BEAMS
AND GEOPHYSICAL DATA BASES

Krishin H. Bhavnani
William J. McNeil
Maurice F. Tautz

RADEX, Inc.
192 Log Hill Road
Carlisle, MA 01741

Final Report
May 1980 - May 1983

31 July 1983

Approved for public release; distribution unlimited

DTIC
ELECT
MAR 7 1984

A

84 03 06 039

This report has been reviewed by the ESD Public Affairs Office (PA) and is releasable to the National Technical Information Service (NTIS).

This technical report has been reviewed and is approved for publication
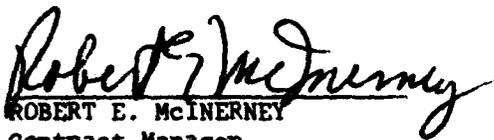
ROBERT E. McINERNEY
Contract Manager

ROBERT E. McINERNEY
Branch Chief

FOR THE COMMANDER

EUNICE C. CRONIN
Division Director

Qualified requestors may obtain additional copies from the Defense Technical Information Center. All others should apply to the National Technical Information Service.

If your address has changed, or if you wish to be removed from the mailing list, or if the addressee is no longer employed by your organization, please notify AFGL/DAA, Hanscom AFB, MA 01731. This will assist us in maintaining a current mailing list.

Do not return copies of this report unless contractual obligations or notices on a specific document requires that it be returned.

REPORT DOCUMENTATION PAGE	READ INSTRUCTIONS BEFORE COMPLETING FORM

1. REPORT NUMBER	2. GOVT ACCESSION NO.	3. RECIPIENT'S CATALOG NUMBER
AFGL-TR-83-0140	AD-A138632	

4. TITLE (and Subtitle)	5. TYPE OF REPORT & PERIOD COVERED
ANALYSIS OF SPACECRAFT CHARGING, PARTICLE BEAMS AND GEOPHYSICAL DATA BASES	Scientific-Final May 1980–May 1983
	6. PERFORMING ORG. REPORT NUMBER

7. AUTHOR(s)	8. CONTRACT OR GRANT NUMBER(s)
Krishin H. Bhavnani William J. McNeil Maurice F. Tautz	F19628-80-C-0127

9. PERFORMING ORGANIZATION NAME AND ADDRESS	10. PROGRAM ELEMENT, PROJECT, TASK AREA & WORK UNIT NUMBERS
RADEX, Inc. 192 Log Hill Road Carlisle, MA 01741	9993XXXX

11. CONTROLLING OFFICE NAME AND ADDRESS	12. REPORT DATE
Air Force Geophysics Laboratory Hanscom AFB, Massachusetts, 01731 Contract Monitor: Robert E. McInerney/RMY	31 July 1983
	13. NUMBER OF PAGES
	121

14. MONITORING AGENCY NAME & ADDRESS(If different from Controlling Office)	15. SECURITY CLASS. (of this report)
	Unclassified
	15a. DECLASSIFICATION/DOWNGRADING SCHEDULE

16. DISTRIBUTION STATEMENT (of this Report)

Approved for public release; distribution unlimited

17. DISTRIBUTION STATEMENT (of the abstract entered in Block 20, if different from Report)

18. SUPPLEMENTARY NOTES

Tech, Other

19. KEY WORDS (Continue on reverse side if necessary and identify by block number)

SPACECRAFT CHARGING	SCATHA	GEOMAGNETIC FIELD
ELECTRON-ION BEAMS	GRAPHICS	PARTICLE TRACKING
MATERIALS CHARGING	CONTOUR	ATMOSPHERIC DENSITY
NASCAP	ISOMETRIC	ATMOSPHERIC WINDS
PLASMAS	IONIZATION	ROCKET SPHERE

20. ABSTRACT (Continue on reverse side if necessary and identify by block number)

This report documents investigations and computer programs developed for study of spacecraft charging, ionization effects of beams, and analyses of geophysical data bases.

Spacecraft charging studies have been performed utilizing NASCAP and the associated program MATCHG.

(over)

DD FORM 1473 EDITION OF 1 NOV 65 IS OBSOLETE

1

The present operational system at AFGL, and procedures for representing spacecraft models and environmental parameters are described. Specific SCATHA satellite charging events were simulated in detail. Special studies of HELIOS 1, GEOS, and a simple Space Based Radar are also described.

Investigations for plasma definition and for determining threshold conditions for materials charging are summarized.

Ionization and charging characteristics due to electron and ion beam currents are simulated for simple spherical or cylindrical symmetries, and includes flight simulation predictions.

Particle trajectory studies were conducted for some basic electric field configurations, as well as for tracking particle beams in the geomagnetic field.

Atmospheric density and winds have been determined for a series of rocket sphere flights in the lower thermosphere. Analytical and data processing procedures are described.

An interactive graphics program (SUATEK) has been advanced. This system as well as some three-dimensional plotting packages, now available on-line, are summarized.

ACKNOWLEDGEMENTS

TABLE OF CONTENTS

TABLE OF CONTENTS (continued)

LIST OF FIGURES

LIST OF FIGURES (continued)

LIST OF TABLES

1.0 Spacecraft Charging

Magnetospheric substorms at high altitudes are characterized by
hot tenuous plasmas which can charge a satellite negatively to
many kilovolts. The reliable estimation of the charging effects
on present and future space vehicles has been a concern of the
Air Force and NASA for several years, and a subject of consid-
erable R&D activity. The inclusion of all factors that are
significant for spacecraft charging presents a formidable
problem. Complex three dimensional geometries with diverse
surface materials and internal electrical propertie have to be
taken into account. The surface-plasma interactio which
involve secondary emission, backscattering, photoer sion and
charge transport must be considered in detail. Th gneto-
static environment may include solar, magnetic field, substorm
and space charge effects. Charging dynamics can exist due to
varying photoemission over a rotating or eclipsing satellite,
changing plasma conditions, active control by electron or ion
beams, and switching of electrically connected satellite
configurations. Investigators at AFGL are widely involved in
SCATHA satellite and other plasma physics research experiments.

For a number of years the analytical tool which most compre-
hensively represents these processes has been the NASCAP program
developed by S-CUBED.[1,4] This program represents an attempt
to realistically simulate and depict spacecraft charging by
numerically solving the full three dimensional problem. The
NASCAP model uses a quasi-static Vlasov equation approximation to
obtain surface charging fluxes, given potential distributions and
the ambient environment conditions. Following calculation of

dielectric charge transport and surface charge distributions, the spatial potential problem (Laplace's equation) is solved using a finite element, nested-mesh technique. The iterative cycle then returns to the Vlasov flux charging equation. Elaborate plasma and material characteristics may be formulated in NASCAP, along with complex geometries and electrical connectivities of the surfaces.

Thus NASCAP is a major evolving engineering level program, as well as a tool for research on plasma sheath models and spacecraft charging experiments such as SCATHA. The NASCAP program was installed at AFGL in 1978 for the purpose of verification and validation, and as a means of support for investigations of charging phenomena.

Since installation, the program has been run extensively to analyze charging effects and to carry out simulation studies for SCATHA and other space vehicles. The early work focused on the identification of program bugs and computational instabilities. These studies were served by examining the charging behavior of simple objects such as NASCAP quasispheres and cylinders. Further testing of the NASCAP program was done by calculating sunlight charging of quasi-spheres for fixed sun direction and rotational motion.[3] Preliminary SCATHA simulations were completed assuming simplified plasma environments.[6,8] These runs included quasispheres, 2-grid and 4-grid SCATHA models. The effect of electron emitter beams on SCATHA charging was also examined.[7] The most recent SCATHA simulations have implemented time dependent specification of the plasma environment and of solar flux.[9,15]

12

1.1 Operational System and Simulation Procedures

The NASCAP source code is provided by S-CUBED on magnetic tape in
blocked EBCDIC format.   A number of steps are necessary in order
to set up the system at AFGL:

a) read the source tape and convert to CDC compatible format
b) convert the NASCAP routines to UPDATE format and compile
c) form a segmented version of the program which is small enough
   to fit on the CDC 6600

The final segmented binary file requires 276 K_8 to run.   Also
contained on the source tape are three NASCAP auxiliary programs:

PLOTREAD - reads plot files created by NASCAP and outputs
           microfiche

TERMTALK - reads the results files created by NASCAP, giving
           access to summary information.

MATCHG - uses NASCAP algorithms to calculate charging of
           material surfaces.

In addition, S-CUBED provides an auxiliary file, NASFILES, which
contains default values for the surface material parameters, and
object definition specifications for SCATHA models.

A number of major revisions of the NASCAP code and its auxiliary
programs have been installed on the CDC-6600 system.
A comprehensive system has been implemented to facilitate program
maintenance and operational logistics.   Considerations provided
for at AFGL are:

13

a) coordination and compatibility with the UNIVAC 1100 version of NASCAP at S-CUBED)

b) prompt revision of source, relocatable, and absolute codes

c) tape storage of source codes and results files

d) generation of microfiche plots using the auxiliary program PLOTREAD

e) maintenance and modification of auxiliary programs MATCHG and TERMTALK.

f) availability of SLATEK plotting routines for display of MATCHG and TERMTALK results

g) maintenance and modification of program ALLES which calculates Maxwellian fits to spectra, for input to NASCAP

h) generation of tapes and associated materials for external distribution of programs

The NASCAP simulation of a complex charging event entails considerable operational management. Input files containing the material parameters and the object definition information are required. A flux definition file, which describes the plasma environment, must be constructed. Provision for inputting the flux files to the auxiliary MATCHG program for trial run testing is advantageous. It is necessary to form a run options file from the NASCAP keyword list, in accordance with the rules of syntax and precedence. The run options file may contain repetitive modules for generating variable sunlight intensity or rotational motion. Special card blocks may be needed for specification of onboard beam emitter or detector character-istics. After completion of a NASCAP run the printed output and microfiche must be examined and interpreted, and the restart files either archived or reset for a continuation run. Inspection of the restart file information and plotting of summary and comparative results is made available through the auxiliary TERMTALK program. Figure 1.1 shows a schematic of the AFGL operational system for a NASCAP simulation study.

14
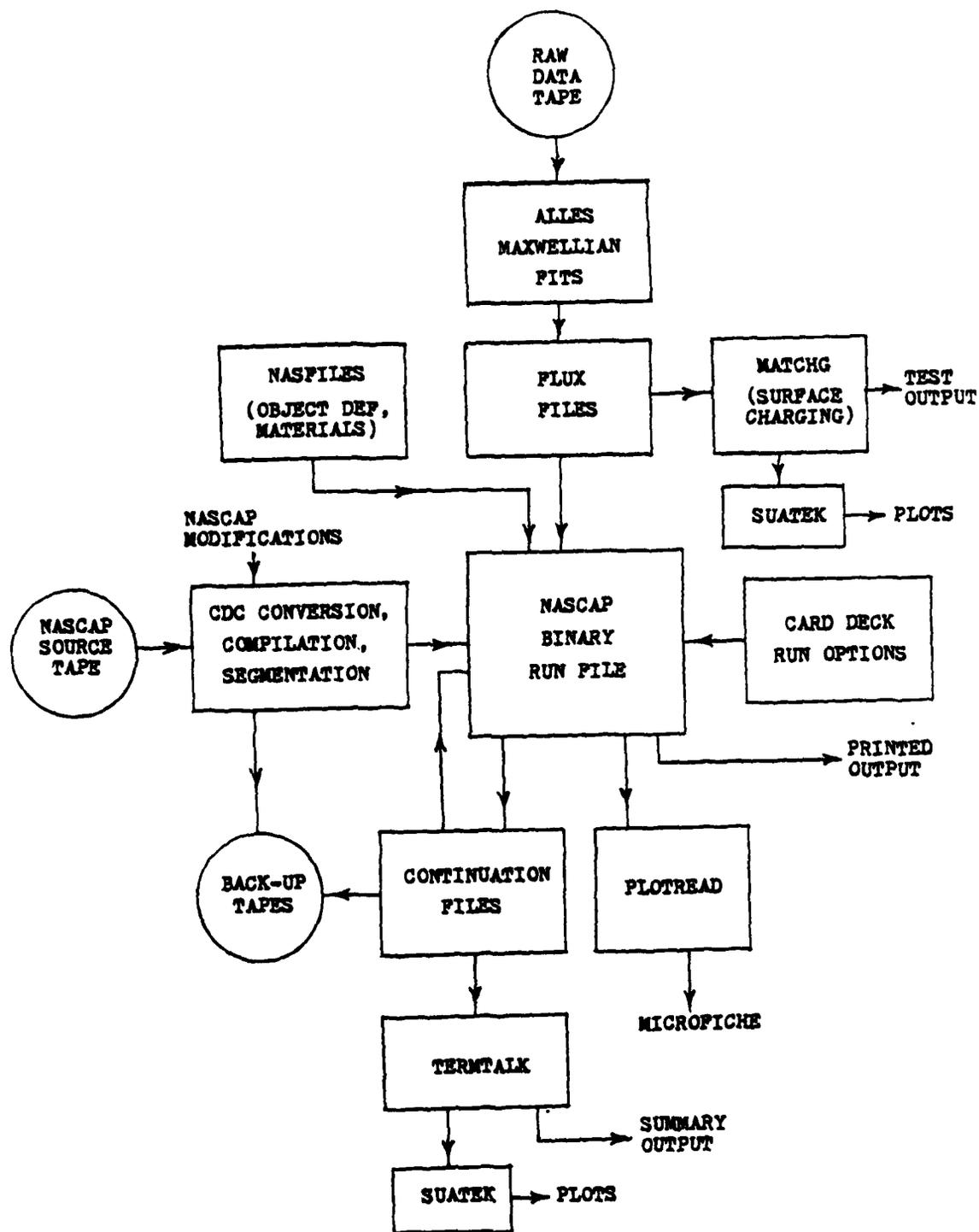
Figure 1.1 NASCAP Simulation Operational System

15

In the SCATHA simulations, the ambient plasma has been
represented by single or double Maxwellian fits to measured data,
as determined by the ALLES program.   The material properties
have been set to default values provided by S-CUBED.   For the
vehicle object specification, the 1, 2, 3 and 4-grid models of
the SCATHA satellite have all been utilized.
The 1-grid and 3-grid models of SCATHA are shown in Fig. 1.2.
The main difference between these two models is that the 3-grid
version has a more detailed representation of the external booms.
Since the computation time goes up repidly with grid size, most
of the analysis has been done with the 1-grid model.

1.2   Plasma Environment Specification

The accurate simulation of charging events requires a detailed
representation of the ambient plasma.   This is, in itself, a
difficult problem and a substantial effort has been applied to
the development of a program, ALLES, to generate parameter files
to specify the environment.   The program makes double Maxwellian
fits to measured spectra data, with the plasma temperatures and
densities as the floating parameters. .
Plots of the individual fits versus the data, and summary plots
of the fit parameters versus time are available.   The following
describes the fitting procedures that were used in the analysis
of the day 114 (1979) charging event,[9] based on spectra
obtained from the SC9 experiment.
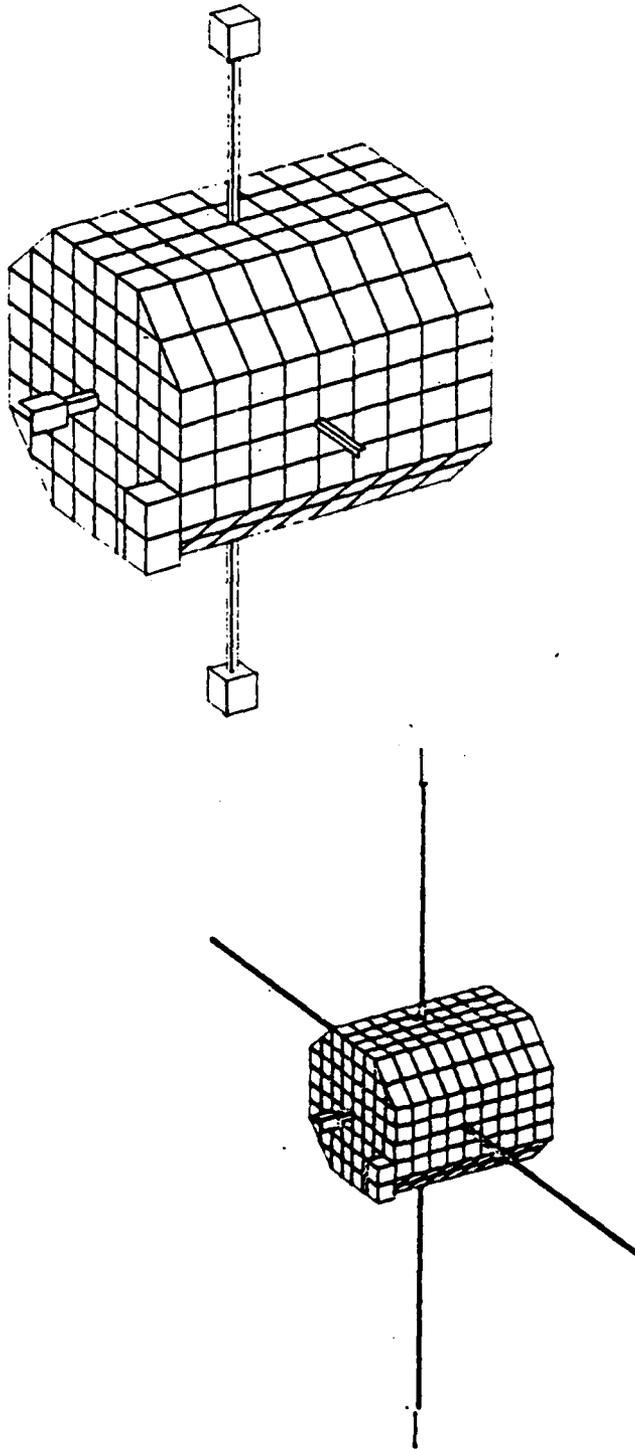
Figure 1.2 NASCAP 1-grid and 3-grid Models of SCATHA

17

The SC9 plasma data resides on magnetic tape in the form of electron and ion detector counts. The data was recorded at 16 sec intervals and the counts are distributed into 64 energy bins ranging from 0 to 80 KeV. In ALLES the raw counts are converted to phase space distribution functions f (units are sec^3/cm^6) by multiplying by appropriate calibration and phase space factors. Figure 1.3 shows a typical spectrum (UT=27368 secs). The lower two plots give ln(f) for the electrons (left) and ions (right). The upper plots give expanded views of the low energy region (0-10KeV).

In the analysis, the 15 lowest energy bins are disregarded. Also, the data points are corrected for the shift in the spectra due to vehicle charging. In the plots, the circles show the shifted points and the crosses denote the unshifted distribution. The method employed to fit the shifted spectra is outlined below:

1) The spectra are first split int high and low regions (the low energy range extends from vehicle ground plus 2 KeV up to the separation cut which was set at 15 KeV).

2) The high energy range (>15 KeV) is fitted with a single Maxwellian function.

3) This high energy fit is extrapolated back into the low region and subtracted from the data.

4) A second Maxwellian is fitted to the difference spectrum in the low energy region.

18
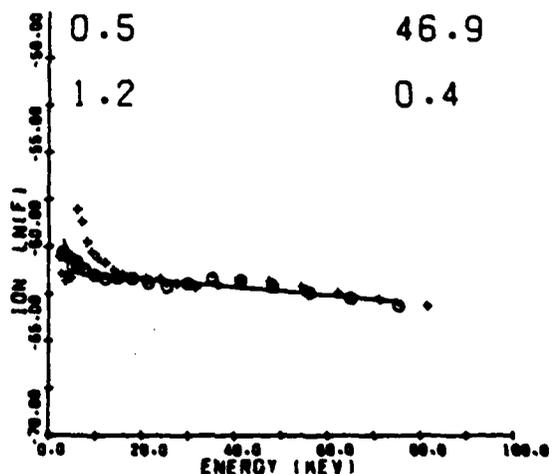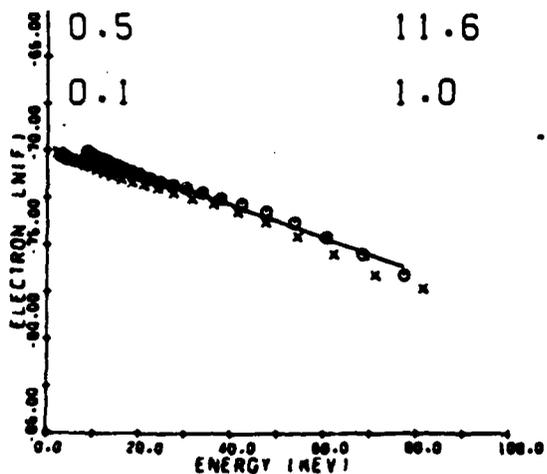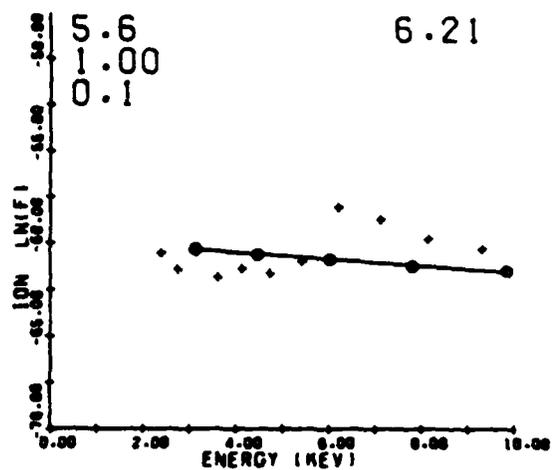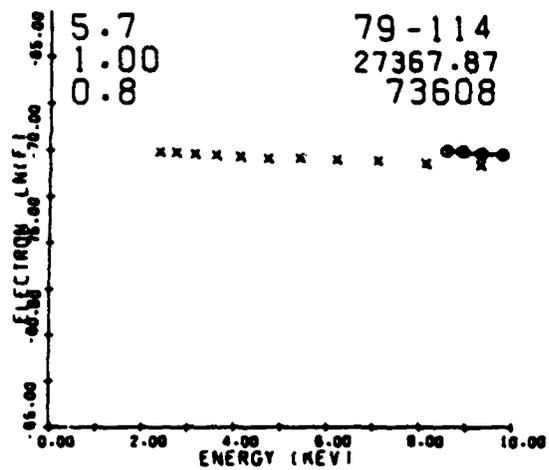
Figure 1.3 ALLES Fits to SC9 Spectra at 27368 sec. UT

19

A virtue of the above method is that it clearly separates the fits into high and low energy components. However, when the method was applied, it was found the the solutions reached could be very sensitive to the location of the separation cut. Moreover, sometimes no reasonable physical values were obtained from the fit. To remedy this situation, a second level of analysis was employed. The results from the above method were input as starting values for a general least squares fitting routine (if the first method fails, the values from the last previous successful case are input). This additional least squares fitting was invoked whenever it could improve the RMS error of the fit.

A typical fit to the data is displayed by the solid lines in the lower plots of Figure 1.3. The numbers in the upper corners give the fit parameters (temperatures and densities corresponding to the low and high regions). The solid lines in the upper plots show low energy single Maxwellian fits for comparison which were not used in the NASCAP simulation.

In Figures 1.4 (a)-(d) we summarize the derived plasma parameters for the day 114 full eclipse period. Although there are some fluctuations, the temperatures and densities are seen to be relatively flat over this time period.

Before being used for NASCAP simulations, a further change was made to the double Maxwellian fit parameters. The electron densities were renormalized to the ion densities to provide for charge neutralization and a correction was made for the O_2 content of the plasma.
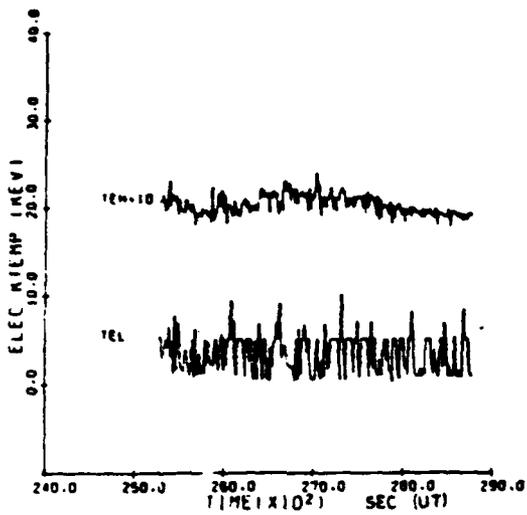
Fig. 4a. Electron temperatures
vs. UT
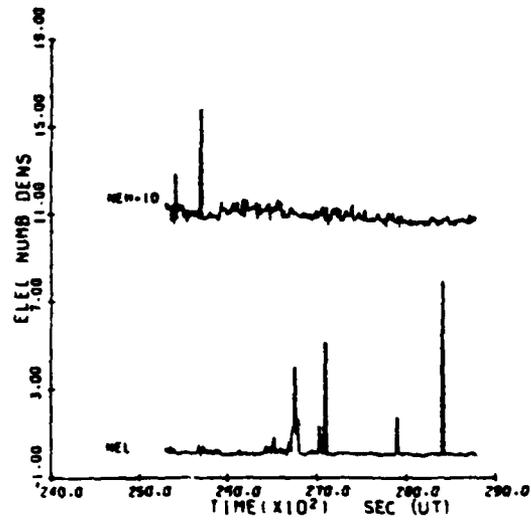
Fig. 4b. Electron number densities
(cm^{-3}) vs. UT
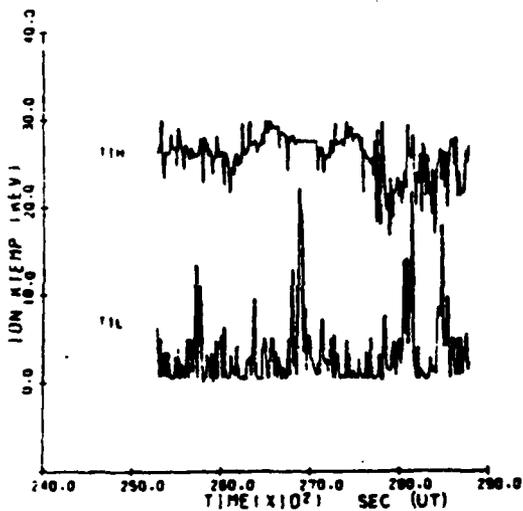
Fig. 4c. Ion temperatures
vs. UT
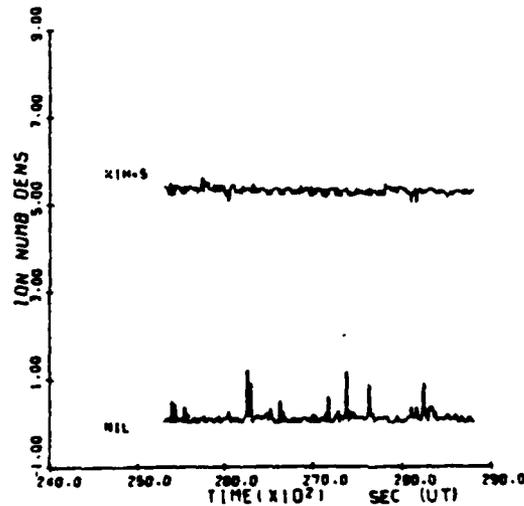
Fig. 4d. Ion number densities
(cm^{-3}) vs. UT

Figure 1.4   Plasma Parameters for Full Eclipse Period (Day 114/79)

1.3 Materials Charging Studies

The auxiliary program MATCHG provides an effective instrument for
studying the interactions between a vehicle surface and a given
plasma environment.   The code calculates the equilibrium
potential for any material, from the current balance equation,
for cases where surface conductivity, photoemission, and multi-
dimensional effects may be neglected.   The MATCHG program has
been run extensively to investigate the eclipse charging behavior
of many different materials.[5]   The code has been utilized for
sensitivity studies of the material properties, comparisons of
the potentials for single and double Maxwellians, testing of
alternate formulations for secondary emission equations, and
various other studies of the surface-plasma interaction.   The
MATCHG code has been adapted so that it can read in the NASCAP
flux definition files.   In this way, the ALLES fits to spectra
data can be input to MATCHG and time histories of the eclipse
charging voltages can be produced.   The results can be used to
compare the effects of different fitting methods on the charging
strength, or for making trial passes through the data, before
employing the NASCAP code which consumes much more computer time.
Figure 1.5 shows a time history of the MATCHG equilibrium
voltages, corresponding to ALLES fits to the day 113, 1981
spectra data.[15]   Time histories can also be generated for all
of the contributing currents at the material surface (primary
plasma currents, secondary emission and backscatter currents, and
bulk conductivity currents).   This information can be quickly
obtained and gives an indication of the relative importance of
these effects throughout the charging simulation.

A series of MATCHG runs have been done to investigate systemati-
cally the threshold conditions for materials charging based on
the current balance condition.[14]   The dynamics of the charging

22
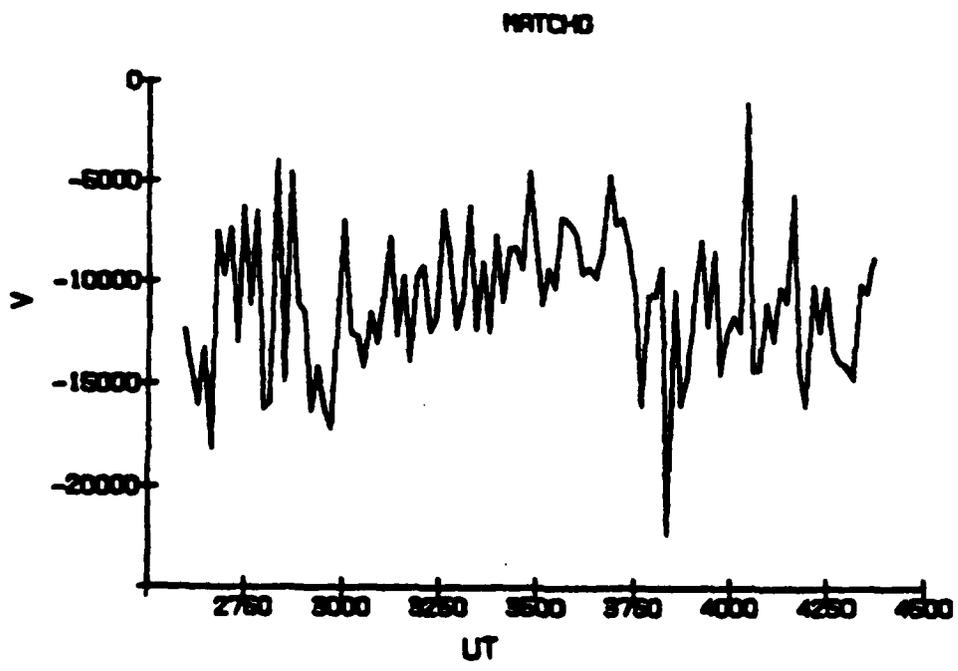
Figure 1.5 MATCHG Potentials versus UT for
Single Maxwellian Fits (Day 113/81)

is illustrated in Figure 1.6(a) which shows the MATCHG electron
and ion currents $-J_e(V)$ and $J_i(V)$ versus V for ASTROQ material.
Each curve corresponds to a different Maxwellian temperature
(T_e, T_i = 5,10, 15, 20, 25). The plasma densities are taken as
$n_e = n_i = 1$. The intersection of any two curves determines the
equilibrium voltage V. The curve for $-J_e(V)$ with $T_e = 5$ lies
below the origin and hence can never intercept a $J_i(V)$ line.
This is an example of a case where the electron temperature is
below the threshold and no charging can occur. The remaining
$-J_e(V)$ curves start above the $J_i(V)$ lines at $V=0$ and charging
takes place.

We have examined the threshold conditions for charging of a
surface material immersed in a Maxwellian plasma. The threshold
relations depend on the plasma temperatures and densities and on
the material properties through the secondary emission coeffi-
cients $\delta^S(T_e)$, $\delta^S(T_i)$ and the backscatter ratio $\delta^B(T_e)$.
For a single Maxwellian plasma, the necessary condition for
charging is that the electron temperature must be greater than
the threshold temperature defined by

$$\delta(T_e) \quad = \quad -1 + \delta^S(T_e) + \delta^B(T_e) \quad = \quad 0$$

The values of this threshold function, calculated by MATCHG, are
shown in Figure 1.6(b) for five different NASCAP materials.
For a multi-Maxwellian plasma at least one of the electron
temperatures must be above threshold and the net electron induced
current must be negative. To arrive at necessary and sufficient
conditions for charging, one has to take into account the ions as
well as the electrons. Explicit formulas have been given for
single and double Maxwellians. For a double Maxwellian, the
threshold condition defines a linearly bounded region in the
density space (n_{e1}, n_{e2}).

24

a) $J_e(V)$ AND $J_i(V)$
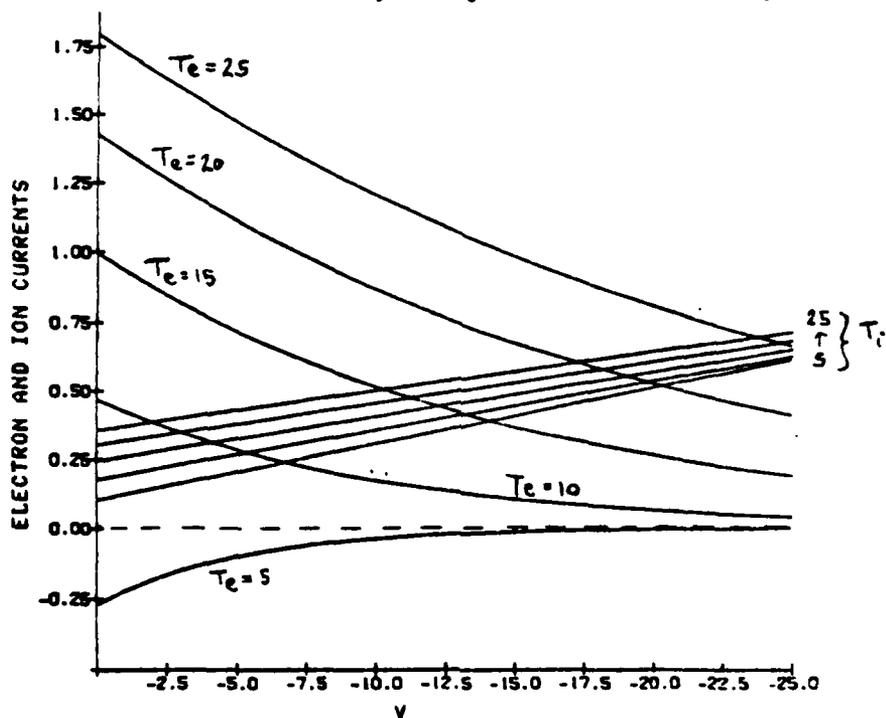
b) $\delta(T_e) = -1 + \delta^S(T_e) + \delta^B(T_e)$
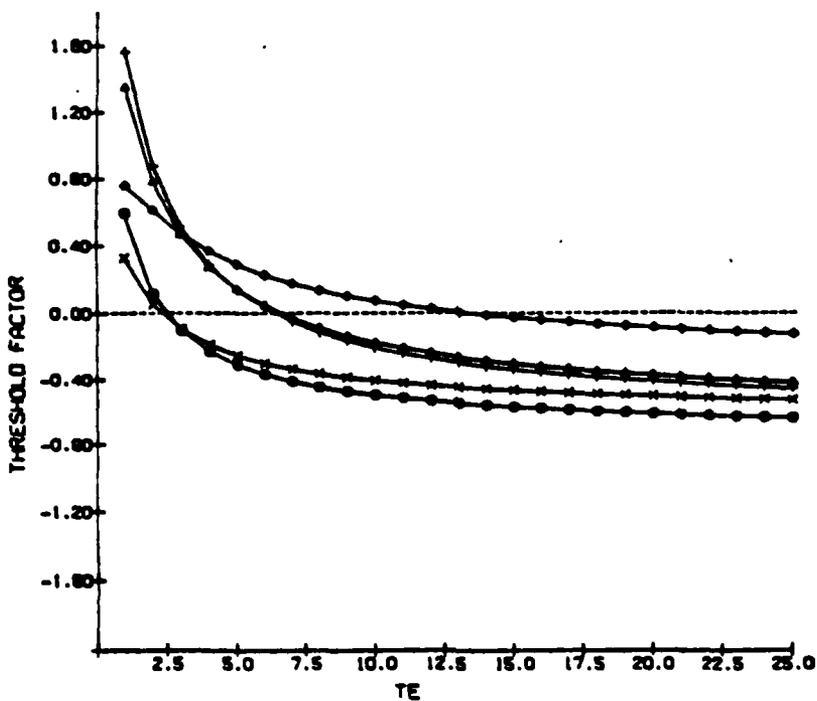
Figure 1.6   Threshold Conditions for Charging for ASTROQ Material

1.4 Special Simulations

The NASCAP model has been applied to several different space vehicles.   A simple geometry was configured in order to represent the Helios 1 satellite and its external antenna boom.[10] The NASCAP configuration that was used is shown in Figure 1.7. The satellite body is a 2x2 mesh cube.   Attached is a single 16-segmented cylindrical boom (radius = 7mm) which is connected to a separate conductor (other than the vehicle ground) through a 200 pf condenser (the Helios antenna capacitance).   In order to scale the system to correspond to the Helios dimensions, the mesh size was set to 1 meter.

Figure 1.7 also shows the boom potentials calculated during one cycle of the NASCAP rotate mode.   Two curves are given: one for a cell at the base of the boom, and one for a cell at the boom tip. As can be seen, there is only a small variation of potential (≈ 1 volt) along the boom.   Both curves show the expected spin modulation.   When the boom is perpendicular to the sun direction ($\phi = +90, -90^{\circ}$), the photo current is a maximum and the voltage goes positive.   When the boom is aligned with the sun ($\phi = 0, -180^{\circ}$) the cells go a few volts negative.

A comparison of Figure 1.7 with the Helios measurements of boom potential indicate that the amplitude of the oscillations are of the right order of magnitude.   Considering the very simplified model that has been employed here, the above agreement is satisfactory.   It demonstrates that the NASCAP program can successfully predict the spin modulated potential variations on a rotating boom, and that the details of the model are not significant for this case.

26
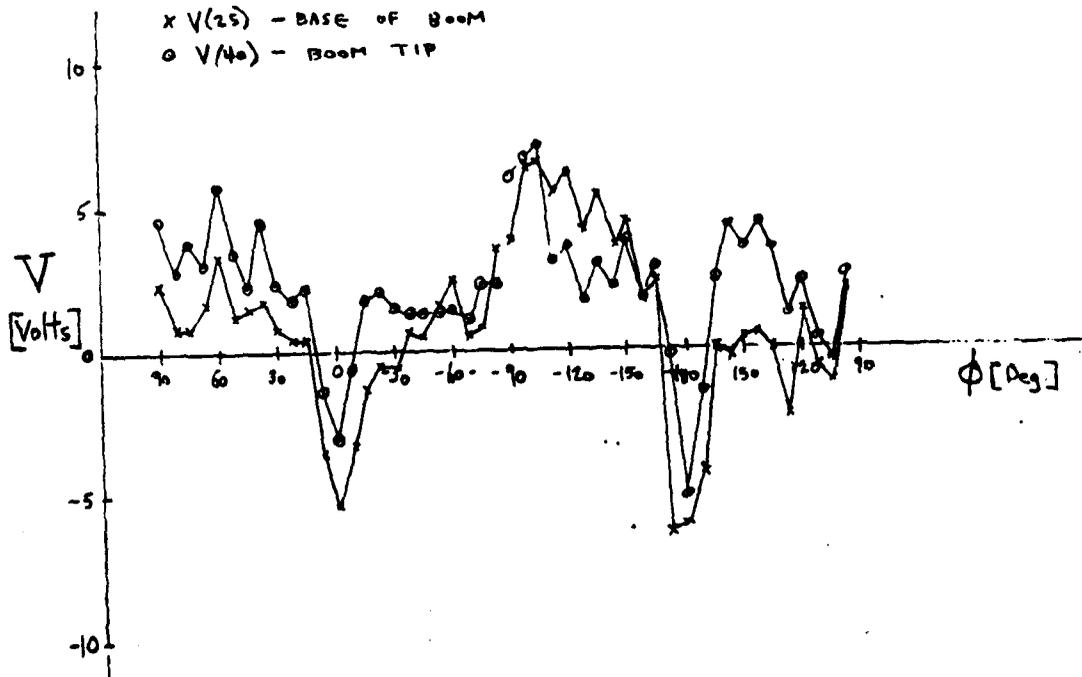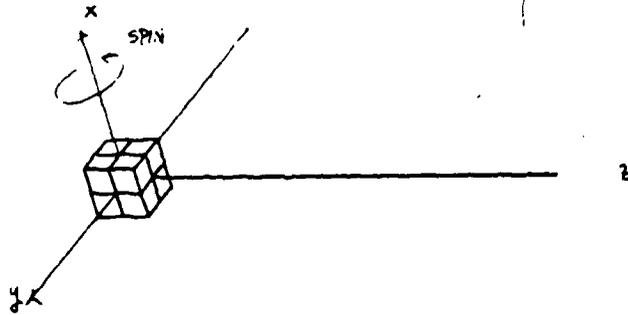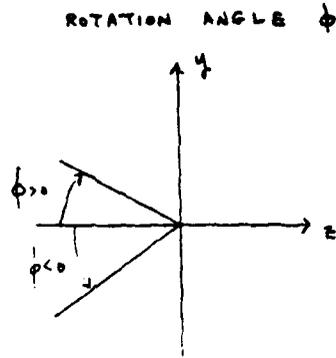
Figure 1.7   Helios Model and Boom Potentials vs Rotation Angle

27

The NASCAP program has been used to configure a model of the GEOS
spacecraft and SPA sensor unit.[13]   The GEOS satellite consists
of a cylindrical body with projecting booms.   The Suprathermal
Plasma Analyzer detector is mounted on one of the booms.
The corresponding NASCAP model is described in Figure 1.8(a).
The main features of the model are:

a) The satellite body is built up from 5 vertically stacked
   8x4 mesh octagons. The mesh size was taken as .2 m so the
   effective diameter is 8x.2 = 1.6 m and the height is
   5x.2 = 1.0 m.

b) Two external cylindrical booms of length 11x.2 = 2.2 m
   extend out from the top of the satellite body.

c) The SPA sensor unit is represented by a 1x1x1 mesh cube.
   The effective dimensions are thus 20x20x20 cm, which is
   slightly larger than actual size. The SPA cube was put on
   a separate conductor to allow for independent biasing.

d) The lower 3 mesh units (.6m) of the satellite body is
   covered with the material Indox.

e) All other surfaces (the top of the satellite, the booms, the
   SPA unit) are covered with Goldpd.

Sunlight charging of a GEOS satellite model for three repres-
entative voltages on the SPA detector were studied.

28
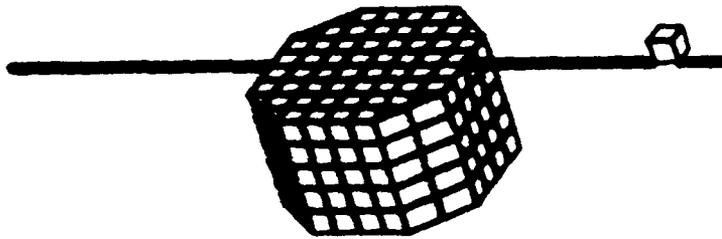
Figure 1.8(a)   NASCAP Model of GEOS Satellite
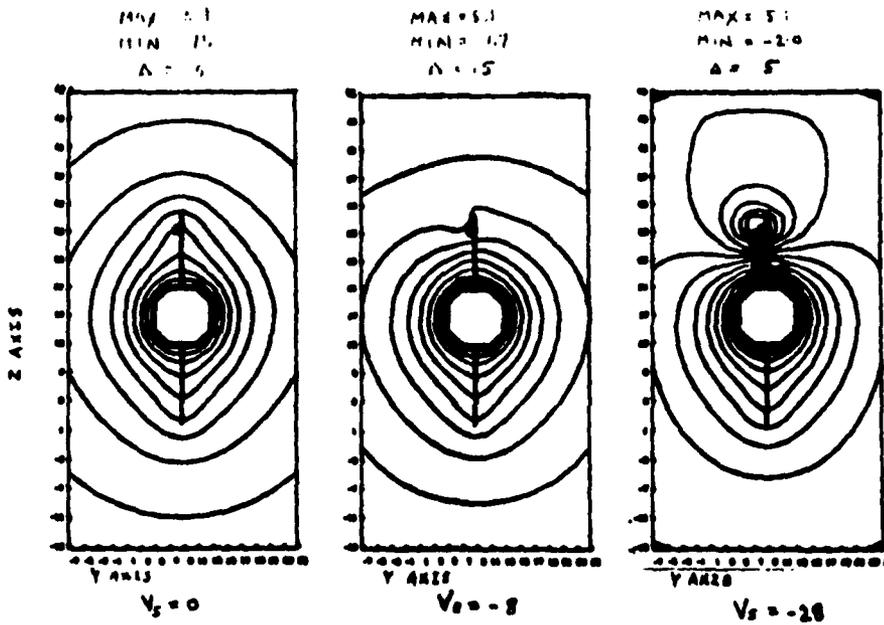
Figure 1.8(b)   GEOS Potential Contours (Top View)

The primary questions to be examined were:

1) Are the local electrostatic fields around the detector
   significantly perturbed by changes in sensor bias?

2) Are the trajectories of low energy particles near the SPA
   instrument significantly altered by the sensor bias?

When the model is exposed to the expected plasma environment and
sunlight, the vehicle frame potential goes a few volts positive.
If the bias on the SPA surface is varied from 0 to -28 volts. the
local field near the unit is modified and there is a significant
change in the low energy trajectories.   Figure 1.8(b) shows a
top view of the potential contours around the GEOS model.   The
influence of the detector biasing on the contours is clearly
evident.

The proposed Space Based Radar structure was modeled by
NASCAP.[12]   The SBR vehicle is composed of three main
components:

1) the lower side package (LSP) consisting mainly of the large
   antenna array.
2) the upper side package (USP) consisting of two gimbaled solar
   arrays.
3) the mast connecting LSP to USP.

The corresponding NASCAP model is given in Figure 1.9(a).
The mesh size is 8 meters. The large antenna (LSP) is
represented by an octagon of diameter 8 meshes = 64 meters
(actual diameter = 71 meters).

The mast is a boom cylinder of diameter 2 meters and length 12
meshes = 96 meters (actual length 102.5 meters). The solar
arrays (USP) are represented by a 2x2 mesh = 16 meter x 16 meter
square.

The surface material on the large antenna (LSP) is mainly KAPTON
with a small amount of ALUMINUM edge tape and the USP solar array
is assumed to be borosilicate glass.[1] For the NASCAP model we
have assumed that the LSP and the mast are covered with KAPTON
and the USP with SOLAR material.

The SBR will be in polar orbit going through the auroral region
at altitude $\approx$10,000 Km. The LSP antenna always points earth-
ward, while the gimbaled solar arrays align themselves with the
sun direction. Relative to a coordinate system fixed on the SBR
the sun appears to rotate through 360° on each orbit. We chose
two representative positions, at $+45^\circ$ and -45°, for the NASCAP
simulations.

Two test plasma cases were set up:

   1) a "cool" plasma with T_e=5, T_i=10
   2) a "hot" plasma with T_e=10, T_i=20

The densities were assumed to be 1 cm^{-3}. In the cold plasma the
materials ALUMINUM and KAPTON would charge (in eclipse) but SOLAR
would not. For the hot plasma all the materials would charge.

31
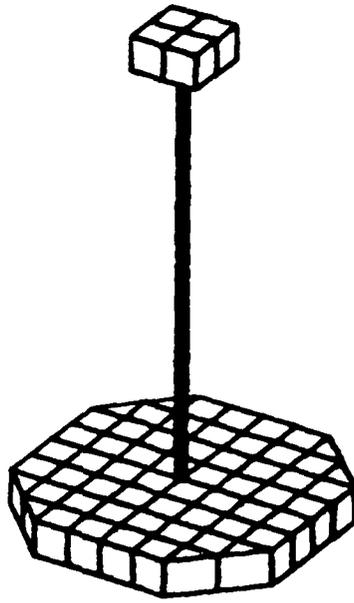
Figure 1.9(a)   NASCAP Model of Space Based RADAR
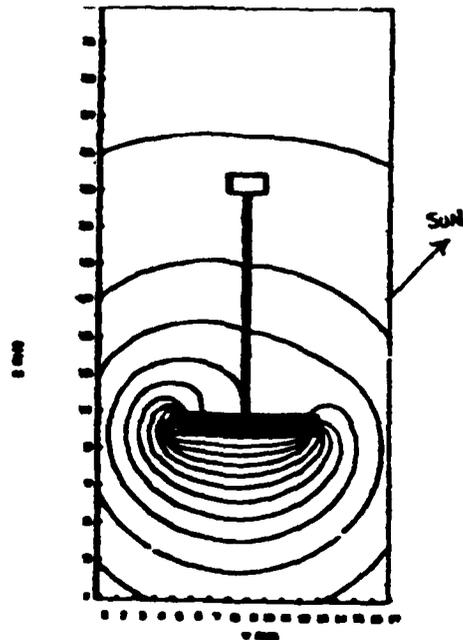
Figure 1.9(b)   Potential Contours for 45° Sun Direction

32

The NASCAP runs that were considered are summarized in Table 1.1.
The vehicle ground voltage and the potentials on selected surface
cells are listed.

For case (1), the cool plasma is used and the sun is at angle
+45°. The vehicle ground charges to -1.8 KV. The potential
contour plots indicate that charge builds up on the shade side of
the LSP. The solar array does not charge and therefore the field
lines are unperturbed near the USP.

Case (2) is the same as case (1) except that the hot plasma
replaces the cool plasma. The vehicle ground thus increases to
-5.1 KV. The potential contours are similar to those of case (1)
but now the USP charges up and perturbs the potential lines in
its vicinity.

Case (3) differs from case (2) in that the sun angle is changed
from +45° to -45°. Here the contour lines build up on the
topside of the LSP, which is now in the shade. The vehicle
ground is about the same as for case (2).

The simplified NASCAP model of the SBR provides a possible
scenario for vehicle charging. As it follows a polar orbit,
the top and bottom sides of the LSP revolve into and out of the
sunlight. If there is a low density ambient plasma present,
with electron temperature greater than 3KeV, then the shade side
of the LSP can charge up to the equivalent eclipse equilibrium
voltage. If the plasma temperature is high enough ($\approx$6KeV), then
the shade side of the USP will charge. The potential contours
are of the type shown in Figure 1.9(b).

TABLE 1.1   NASCAP RESULTS FOR SBR CHARGING

			CASE (1)	CASE (2)	CASE (3)
PLASMA			cool	hot	hot
SUN ANGLE			$+45^{\circ}$	$+45^{\circ}$	-45°
ITERATION STEP			17	15	15
TIME			1.02×10^{5}	3.2×10^{4}	3.2×10^{4}
	CELL#	MATERIAL	V	V	V
GROUND VOLTAGE	-1		-1803	-5149	-5174
LARGE ANTENNA LSP, bottom	2	KAPTON	-2681	-7467	-3010
LARGE ANTENNA LSP, top	1	"	-1329	-3802	-7468
MAST- bottom	161	"	-1006	-3795	-7468
middle	166	"	-735	-2298	-3297
top	172	"	-473	-2638	-2523
SOLAR ARRAY USP, bottom	65	SOLAR	-489	-3007	-2407
SOLAR ARRAY USP, top	64	SOLAR	-408	-1922	-3008

SCATHA charging in sunlight has been studied for a "worst case" plasma environment, based on SC5 measurements.[2,11] In the NASCAP simulations an averaged double Maxwellian fit to the plasma spectrum was used. Due to uncertainties in the environment parameters we have not attempted to predict absolute potentials with NASCAP but, instead, have looked at the behavior of SCATHA charging, under a variety of input conditions, for comparative studies. The results of the NASCAP runs are given in Tables 1.2 and 1.3. The cases that have been considered are labelled from 1 to 8 as indicated.

Cases (1) and (2) compare eclipse charging for the 1-grid SCATHA model using secondaries of normal incidence (NORMAL) or with an isotropic distribution (ANGLE). It can be seen that the ground voltage is decreased from -10.9 KV to -7.0 KV when ANGLE replaces NORMAL. This reduction is due to the fact that more secondaries are emitted when the particles impinge on a surface isotropically. The ANGLE result is in good agreement with the voltage that was actually measured ($\approx$ -8 KV) in the eclipse that occurred about 25 minutes later.

Cases (3) and (4) again make the comparison between NORMAL and ANGLE secondaries, but for a sunlight environment. Here the SPIN mode of NASCAP, set to give spin averaged illumination around the X-axis, has been employed. Again there is a large difference (-3.2 to -.74 KV) between NORMAL and ANGLE results for the ground voltage. The voltage for the ANGLE calculation is about a factor of two greater than than the maximum measured sunlight potential (-.34 KV).

In the preceding runs, it was assumed that there was no biasing of the conductors 2 and 3 of the 1-grid model. To be consistent with the S-CUBED configuration, these conductors were biased to zero volts relative to conductor 1. Case (5) was run to test

35

TABLE 1.2 SUMMARY CASES 1 to 4 (WORST CASE)

| | CELL | MATERIAL | ECLIPSE | | SPIN | |
			NORMAL	ANGLE	NORMAL	ANGLE
	-1	GROUND	-10,886	-7039	-3155	-736
	-2	BOOMTIPS	-14,473	-9885	-1496	-498
	-4	REF BAND	-11,512	-7559	-2576	-1114
	279	KAPTON	-14,450	-9891	-2122	-614
SC1-1	311	SOLAR	-15,160	-9731	-2136	-612
	309	INDOX	-10,890	-7039	-3155	-736
	419	GOLD	-11,860	-7695	-2108	-612
SC1-2	135	KAPTON	-14,450	-9891	-2174	-802
	352	GOLD	-10,890	-7039	-3155	-736
SC1-3	353	TEFLON	-13,250	-8168	-13,220	-8145
	362	KAPTON	-14,450	-9891	-14,440	-9865
	363	ASTROQ	-10,930	-7060	-3455	-1081
BOTTOM	2	WHITEN	-11,550	-7722	-5285	-2791
TOP	359	GOLDPD	-10,890	-7039	-3155	-736
JOB			TZWCEGR	TZWCE2F	TZWCS13	TZWCSAY
STEP			50	40	20	26
ΔV(step)			-169	-145	-1	-7
CASE			1	2	3	4

TABLE 1.3 SUMMARY CASES 5 to 8 (WORST CASE)

	CELL	MATERIAL	SPIN		ROTATE	
			1-grid	3-grid	1-grid	3-grid
SC1-1	-1	GROUND	-689	-1371	-1231	-1908
	-4	REF BAND	-1087	-1639	-1540	-2123
	279/280	KAPTON	-585	-1477	-1453	-2244
	311	SOLAR	-583	-1284	-1389	-1734
	309/310	INDOX	-689	-1371	-1231	-1908
	419	GOLD	-584	-1638	-1603	-2123
SC1-2	135	KAPTON	-777	-1514	-1230	-1959
	352	GOLD	-689	-1371	-1230	-1908
SC1-3	353/354	TEFLON	-8153	-8163	-8601	-8675
	362/363	KAPTON	-9880	-9894	-10,360	-10,410
	363/364	ASTROQ	-1035	-1704	-1566	-2222
BOTTOM	2	WHITEN	-2818	-3355	-3340	-3887
TOP	359	GOLDPD	-689	-1371	-1230	-1908
JOB			TZWCS3H	TZWCSBG	TZWCR3X	TZWCTIF
STEP			20	35	77(229)	51(225)
ΔV(step)			-19	-32	+40	-113
CASE			5	6	7	8

37

the effect of this change. By comparing cases (4) and (5) we
see that this modification makes negligible difference to the
charging. On subsequent runs, the zero biasing of conductors 2
and 3 was maintained.

Figure 1.2 shows the NASCAP 1-grid model of SCATHA and the
corresponding 3-grid model. The only difference between the
models is that the external booms have been modified. In the 3-
grid model the booms extend out to actual length, and the surface
material is changed from BOOMAT to KAPTON. The cell numbering
differs slightly for the two models. In column 1 of Table 1.2
both numbers are given (1-grid first), where differences occur.

The 3-grid model was run in eclipse, and it was found to give
virtually the same potentials as for the 1-grid model (case 2).
This result is expected since the plasma is strong enough to
charge the surface cells independently. The situation can be
quite different in a weak plasma where the "boot strap" mecha-
nism (charging cells influencing neighboring non-charging cells)
can lead to substantial deviations in the potentials obtained
from the two models.

Cases (5) and (6) compare the results for sunlight charging (in
the SPIN mode) with the 1-grid and 3-grid models. It is evident
that the 3-grid model charges higher (-1.37 KV versus -.69 KV).
This result holds true also for cases (7) and (8) which make the
same comparison relative to the ROTATE mode (-1.9 KV versus -1.23
KV). The potential contours for the 3-grid model are quite
different in the region of the booms from those of the 1-grid
model. Otherwise, the main features of the charging are the
same i.e. the WHITEN cells in the bottom shade and the SC1-3
patch in the top-side shade are at the highest potentials.

38

By comparing cases (5) and (7) to cases (6) and (8) we see that the vehicle ground tends to be higher for the rotate mode than with SPIN for both the 1-grid model (-1.23 KV versus -.69 KV) and the 3-grid model (-1.91 KV versus -1.37 KV). This behavior is consistent with earlier NASCAP studies[3] which gave the same result for a uniform quasisphere.

The NASCAP comparative runs illustrate the following characteristics of SCATHA charging:

1) The ANGLE mode for secondary emission produces less charging than NORMAL.
2) The 1-grid model charges up less than the 3-grid model.
3) The biasing of conductors 2 and 3 on the 1-grid model has little effect
4) The SPIN mode tends to give lower charging than for ROTATE.

In the ROTATE runs, the amplitude of the spin modulation can depend on the DVLIM parameter which may have to be adjusted from the default value.

The NASCAP calculation of the vehicle ground potential in sunlight is $\approx$-1300 V (average over cases (5) to (8)), which is higher than the maximum measured value of -340 V. The eclipse charging result of $\approx$ 7.0 KV (from case(2)) is less than the estimated value of -16 KV (from Table 1). On the other hand the NASCAP result is quite close to the actual measured voltage of $\approx$ 8 KV for the eclipse which occurred later. The SSPM results for sunlight charging are mixed; the calculated voltages are found to be high for GOLD and SOLAR, low for QUARTZ, and in rough agreement with the KAPTON and TEFLON samples.

1.5   Extended Simulation Studies

The P78-2 SCATHA satellite was launched in January 1978, into a near-geosynchronous orbit.   The satellite carries thirteen separate experimental payloads for analyzing spacecraft charging effects.   The data from the UCSD charged Particle Experiment (SC9) was used to determine periods of strong eclipse charging, by looking for sharp peaks in the high resolution electrostatic analyser (ESA) ion count measurements.   The channel number of the peak gives an estimation of the shift in energy due to particle acceleration into the detector, and thus of the spacecraft potential.   This effect is clearly evident in the upper-right plot of Figure 1.3 where there is a clear peak in the ion distribution function at about 6.2 KeV corresponding to vehicle charging of 6.2 Kv.   Figure 1.10 gives a summary of the spacecraft potential versus UT for the most active charging days of the 1979 eclipse seasons.   The "worst case" charging event occurred on day 114, 1979 and this was chosen for a NASCAP simulation study.[9]

On day 114, the SCATHA satellite was in full eclipse from UT=26055 to UT=28868.   The NASCAP simulation runs were started at UT=25950, with the vehicle initially uncharged and the sun intensity equal to zero.   This procedure approximates the actual situation where the vehicle was charged slightly ($\approx$ 400 volts) in sunlight and the sun intensity rapidly decreased to zero.

The NASCAP 1-grid model (see Figure 1.2) was used to represent the SCATHA satellite.   The charging simulation was carried out in the UPDATE mode.   That is, on each time-step, the program searches an input file for the most recent spectrum and updates the flux description to the corresponding double Maxwellian fit.
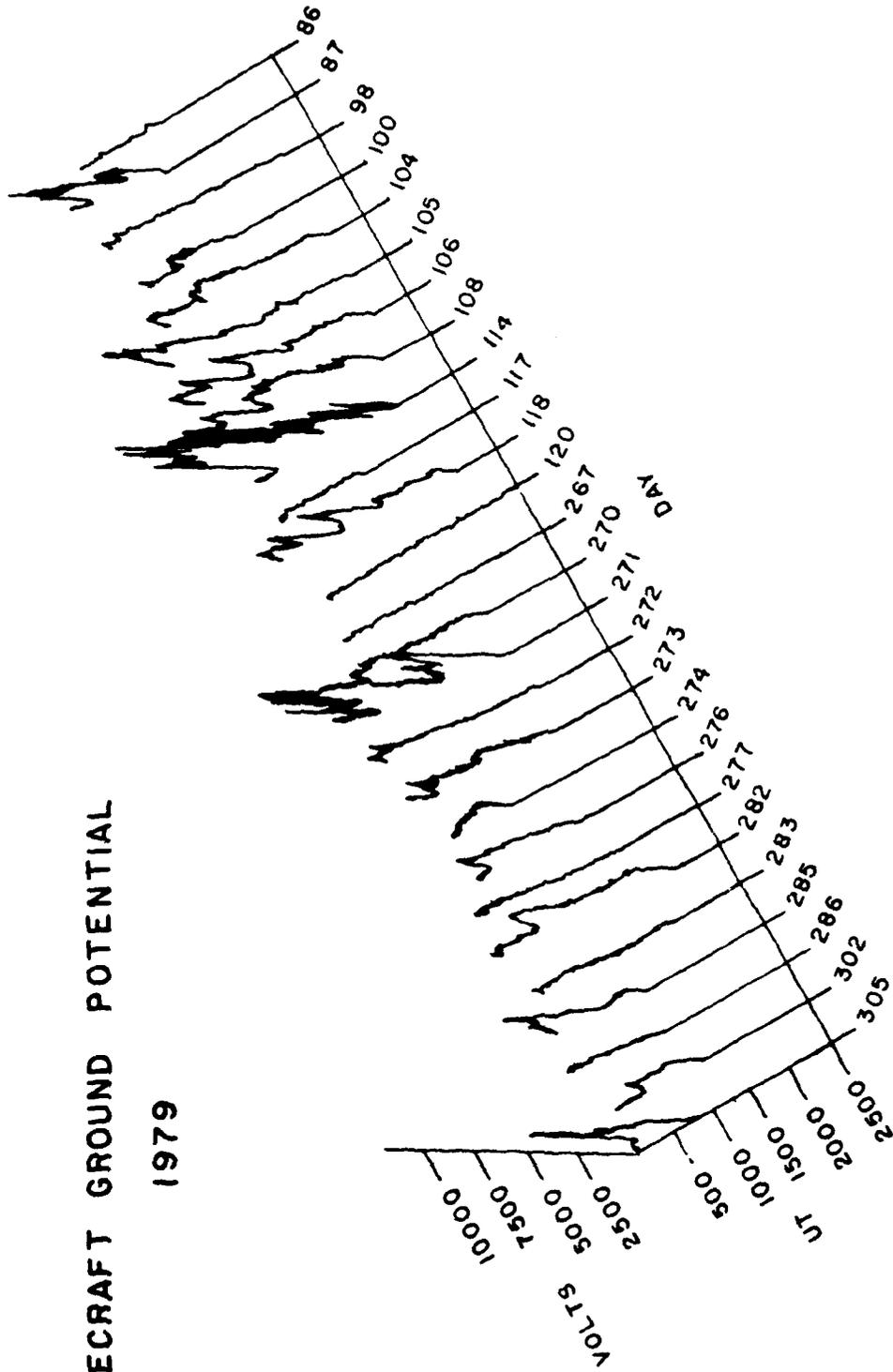
Figure 1.10 Spacecraft Potential Measured over a Five Month Span

41

Figure 1.11 displays the NASCAP results for the complete pass through the data. As can be seen from the plot, the overall agreement with the measured SC9 voltages is quite good. The potential contours, for a point mid-way through the second pass run, are shown in Figure 1.12. Near the surface, the contour lines tend to follow the satellite geometry, with some deviations due to the booms. Beyond a few meters from the satellite, the monopole field dominates.

The most complex NASCAP simulation that has been attempted is the day 113 (1981) case, where transit into and out of eclipse was considered.[15] Here, in addition to the temporal plasma environment, we have time dependent sun illumination in the penumbra regions.

The SC9 instrument sweeps through 64 energy channels ($0 < E < 82$ KeV). The measurements were made once every 17 seconds during the day 113 eclipse period. The ALLES program reads the SC9 data from magnetic tape, converts the electron and ion counts to the corresponding phase space distribution functions, and makes Maxwellian fits to each spectrum. Figure 1.13 shows the SC9 distribution functions versus UT.

To obtain an overview of the charging strength of the day 113 plasma environment, a number of trial runs were done with the auxiliary program MATCHG. The MATCHG program was adapted so that it could read in the spectrum fits, one-by-one, and calculate the equilibrium potential for each of them. The surface material was chosen to be SOLAR, which is the most prevalent cell on the NASCAP model of SCATHA. From previous work it has been found that SOLAR is a good indicator of the eclipse charging behavior of the 1-grid model i.e. when SOLAR charges, the NASCAP model does so also, usually reaching a value $\approx 30\%$ below that of MATCHG.

42
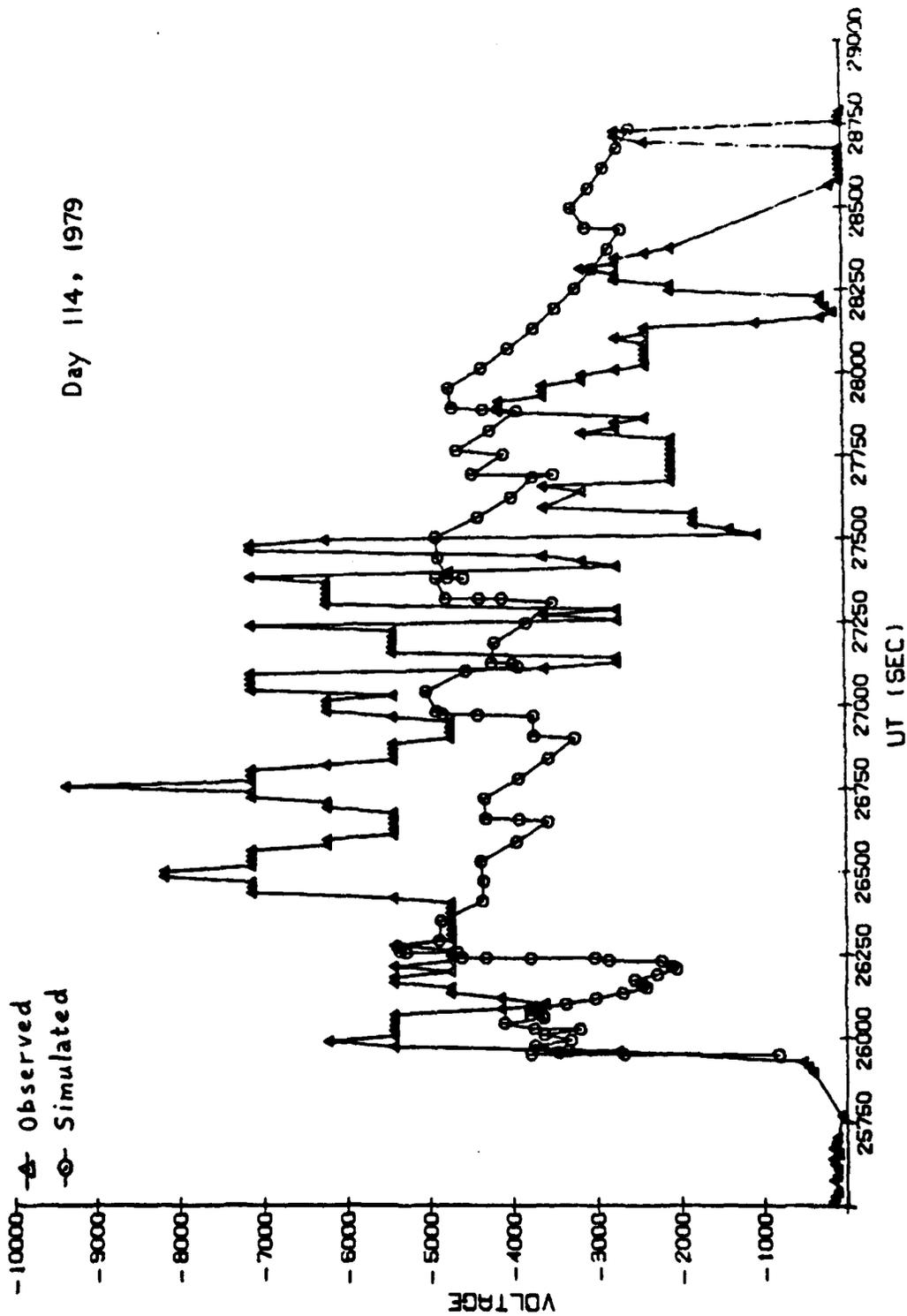
Figure 1.11 Comparison of simulated (2nd pass) and observed ground potentials

POTENTIAL CONTOURS ALONG THE X-Y PLANE OF Z = 7
VMIN = -5.5510E+03 VMAX = -1.2949E+03 DV = 5.0000E+02
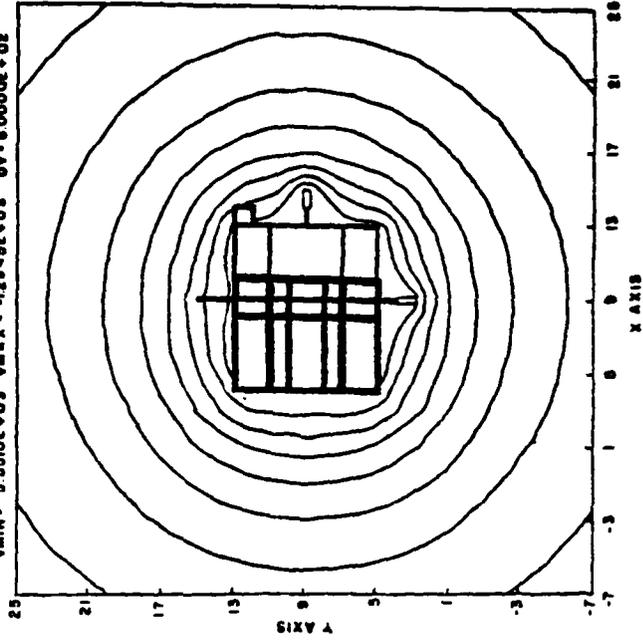
Fig 1.12c X-Y plane

POTENTIAL CONTOURS ALONG THE Z-Y PLANE OF X = 8
VMIN = -5.4130E+03 VMAX = -8187.0E+02 DV = 5.0000E+02

Fig 1.12b Z-Y plane

POTENTIAL CONTOURS ALONG THE X-Z PLANE OF Y = 9
VMIN = -5.0980E+03 VMAX = -8187.0E+02 DV = 5.0000E+02

Fig 1.12a X-Z plane

Potential contours for SCATHA model at 27368 sec. UT

44
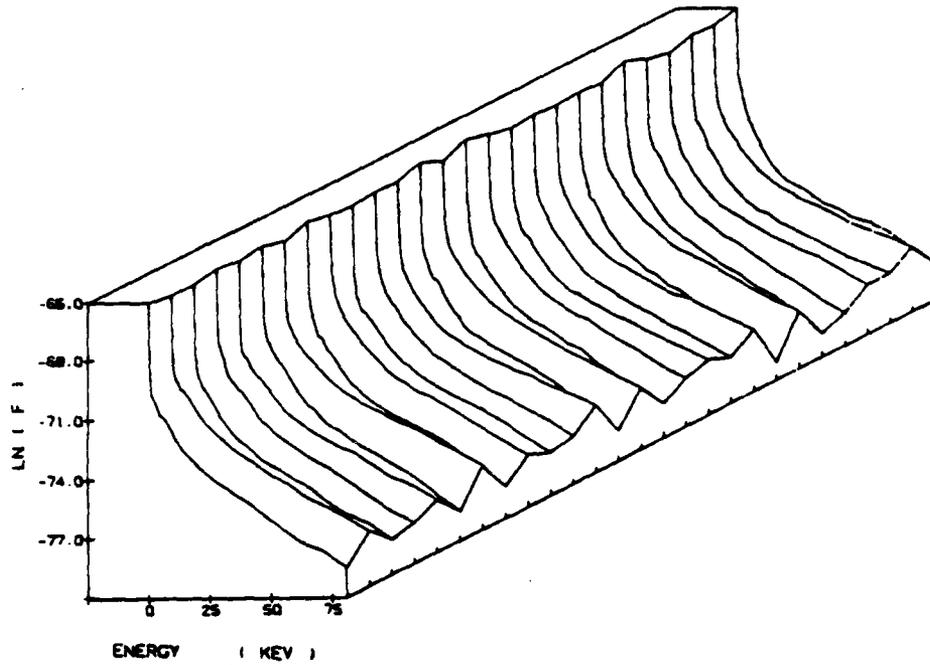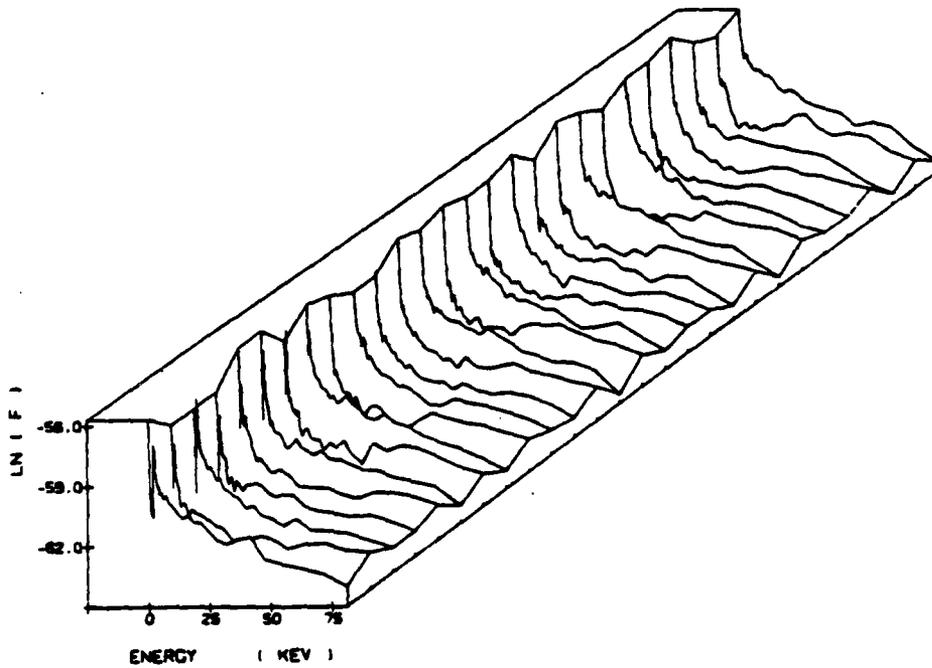
Figure 1.13 Electron and Ion Phase Space
Distribution Functions for Day 113

45

These studies indicated that adequate charging voltages in the
eclipse region could be obtained by using the single Maxwellian
fits from ALLES.   Figure 1.5 gives the MATCHG equilibrium
potentials versus UT corresponding to these fits.   In order to
reduce fluctuations, the electron densities and temperatures were
smoothed using a ten point running average.   The final input
temperatures and densities are given in Figure 1.14.

To conserve computing time, the NASCAP 1-grid model of SCATHA was
employed.   This model gives an adequate representation of the
vehicle geometry and surface materials (the material properties
were assumed to have the default values set by S-CUBED).
However, the booms are truncated and this will lead to some
inaccuracy in the sunlight regions.   Also, to save time, the sun
illumination was represented by the SPIN approximation, rather
than ROTATE.   Again this will introduce uncertainties into the
calculation of sunlight effects.

The NASCAP simulations were carried out in the UPDATE mode i.e.
on each iteration the program searches an input file containing
the spectra fits and picks out the one that is closest (earlier)
to the current time.   Also, by means of RDOPT cards, the sun
intensity is adjusted on each step to define the variation in sun
illumination in the entrance and exit penumbra regions.
The NASCAP time-step was set to 17 secs, which is the interval
between SC9 measurements, so that each spectra would be sampled
at least once during the run.   A complete pass through the data
-- into and out of eclipse -- takes about 6 hours running time on
the CDC 6600, using the 1-grid model.

The vehicle frame potential, as determined from SC9 measurements,
is plotted versus UT in Figure 1.15.   The circles represent the
measured voltages in KV.   The solid line in the figure gives the
sunlight intensity during passage through eclipse.   The voltage

46
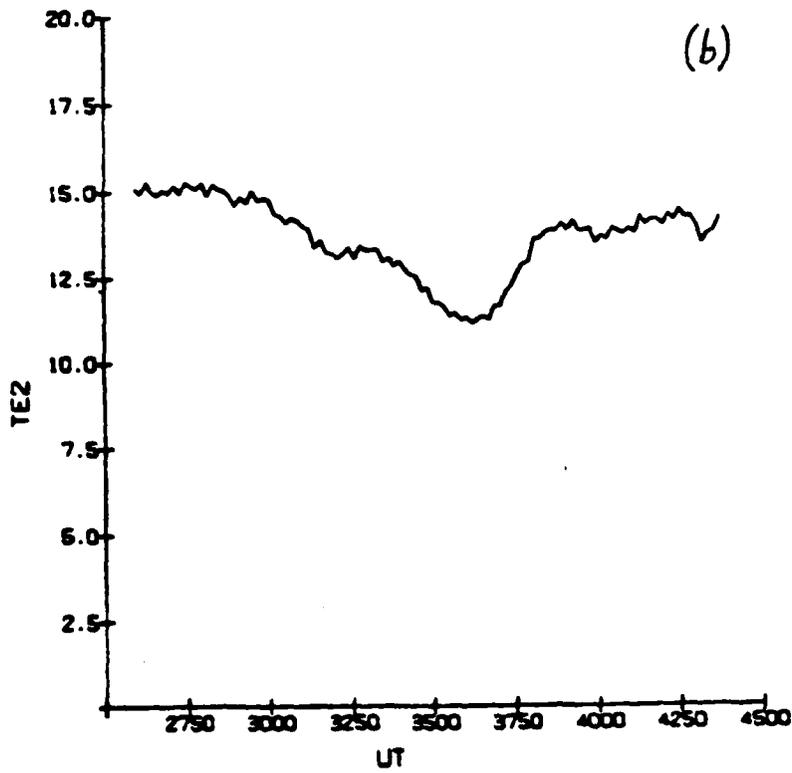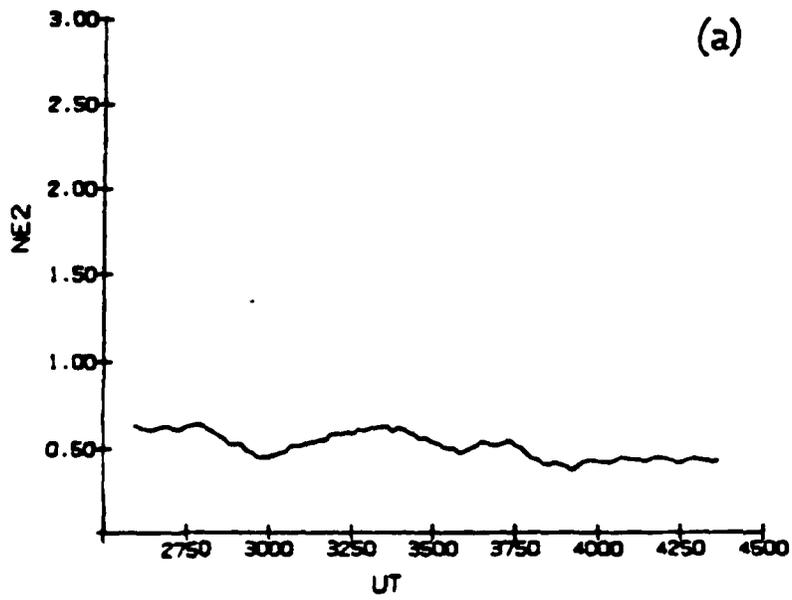
Figure 1.14   Corrected and Smoothed Electron Density
and Temperature (Single Maxwellian)

47
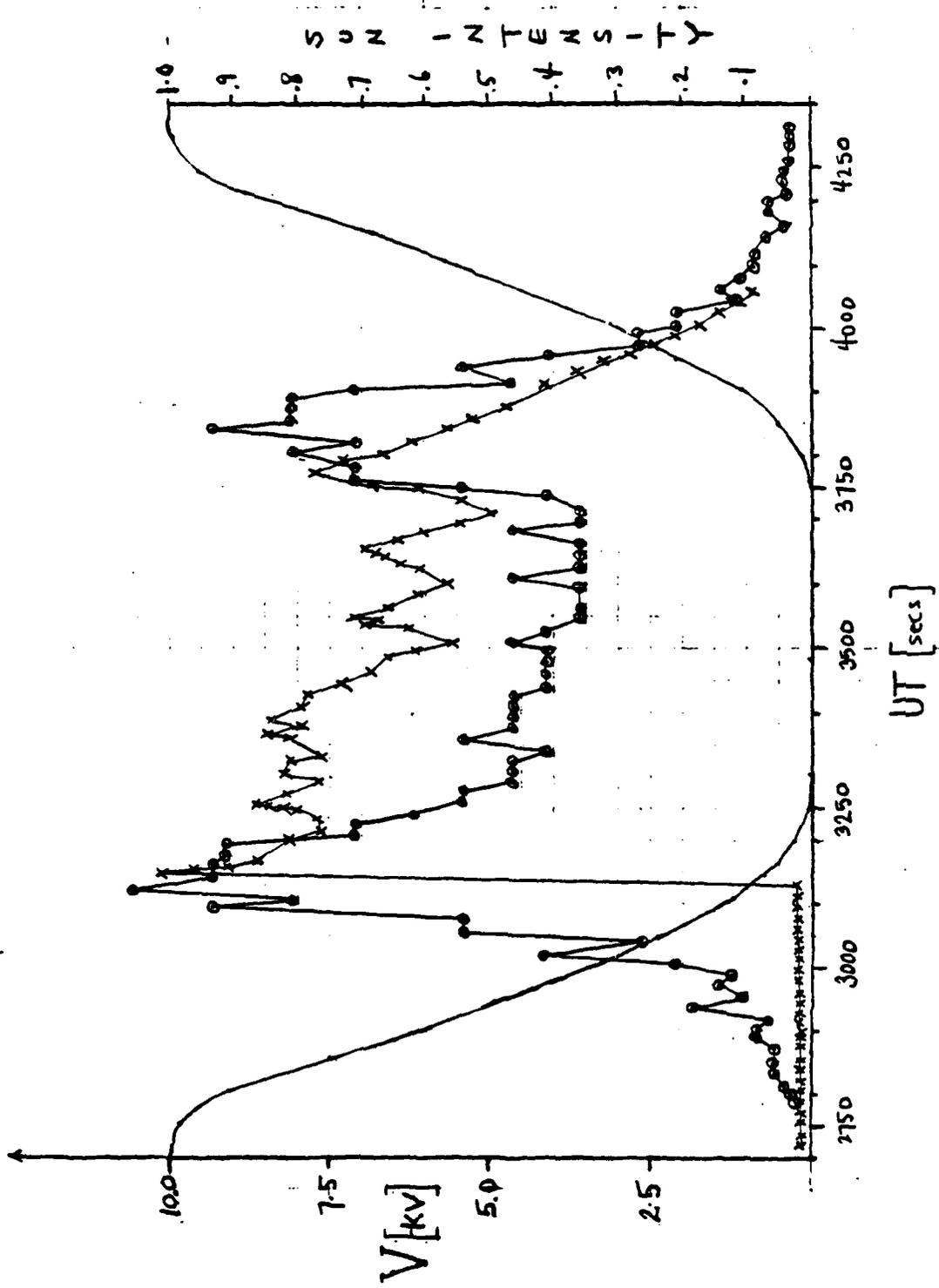
Figure 1.15 NASCAP Ground Potentials vs. UT for Single Maxwellian Fit (Day 113/91)

48

plot has two peaks; the first peak is correlated with entry to
eclipse and the second one occurs in the exit penumbra.

A straightforward physical picture may be used to explain the
main features of the day 113 charging event.   Assume that there
was present a severe charging plasma environment.   In sunlight,
any shaded surfaces would charge up, but those cells that are
exposed to the solar UV would lose photo-electrons, so that the
charging would be inhibited.   The net effect is that the vehicle
ground typically goes a few hundred volts negative.   When the
spacecraft enters penumbra, the photoemission is reduced and
eventually a point is reached where the plasma current dominates.
The vehicle then rapidly charges and maintains a high voltage
through eclipse.   In the exit penumbra region, the photoemission
again builds up and the charging is suppressed.

Figure 1.15 gives the NASCAP predictions for the day 113 event
assuming a DVLIM parameter of 500 (a comparison run with value
5000 was also done).   The following aspects of the simulations
are worthy of note:

a) in sunlight, the vehicle frame potential goes a few hundred
   volts negative, as expected.

b) when the sun illumination in the entrance penumbra is suffic-
   iently reduced (to $\approx$ 25%) there is rapid charging.   With the
   smaller DVLIM setting (500), the charging peak is $\approx$ 10KV, in
   agreement with measurements.

c) in the full eclipse region, the vehicle frame falls to $\approx$ 6KV,
   which is a few kilovolts higher than the measurements.   This
   result is independent of DVLIM.

49

d) the second peak structure in the data is too high when
   DVLIM = 5000, and slightly low for DVLIM = 500.
   The latter case should be more accurate.

e) in the exit penumbra, the solar UV brings down the frame
   potential, roughly in accordance with measurements.   The
   region is almost independent of DVLIM even though there are
   frequent cut-backs with DVLIM =500 and none with DVLIM =5000.

The primary weakness in the simulation appears to be near the
entrance penumbra region where the NASCAP frame potential starts
to rise later than for the measurements and then goes up much
more rapidly.   This is an inherently difficult part of the
event to model, requiring precise values of the sun illumination
and correlated plasma enviroment.

The SPIN approximation, which averages the sun intersity over
many cycles is probably inadequate here (the jogs in the measured
voltage during charging are probably due to rotational effects).
Also, neglecting the low energy electrons is less valid in this
region where the vehicle potential is low.   For these reasons,
it is not surprising that the NASCAP code does not track the
measurements better through the initial charge-up phase.

The overall agreement of the 1-grid frame potential with the SC9
voltages is quite good considering that:

   1) we have neglected the low energy Maxwellian components

   2) there are uncertainties in the materials properties

3) there are approximations in the model (truncated booms, SPIN mode instead of ROTATE)

4) there is uncertainty in the O_2 content of the environment

5) there were large fluctuations in the charging strength from one plasma spectrum to the next.

The first point above is the most crucial one.   The low energy electrons, in particular, form a critical part of the plasma specification.   But the low energy part of the SC9 spectra is not known during periods of strong charging because these particles are repelled by the electric field surrounding the vehicle.   Thus some guess has to be made as to the shape of the low energy electron spectrum.   If we use extrapolated fits to the region (the double Maxwellian fit) then we find that the charging is suppressed.   If we neglect the low energy components entirely (the single Maxwellian) then we get charging that is a few kilovolts too high in the central eclipse region.   A definitive test of the NASCAP program can only be made if a complete specification of the particle spectrum is available.

References

1. Katz, I. et al, "Extension, Validation and Application of the Nascap Code", Final Report, SSS-R-79-3904, January 1979.

2. Mullen, E.G. et al, "A Worst Case Spacecraft Environment as Observed by SCATHA on 24 April 1979", AFGL-TR-81-0231.

3. Rubin, A.G., Bhavnani, K.H., and Tautz, M.F., "Charging of Spinning Spacecraft", AFGL-TR-79-0261

4. Stannard, P.R. et al, "NASCAP Programmer's Reference Manual", SSS-R-82-5443, March 1982.

5. Tautz, M.F. et al, "Prediction of Materials Charging in Magnetospheric Plasmas", AFGL-TR-81-0088

6. Tautz, M.F. et al, "SSPM Experiment Simulation Study for the April 24, 1979 Charging Event", AFGL-TM #23

7. Tautz, M.F., Rubin, A.G., and Saflekos, N.A., "Preliminary Simulation of Electron Emitter Events on March 29, 1979", AFGL-TM #33

8. Tautz, M.F. et al, "SSPM Experiment Simulations for 1979 Day 87 and Day 114 Charging Events", AFGL-TM #39

9. Tautz, M.F., Rubin, A.G., and Saflekos, N.A., "NASCAP Simulation of Charging Event for Temporal Plasmas of April 24, 1979", AFGL-TM #58

10. Tautz, M.F., Rubin, A.G., and Saflekos, N.A., "NASCAP Simulation of Helios 1 Antenna Boom Potentials", AFGL-TM #61

11. Tautz, M.F., Rubin, A.G., and Saflekos, N.A., "NASCAP Simulation of SCATHA Charging in Worst Case Plasma of April 24, 1979", AFGL-TM #70

12. Tautz, M.F., Rubin, A.G., and Saflekos, N.A., "Preliminary NASCAP Model of the Space Based Radar", AFGL-TM #71

13. Tautz, M.F., Rubin, A.G., and Saflekos, N.A., "NASCAP Model of GEOS Satellite and SPA Sensor Unit", AFGL-TM #72

14. Tautz, M.F., and Rubin, A.G., "Threshold Conditions for Materials Charging in Maxwellian Plasmas", (in publication)

15. Tautz, M.F., Rubin, A.G., and Saflekos, N.A., "NASCAP Simulation of SCATHA Charging on Transit through Eclipse for Day 113, 1981", AFGL-TM #80

52

2.0   Ionization and Charging Effects of Beam Currents

When a charged probe is placed in a plasma environment, it draws
from the plasma a current of oppositely charged particles.
Since particles of like charge are repelled by the probe, a
sheath develops, depleted to some degree in the repelled species.
The application of this system to the charging of beam emitting
spacecraft was first detailed by Beard and Johnson.[1]   Later,
the physics of the probe sheath was studied in depth by Lam.[3]
More recently, Leadon, et.al.[4] developed a numerical model to
introduce into the Lam model the effect of ionization of neutral
gas molecules by current returning to the probe.   Figure 2.1
illustrates schematically the physical processes in the sheath
region.   The case of a spherically symmetric electron beam
emitter was considered and it was found that ionization served to
reduce probe charging.   This was significant in that experi-
mental results then available indicated low probe potentials at
high beam currents.   However, the study by Leadon, et.al. was
not entirely conclusive in that the PLAS3 program developed to
implement the model failed to converge at high beam currents.
The work on this project was initiated with the aim of deter-
mining the origin of the convergence problems and extending the
model to higher currents.

The further development of the PLAS3 code is a step towards a
synthesis of spacecraft charging models.   PLAS3 is an
intermediate level program which treats the basic physical
processes without dealing with the complications of spacecraft
structural detail.   Thus it can be used to generate benchmark
cases, for comparison with much slower particle pushing methods,
or with complex existing codes such as NASCAP and POLAR that do
not address the low altitude ionization problem.

53
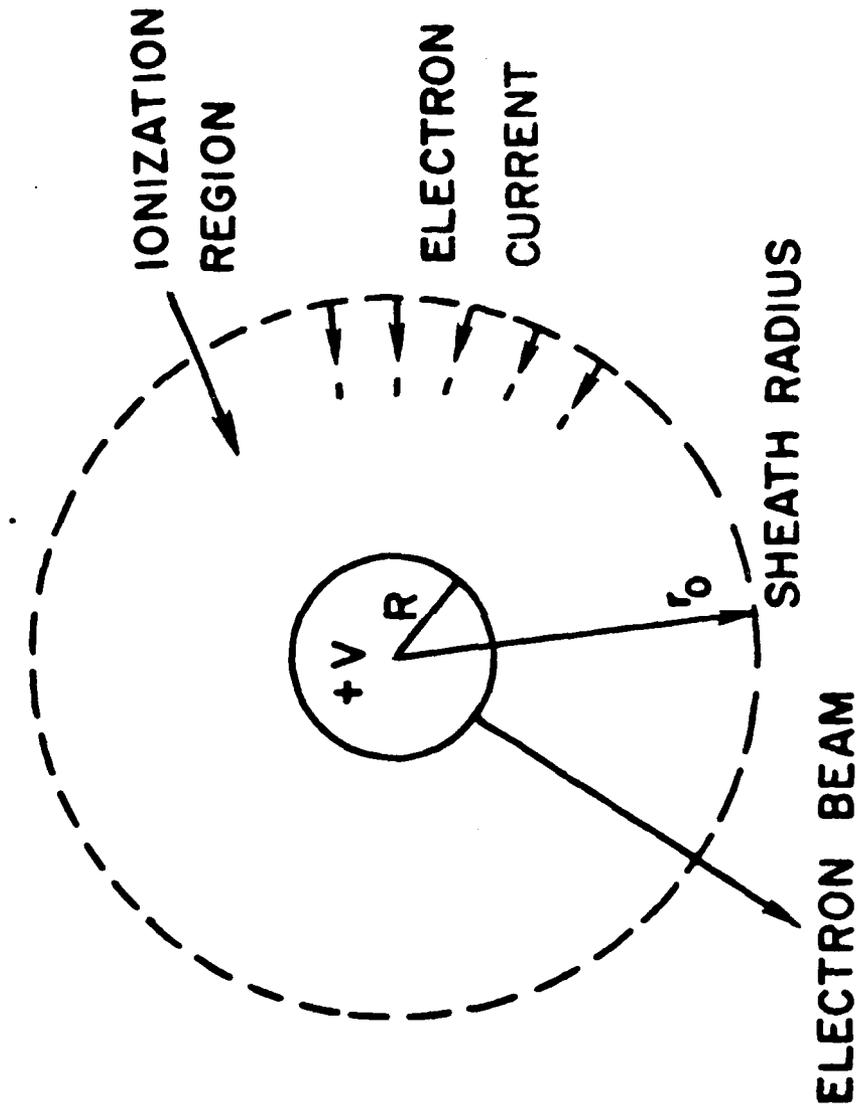
Figure 2.1 Schematic of Ionization Process

2.1 The PLAS3 Model

The model is essentially the same as that used in the previous studies.[3,4] The spherical probe is assumed to be surrounded by a sheath of radius R_o. At the sheath boundary, the field and potential are set to zero, and electron density is equal to the ambient plasma density n_e. Ambient ions, however, are assumed to be repelled from the probe so that their density is zero both inside the sheath and at the boundary. The sheath boundary is determined by the condition that the inward thermal electron flux is equal to the beam current I_b, thus

$$4 \pi q R_o^2 V_{th} n_e = I_b \qquad (1)$$

Once inside the sheath, the electrons are assumed to travel by free fall toward the probe. Conservation of energy then gives

$$\tfrac{1}{2} m U^2 = \tfrac{1}{2} m U_{th}^2 + q \Phi \qquad (2)$$

On their way to the probe surface, electrons strike neutrals, at a density n_o, and ionization occurs with frequency

$$P(V_e)/n_o \sigma \qquad (3)$$

Where $P(V_e)$ is a velocity dependent probability curve, normalized to unity, and σ is the maximum cross section for ionization, around 2×10^{-16} cm^2 for O_2 targets, with a peak around 70 eV. The ion pairs thus created are accelerated away by the field and give rise to a secondary electron and ion flux. The number of secondary pairs produced per second throughout the sheath is

$$N = 4 \pi \int_{R_b}^{R_o} r^2 \left(\frac{dn}{dt}\right) dr \qquad (4)$$

where R_b is the probe radius.

55

The potential inside the sheath is related to the charge density by Poisson's equation

$$-\nabla \cdot \nabla \phi = \frac{-1}{r^2} \frac{\delta}{\delta r} \left(r^2 \frac{\delta \phi}{\delta r} \right) = \frac{e}{\epsilon_o} \left(n_s^+ - n_p^- - n_s^- \right) \tag{5}$$

To use (5) we need another equation relating ϕ and n.
The charge density is derived from three sources.

(1) The primary electron density is found by equating the flux at a point r to the primary flux, thus

$$r^2 n_p^- V_p(r) = R_o^2 \, n_e \, V_{th}$$

Using (2) for $V_p(r)$,

$$r^2 n_p^-(r) = \frac{n_o \, V_{th} \, R_o^2}{\left(V_{th}^2 + \frac{2q}{m_e} \phi(r) \right)^{1/2}} \tag{6a}$$

(2) The secondary contribution to electron density is found by examining the flux at r from electrons originating at ρ.

$$r^2 n_s^-(r) \, V_s(r) = \left(\frac{dn}{dt} \right) \rho^2 \, d\rho$$

From energy conservation,

$$\tfrac{1}{2} m \, V_s^2(r) = q \left(\phi(r) - \phi(\rho) \right)$$

since pairs are assumed to originate with zero initial velocity. Summing contributions to n_s from all $R_o > \rho > r$ gives

$$r^2 n_s^-(r) = \int_r^{R_o} \frac{\left(\frac{dn}{dt} \right) \rho^2 \, d\rho}{\left(\frac{2q}{m_e} \left(\phi(r) - \phi(\rho) \right) \right)^{1/2}} \tag{6b}$$

56

(3) A treatment equivalent to (2) for secondary ions gives

$$r^2 \, n_s^+(r) \;=\; \int_{R_o}^{r} \frac{\left(\frac{dn}{dt}\right) \rho^2 \, d\rho}{\left(\, V_s^2 + \frac{2q}{m_i}\left(\phi(\rho)-\phi(r)\right)\right)^{\frac{1}{2}}} \tag{6c}$$

Here the ions are assumed to be swept out by the motion of the probe at velocity V_s so that energy conservation appears as

$$\tfrac{1}{2}\, m \, V^2 \;=\; \tfrac{1}{2}\, m \, V_s^2 + \frac{2q}{m_i}\,|\phi-\phi_b|$$

where ϕ_b is the potential at which the ion was created.

When Eqns. (6a – 6c) are substituted for the RHS of (5) and the boundary conditions

$$\phi(R_o) = 0, \qquad \phi'(R_o) = 0$$

are imposed, we arrive at a closed integro-differential equation for ϕ, which we solve by the following numerical scheme.

In order to solve Eq. 5, we define

$$E = -\nabla\phi \tag{7}$$

and consider a corresponding difference equation. The sheath region is divided into N shells of width

$$\Delta r = (r_o - r_b)/N$$

Each shell begins at a radius $\rho_i = r_b + (i-1)\Delta r$

and has as its midpoint the radius $r_i = r_b + (i-\tfrac{1}{2})\Delta r$

57

At each P_i we define a field variable E_i and at each r_i we define a potential Φ_i and a space charge n_i. The potential is related to the field by

$$\Phi_{i+1} - \Phi_i = (E_i + 2E_{i+1} + E_{i+2}) \Delta r / 4 \qquad (8)$$

The densities are found by replacing the integrals in Eq. 6 by trapezoidal rule approximates.

To include the effects of ionization in cell i to the charge density in that same cell, we divide the cell into general subcells and approximate the field as a constant over each region. The integrals in Eq. 6 can than be done analytically.

With the knowledge that

$$E_{N+1} = 0, \qquad \Phi_{N+1} = 0$$

We arrive at a set of N non-linear equations in N unknown field points. These we solve by Newton-Raphson iteration as follows. Define

$$f_i(E_1, E_2, \ldots, E_N) =$$

$$P_{i+1}^2 E_{i+1} - P_i^2 E_i - \frac{e}{\epsilon} \Delta r n_i, \quad i=1, N \qquad (9)$$

Guess an initial vector

$$(E_1^{(o)}, E_2^{(o)}, \ldots, E_N^{(o)})$$

and modify the initial vector in a direction which will minimize the residuals of Eq. 9.

2.2 Method of Approach and Results

After investigating both the model and the previous numerical
implementation, the code was rewritten using a different and more
straightforward method (Newton-Raphson) to solve the equations.
This program was thoroughly cross-checked with the original for
cases where the original converged.   Using the new algorithm,
we were able to obtain solutions for arbitrarily high beam
currents.   The nature of the potential contours was rather
unusual and SUATEK graphics capabilities were added to the
program to facilitate understanding of the underlying physics.
Plots of potential, electric field and total and partial charge
distributions such as are shown in Figures 2.2 and 2.3 were made
available.   A series of runs have been made to calculate the
dependence of the probe charging on the model parameters, namely,
the electron temperature and density, the mean ionization length
and ionization profile, and the beam current.

The effect of mean ionization distance λ on the potential of a
spacecraft emitting a beam is shown in Figure 2.4.   In the
region where ionization is negligible ($\lambda = 10^8$ approximately),
the potential curves are flat, and the potential increases with
beam current.   As the ionization distance decreases (i.e.
ionization is more probable) the potential curve turns down, and
stays constant approximately as the ionization distance λ
decreases further.

The main result from the parameter studies was that the curve of
the probe potential versus current was very similar to that
measured experimentally.   For low electron beam currents, the
potential increases monotonically with the current.   Beyond a
critical current, the returning electrons from the environment
cause ionization, and the potential drops to a lower value.[5]

59
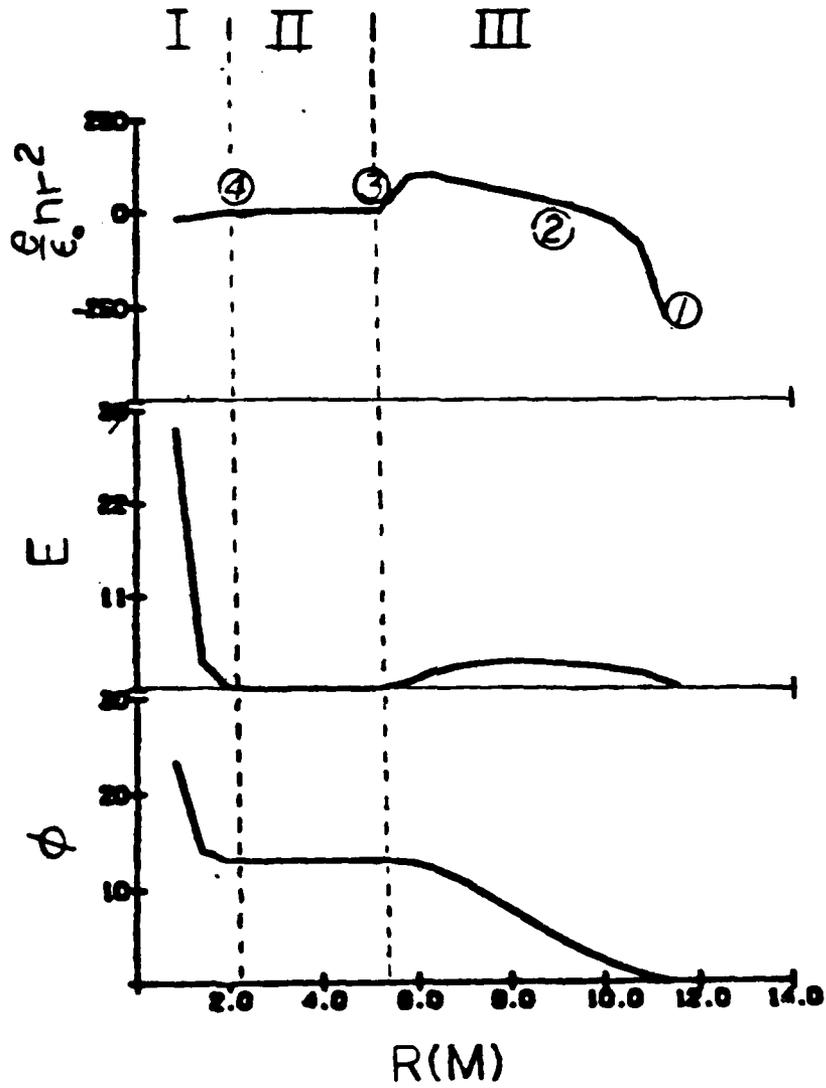
Figure 2.2   Profiles of   (a) Total charge density,
(b) Electric field,   (c) Potential
for a beam of 10 ma and $\lambda = 53$ meters
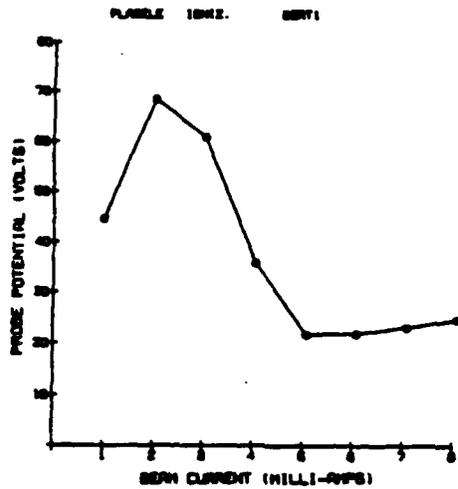
T_e = .037 eV
n_e = 1150/c.c
λ = 53 meters
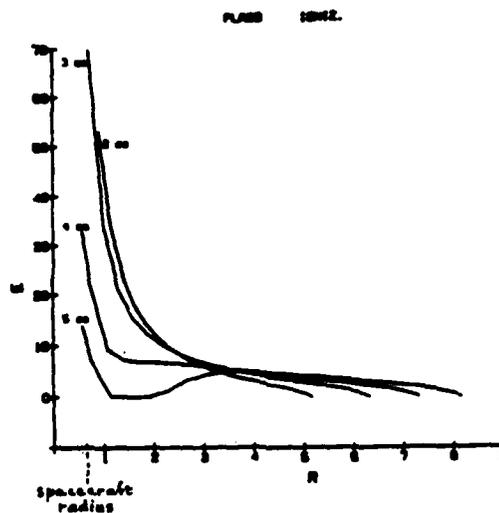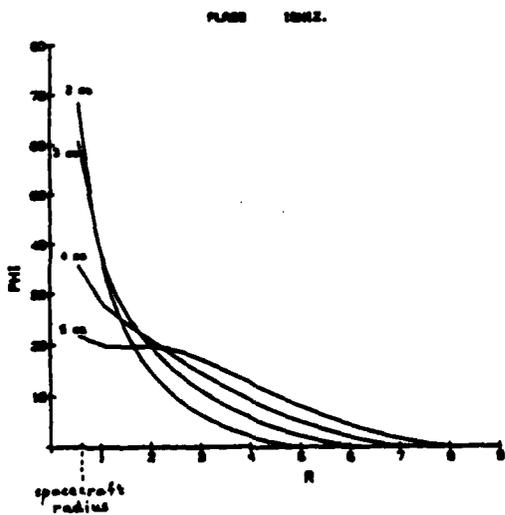
Figure 2.3   Potential and Field Profiles for a Current Sweep

61
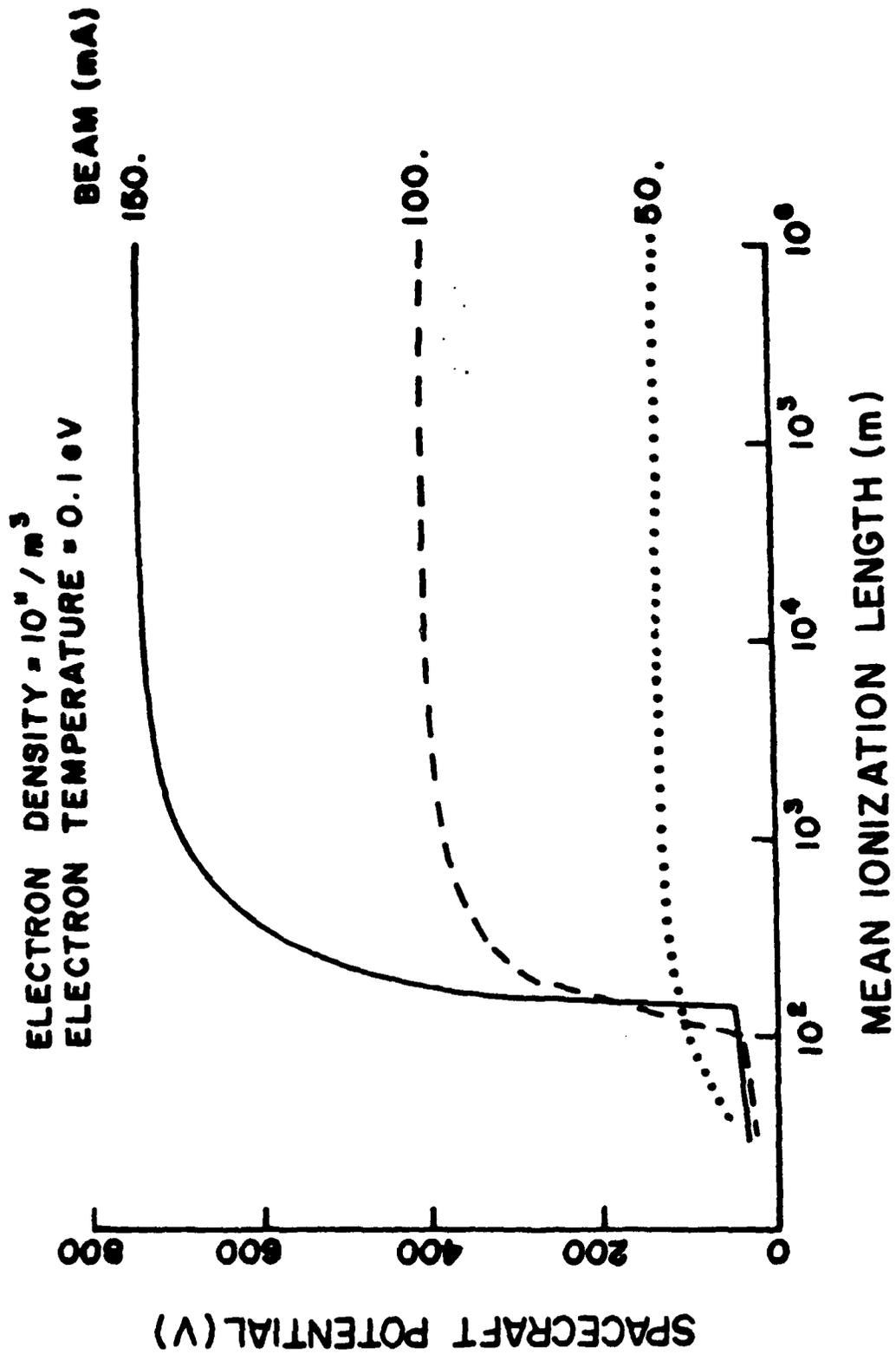
Figure 2.4 Effect of Mean Ionization Length

2.3 Extensions of the Model

The model was applied to two further systems. First, the case
of an infinitely long, cylindrically symmetric electron beam
emitter was considered. The necessity that the cylinder be
infinitely long arises from the fact that this renders the model
one-dimensional, whereas use of further dimensions introduces
problem complications which should initially be avoided.
Results from this study were quite similar to the spherical case.
This shows that the spherical nature of the probe is not essen-
tial in determining charging characteristics.

A case of more immediate interest was the ion emitter.[6] Here
we needed to include one further effect of secondary electron
emission from the probe surface by primary ion collision. We
found that, for ion guns, ionization was less important in
determining charge than for electron guns. In fact, the major
determiner was the enhancement of the return current, mostly from
secondary emission, to increase the effective beam current. The
result of this was to bring down the magnitude of probe charge,
as with electrons, but it became clear that no maximum in the I-V
curve would be encountered for ions.

An analytical model was constructed, based on the Lam solution
and including secondary emission but not sheath ionization.
It was found that this model reproduced the results of the full
model quite nicely for environments of greatest interest to
experimenters. This indicates that ionization may not be
important for typical ion gun experiments.

63

2.4 Flight Simulation

Studies have been carried out to give an indication of the predictive usefulness of the model.[2]   The goal was to duplicate as nearly as possible the environmental conditions to which an upcoming test flight, BERT-1, would be subjected. Simulations were carried out at altitudes between 100 and 250 km for the two electron gun models, spherical and cylindrical, as well as the spherical ion emitter.   The major findings were the following, assuming a maximum beam current of 20 mA:

   a) for electron guns the potential-current curve will exibit
      a local maximum for low altitudes but remain monotonic at
      higher altitudes, and

   b) for ion guns, the potential will reach the limiting value
      of the energy of the ion beam itself for all altitudes.

Figure 2.5 shows the computed results of spacecraft potential as a function of electron beam current at various altitudes.   The non-monotonic behavior of potential current curves is apparent. At low currents, the potential increases with beam current. When the current increases further, ionization occurs inside the sheath, and the potential then turns around.

In addition to the atmospheric simulation, a study was carried out for electron guns at conditions similar to those in a recent ground based test chamber.   In this case, it was shown that the peak voltage and peak current could be matched with reasonable choices of plasma density and temperature in the model.
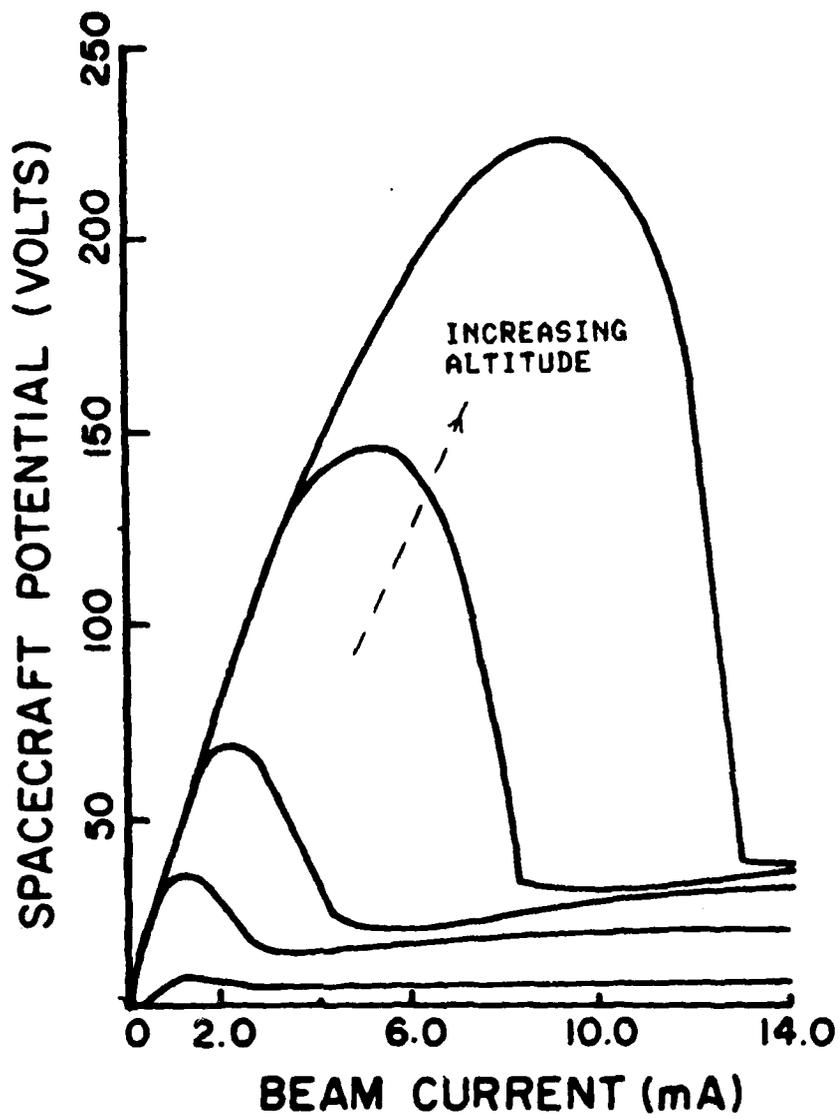
Figure 2.5 Flight Simulation Charging Characteristics

References

1. Beard, D.B. and Johnson, F.S., "Ionospheric Limitations on Attainable Satellite Potential", J. Geophys. Res. Vol. 66, pp. 4113-4122, 1961.

2. Cohen H.A., Lai S.T., McNeil W.J., Wenaas E.P., Leadon R.P., "Spacecraft Charging with Beam Emissions in an Ionizable Environment", EOS Vol. 64, No. 18, p.301, 1983.

3. Lam, S.H., Phys. Fluids 8, 73 (1965)

4. Leadon, R.E. et al, "Analytical investigation of Emitting Probes in an Ionized Plasma", AFGL-TR-81-0138, April 1981.

5. McNeil, W.J., Cohen, H.A., and Lai, S.T., "Effects of Ionization on Charging of Electron Emitting Spherical Probes" AFGL-TM #75, January 1983.

6. McNeil, W.J., Cohen, H.A., and Lai, S.T., "Effects of Ionization on Charging of Ion Emitting Spherical Probes", AFGL-TM #79, February 1983.

3.0 Particle Tracking Studies

3.1 Particle Tracking near Differentially Charged Surfaces

An important aspect of the beam emitter problem is the dynamics
of the beam particles themselves. If a differentially charged
spacecraft is placed in an environment such that little current
is drawn from the surrounding plasma and no sheath develops,
Laplace's equation holds and we can calculate the potential at
all points outside the spacecraft knowing only the charge on the
surface. Once this is known, calculation of the trajectories of
emitted charged particles will answer the question of what frac-
tion of an emitted beam will escape the probe, or return and
thereby neutralize some of the charge.

A number of investigations were conducted to calculate both the
potentials around differentially charged spacecraft and the
trajectories of emitted beams. The major results of these
studies have been the presentation of potential and particle
trajectory plots, and the determination of escape energy as a
function of beam angle for several different charging configu-
rations. Contour plots were used to aid in the presentation of
these data. The final objective of this work is to determine
the time dependence of self-neutralization in a probe which traps
some of its emitted beam. Configurations studied included
quadrupoles, circular concentric disks, and spheres with a
circular cap -- all of which were treated essentially as two-
dimensional problems.

3.1.1 Quadrupole Problem

The potential for two like charges at a distance 'd' on either side of a central charge 'f' is given by

$$\phi(x,y) = \frac{f}{(x^2 + y^2)^{\frac{1}{2}}} - \frac{1}{((x+d)^2 + y^2)^{\frac{1}{2}}} - \frac{1}{((x-d)^2 + y^2)^{\frac{1}{2}}}$$

The equations of particle motion are given by

$$\frac{d^2 x}{dt^2} = - \frac{\delta\phi}{\delta x}$$

$$\frac{d^2 y}{dt^2} = - \frac{\delta\phi}{\delta y}$$

and were solved computationally using Hamming's modified predictor-corrector method. (subroutine HPCG from the IBM Scientific Subroutine Library)

Particle trajectories were plotted using SUATEK with appropriate scaling to overlay on transparencies of the associated potential contour plots.   These contour plots were generated using routine CONREC from the NCAR graphics package.   Figure 3.1 shows a typical plot with four different trajectories for different beam energies.   Other parameters that were studied were quadrupole separation and net charge, beam polarity, and beam origination and angle.

68

Total Energy = -.56, -.06, +.44, +.94
Initial KE = 1.5, 2.0, 2.5, 3.0

QUADRUPOLE MODEL
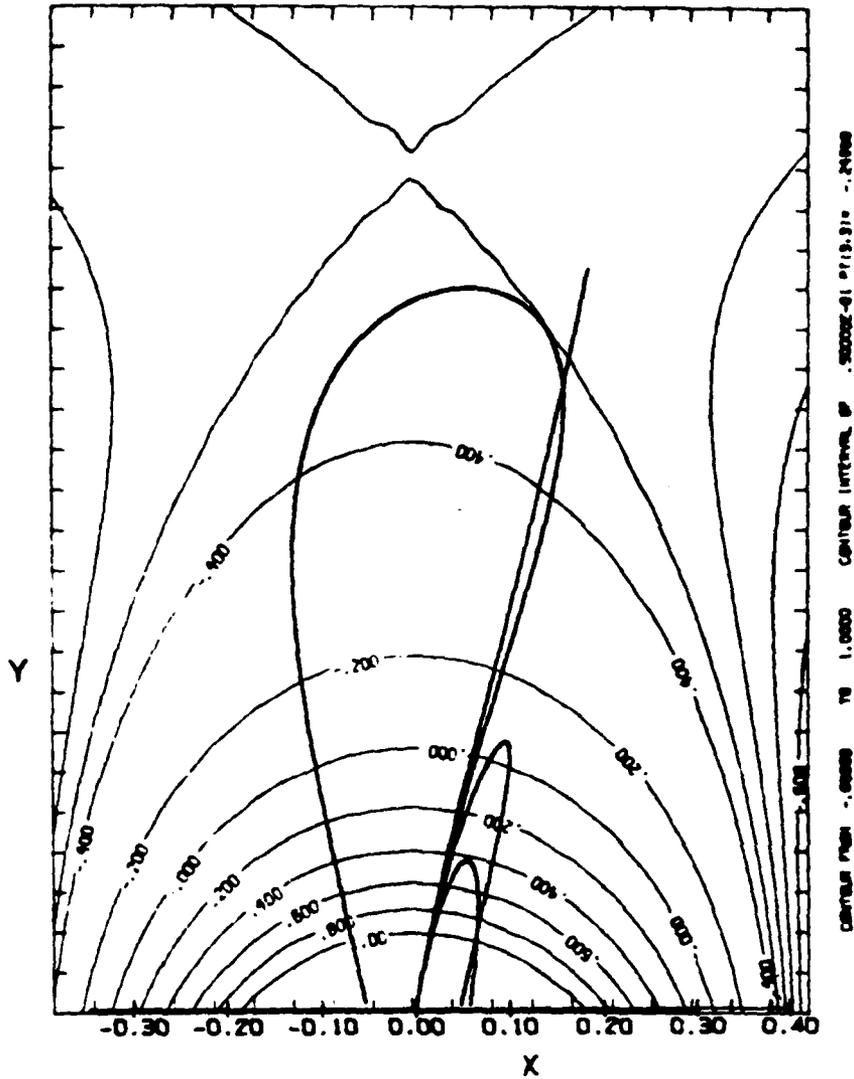
Figure 3.1   Potential Contours and Particle Trajectories
in a Quadrupole Field.

69

3.1.2 Circular Double Disk Problem

The potential for a circular double disk has been derived
analytically[1] as follows:

$$V(\rho,z) = \frac{2}{\pi}\left[\gamma \tan^{-1}\left(\sqrt{2}\left\{\rho^2+z^2-1+\left[(\rho^2+z^2-1)^2+4z^2\right]^{1/2}\right\}^{-1/2}\right)\right.$$

$$+ \frac{1-\gamma}{\sqrt{2}}\int_{\alpha}^{1}\frac{s}{(s^2-\alpha^2)^{1/2}}$$

$$\left.\times\left(\frac{z^2-s^2+\rho^2+\left[(z^2-s^2+\rho^2)^2+4z^2s^2\right]^{1/2}}{(z^2-s^2+\rho^2)^2+4z^2s^2}\right)^{1/2}ds\right]$$
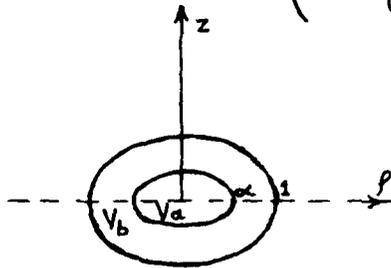
Radii $\alpha, 1$

Potentials V_a, V_b

$$\gamma = \frac{V_a}{V_b}$$

ANALYTICAL CHECKS FOR BOUNDARY CASES

$$V(0,z) = \frac{2}{\pi}\left\{\gamma\tan^{-1}\left(\frac{1}{z}\right)+(1-\gamma)\left[z/(z^2+\alpha^2)^{1/2}\right]\right.$$

$$\left.\times\tan^{-1}\left[(1-\alpha^2)^{1/2}/(z^2+\alpha^2)^{-1/2}\right]\right\}$$

and for $\rho > 1$

$$V(\rho,0) = \frac{2}{\pi}\left\{\gamma\tan^{-1}(\rho^2-1)^{-1/2}\right.$$

$$\left.+(1-\gamma)\tan^{-1}\left[(1-\alpha^2)^{1/2}(\rho^2-1)^{-1/2}\right]\right\}$$

If beam orientation is initially in a plane normal to the disk
surfaces, we can take $x = \rho$ (radius) and $y = z$ (normal to disk)
and consider the problem in rectangular coordinates.

70

The inner disk to outer disk radius ratio α, and the potential ratio γ provide parameters that are similar to the quadrupole problem. The main complexity is due to the integral which must be computed for the potential at each location ρ, z.
Figure 3.2 shows overlaid potential and trajectory plots for positively charged inner and outer disks, with 0.1 radius ratio. Ion beams with three different energies, originating at a distance of 0.2 above the disks are considered. The saddle point introduces the question of beam trapping for many of the studies described in this section.

3.1.3 Circular Cap Problem

The problem is to track particles in the vicinity of a spherical probe with a differentially charged surface.
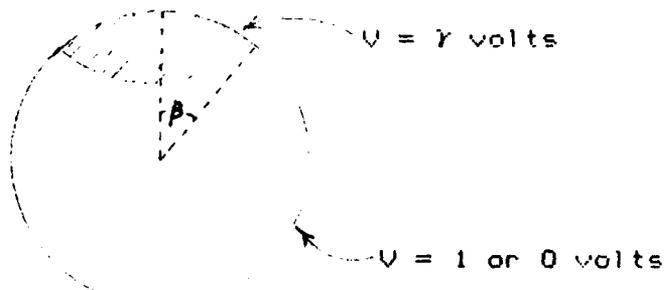
The potential is calculated by noting that the series

$$V(r,\theta) = \sum_{n=0}^{\infty} \left(\frac{a}{r}\right)^{n+1} \alpha_n \; P_n(\cos\theta) \qquad (1)$$

solves Laplace's equation, where a is the probe radius.

CIRCULAR DOUBLE DISK

CIRC. DISKION   A= .1 B=1. VA=   .1 VB= 1.0

$\gamma = +0.1$
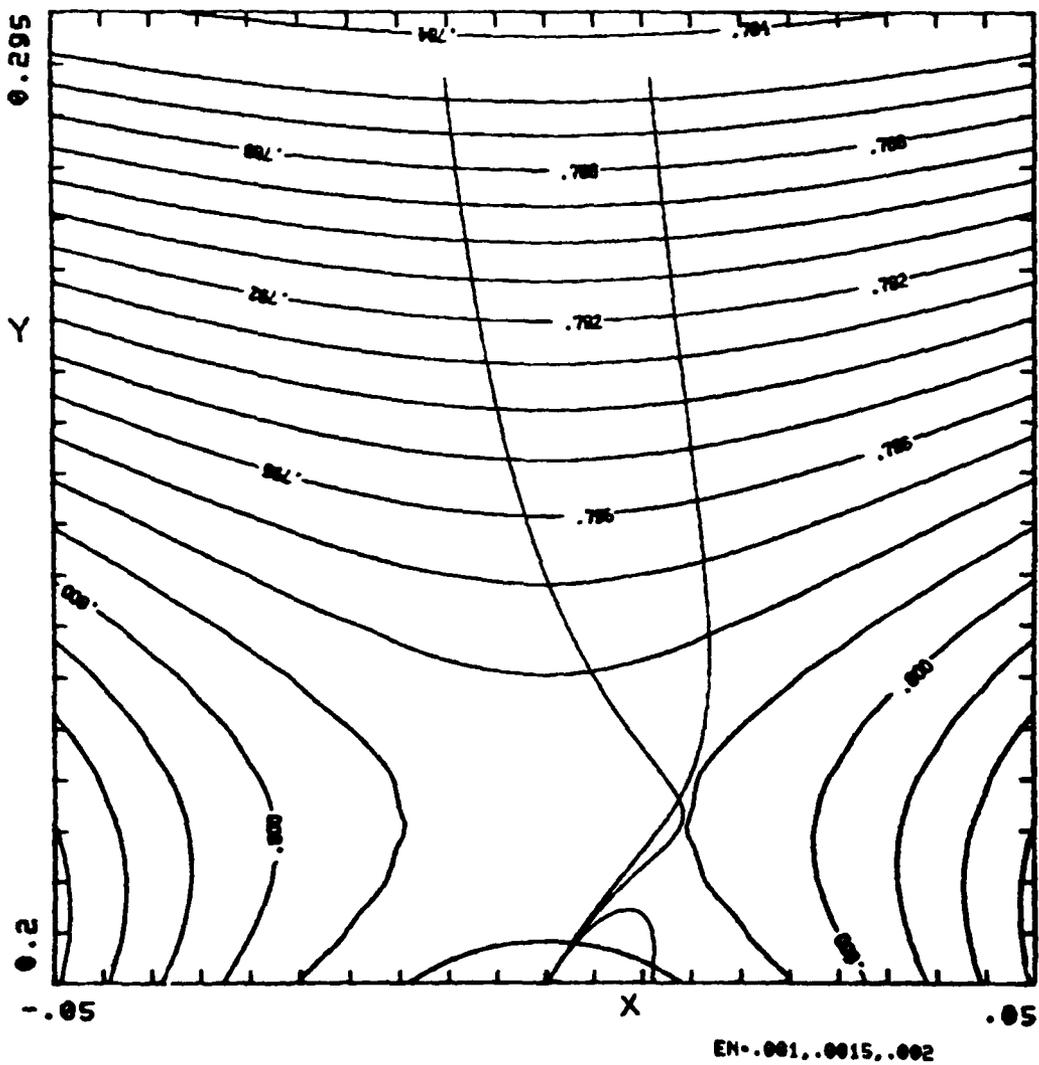
Figure 3.2   Potential Contours and Particle Trajectories
in the Field of a Circular Double Disk.

72

The coefficients are easily found since

$$V(a,\theta) = \begin{cases} \gamma & \theta < \beta \\ 1 \text{ (or } 0) & \theta > \beta \end{cases}$$

and

$$\alpha_n = (n+\tfrac{1}{2}) \int_0^\pi f(\theta) \, P_n(\cos\theta) \, d(\cos\theta)$$

by orthogonality.

Program TRKCOEF calculates these coefficients.   It is run inter-
actively and requires the following inputs:

    NTERM = # of terms in the series

    RRR = cutoff distance for "nearness" to the probe.
     (good convergence is obtained for RRR = 1.1 when NTERM=38)

    B = the angle β in degrees

    G = the charge on the cap

The integrals involved are evaluated analytically; the limit on
NTERM is around 50 due to the difficulty of calculating high
order Legendres.

Whether the charge on the lower portion of the probe is 1 or 0 is
determined by the parameter GAB in subroutine CHECK.   Program
TRKPLOT sets up a file for contour plotting.   TRKCOEF saves the
coefficients on TAPE5 and must be run (or TAPE5 saved) before
other programs are run.

73

Program TRKIONS uses HPCG to track particles from a previously
generated potential.   It allows various starting positions, on
or off the probe, and various beam energies and angles.   They
are defined as follows:
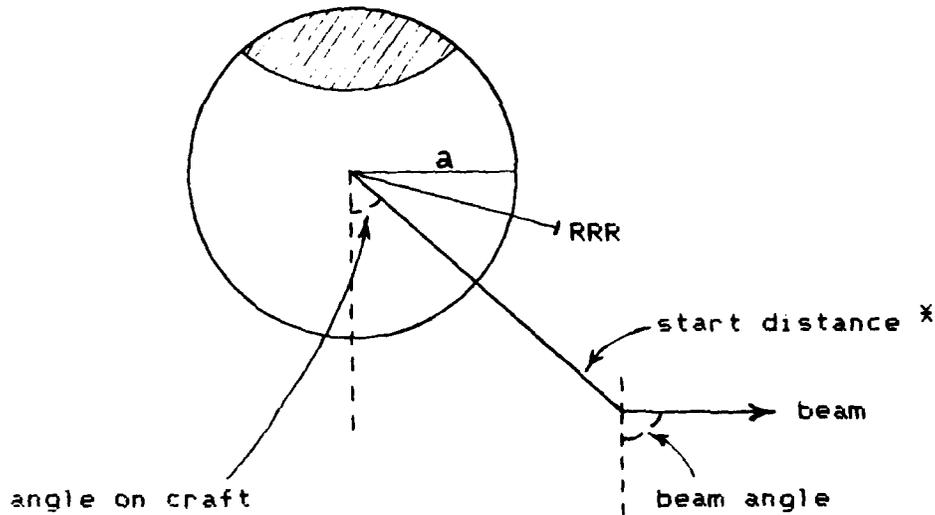
* start distance = 0 will start the particle at r = RRR.

Every 600 timesteps, the program asks whether you wish to stop.
Thus, in its present form it has to be run interactively.

The status of this problem was that the "hot spot" did not seem
to trap the beam when it is released from a point near the craft.
This means, at least, that the situation is more complicated than
was originally imagined.

3.2 Evaluation of Geomagnetic Field Models

Introduction

An important feature in the application of particle beam emitters
is the accuracy with which the beam can be delivered from the
spacecraft to the selected target. Since the beam is charged,
its trajectory is strongly influenced by the geomagnetic field it
must traverse. Thus accuracy of timing is contingent on an
accurate knowledge of the geomagnetic field itself. This study
determines directly the effect of uncertanties in the geomagnetic
field model on targeting by calculating the trajectories of beam
particles with various geofield models. Since the discrepency
within different models is expected to be at least as large as
the difference between the "best" model and the true field, the
study should provide a rough upper bound on the accuracy with
which beams can presently be targeted.

Models

The models are based upon fits of experimental data to an
expansion of spherical harmonics. The coefficients are referred
to a specific year and correction terms are sometimes provided or
subsequent years. The study was conducted for the year 1980.
In addition to yearly variation, there is also a dependence in
the field on time of day and sunspot activity. These effects
were investigated by using additional sets of coefficients,
consisting of correction terms to the reference IGRF80 set, for
0900 and 1300 hours and for noon at sunspot minimum. The models
used and the size of the coefficient sets are given in Table 3.1.

Table 3.1 Geomagnetic Field Models

Model	Order (NMAX = ORDER + 1)
1) IGRF80	10×10
2) Barraclough 80	10×10
3) Barraclough 75	12×12
4) Magsat	13×13
5) WC80	12×12
6) Sq mods (to IGRF80)	

Simulations were carried out for two particle types, two starting altitudes, three initial beam energies and three aiming directions. Thus a total of 36 trajectories were calculated for each model. Trajectories were followed through one gyro rotation and stopped 20 km below the starting altitude. The IGRF80 trajectory was used as the target definition, and deviation of other trajectories from this one was calculated as the nearest approach of a target and test trajectory, without regard to correlation in time.

Procedure

In order to add a set of coefficients to the existing system of programs, the following sequence of runs is carried out:

1) The program CNGMAG is used to convert the Gauss normalized coefficients to Schmidt normalized form and to correct the coefficients to the desired epoch. The correction terms are input along with the coefficients and currently extend to second order in time. The program creates a data block containing the renormalized coefficents to be injected into subroutine NEWMG10 of the trajectory generating program.

2) The simulator[2] was provided by D. Smart (AFGL) and was transferred to a program library called TJPL. There are several copies therein of the field generating subroutine NEWMG10. The highest order spherical harmonic to date is N=14. If a higher order is desired, the program CDNMAG will write a new NEWMG10 subroutine. Some problems in the format statements of CDNMAG, causing intermediate zeros in constants to be eliminated, have been encountered and care should be exercised in any future use. If the dimension of the new coefficient set is 14 or less, one of the existing NEWMG10's in TJPL can be used directly.

3) The data statements written by CNGMAG are injected into NEWMG10 and the program library is updated.

4) The simulation is carried out for a given starting configuration and field model using TJPL. Figure 3.3 shows a typical trajectory for a few gyro rotations.

5) Results from this and previous IGRF80 calculations are compared using program TJCALC, which finds the minimum distance discrepency between test and reference trajectory.

Results

The longest distances travelled occurred for high energy lithium ions at high altitude and were on the order of 700 km. The shortest were for low energy protons at low altitude and were around 15 km. The miss distances from the IGRF 80 trajectory, as a percent of total distance travelled, were 0.08% for WC 80 and 0.01% for MGST 4181 at high altitudes, and 0.14% for WC 80 and 0.025% for MGST 4181 at low altitude. The daily solar corrections added to the IGRF 80 model gave target deviations on the same order of magnitude.

77
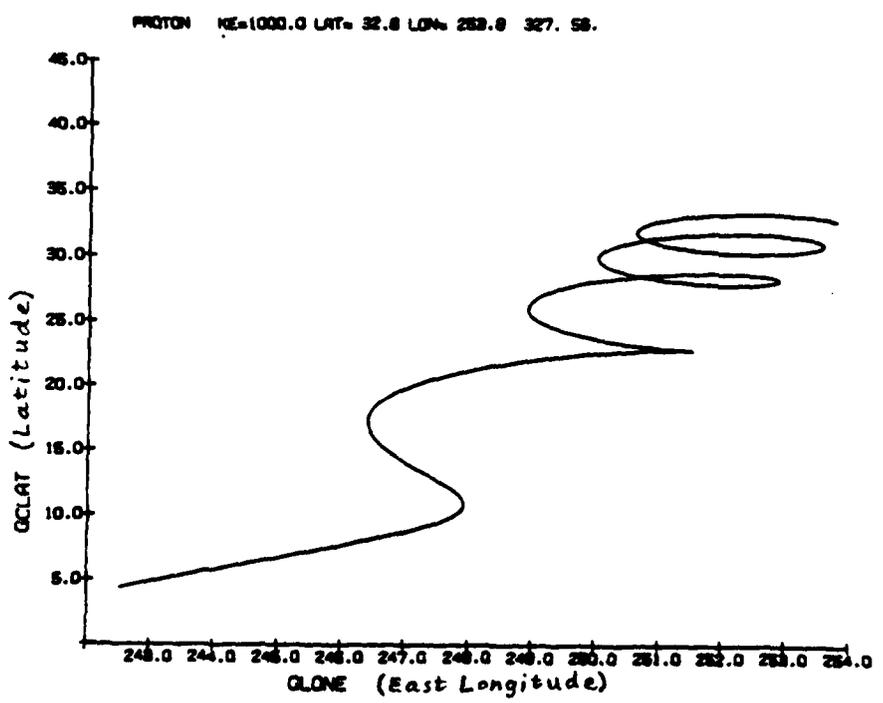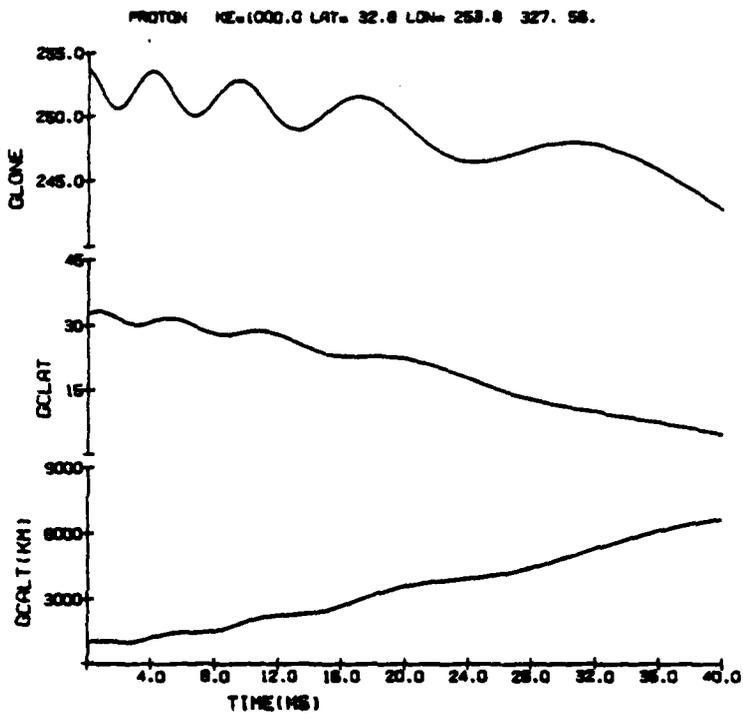
Figure 3.3 Particle Beam Trajectory in the Geomagnetic Field

References

1. Sherman, C. and Parker, L.W., "Potential Due to a Circular Double Disk", J.A.P. Feb. 1971, Vol. 42, No. 2.

2. McCracken, K.G., Rao, U.R., and Shea, M.A., "Trajectories of Cosmic Rays in a High Degree Simulation of the Geomagnetic Field", MIT TR No. 77 (NYO-2670), August 1962.

4.0 Atmospheric Density and Winds from Accelerometer Data

Triaxial accelerometers capable of measuring accelerations in
the tenths of micro-g's are released in rocket launched spinning
spheres.   Once the sensor system is not subject to the large
propulsive forces, the sensitive devices are uncaged and, being
in continuous free fall in the earth's gravitational field, are
able to detect the remaining forces acting on the sensors.
These forces are primarily due to the drag of the sphere in the
earth's atmosphere, but may include centrifugal forces arising
out of module spin and precession.   Since the objective of these
experiments is the study of atmospheric structure in the lower
thermosphere, eccentric forces are an undesirable contaminant,
and are eliminated by design by locating the sensors close to the
dynamic center of the spinning spheres.   Any residual imbalanced
signals are attenuated by special notch filters when the expected
contaminant frequencies are known e.g. spin frequency for spin
axis Z-sensors.   Other undesirable modulation signals must be
totally removed by computational filtering prior to any detailed
processing for analyses of atmospheric density and wind
structure.

In the case of the rocket launched experiments, the sensor unit
resides within a sphere that is released after launch, and
includes the telemetry for transmitting the sensor signals.   The
trajectory is geographically "local", and analyses have been
performed in launcher referenced coordinates in which the spin
axis orientation stays inertially fixed.   Earth curvature must
be accounted for when equating upleg and downleg densities and
wind vectors, and can be accomplished by using actual trajectory
altitudes at all times.   Figure 4.1 shows the coordinate systems
which are appropriate for rocket sphere studies.   The X" system

80

is in the spinning sphere reference frame, with Z" the spin axis
direction.   The X' and X systems are non-spinning and embedded
in the trajectory plane, with Z'(=Z") coincident with the sphere
axis, tilted forward at angle α relative to launcher vertical Z.

Figure 4.1   Coordinate Systems for the Rocket Sphere

Important functions that the data processing system performs are:

1) Telemetry data compaction and splicing

2) Sensor calibrations

3) Signal demodulation and conditioning

4) Trajectory evaluation and integration

5) Maintenance of an evolving Resource File

6) Resolution of sensor orientation and transverse and
in-track winds

81

7) Resolution of consistent density and temperature profiles

8) Tables and graphical presentations in interactive or batch mode

9) Comparison with other concurrent experiments

10) Evaluation of reliability of results

11) Studies of auxiliary associated phenomena

A schematic of the program flow and intermediate files is shown in Figure 4.2, starting from the DECOMM tape and calibration and trajectory data. In addition to the final density and wind profiles in file SPIR, tables, plots and supporting analyses are end products. The scope of each functional area is now discussed. The AC13 sphere experiment at Esrange on Dec.1, 1980 serves as the prototype for the sample results in this report.

4.1 Telemetry Data Compaction and Splicing

The 12-bit PCM coded sensor signals are available over the duration of the flight, after sphere release. It is advantageous if the complete data are available on-line during the initial splicing, calibration, and sensitivity and phase adjustment studies. PACKER routines available in the SUNY program library allow all the data for four X and Y channels, plus three Z and a Nutation channel over the 300+ second span of the experiment to be resident on about 2000 PRU's of perm file. The DECOMM tape is checked for sync losses, and the packed file is augmented from alternate telemetry channels for any missing data. Time track errors of nearly 1 second between channels from different radars have been identified during the splicing process; thus such procedures have enhanced quality control over the data base. Once sensor calibrations and signal demodulation results are completed and saved on reduced files. this large packed file need not be resident on permanent file.

82
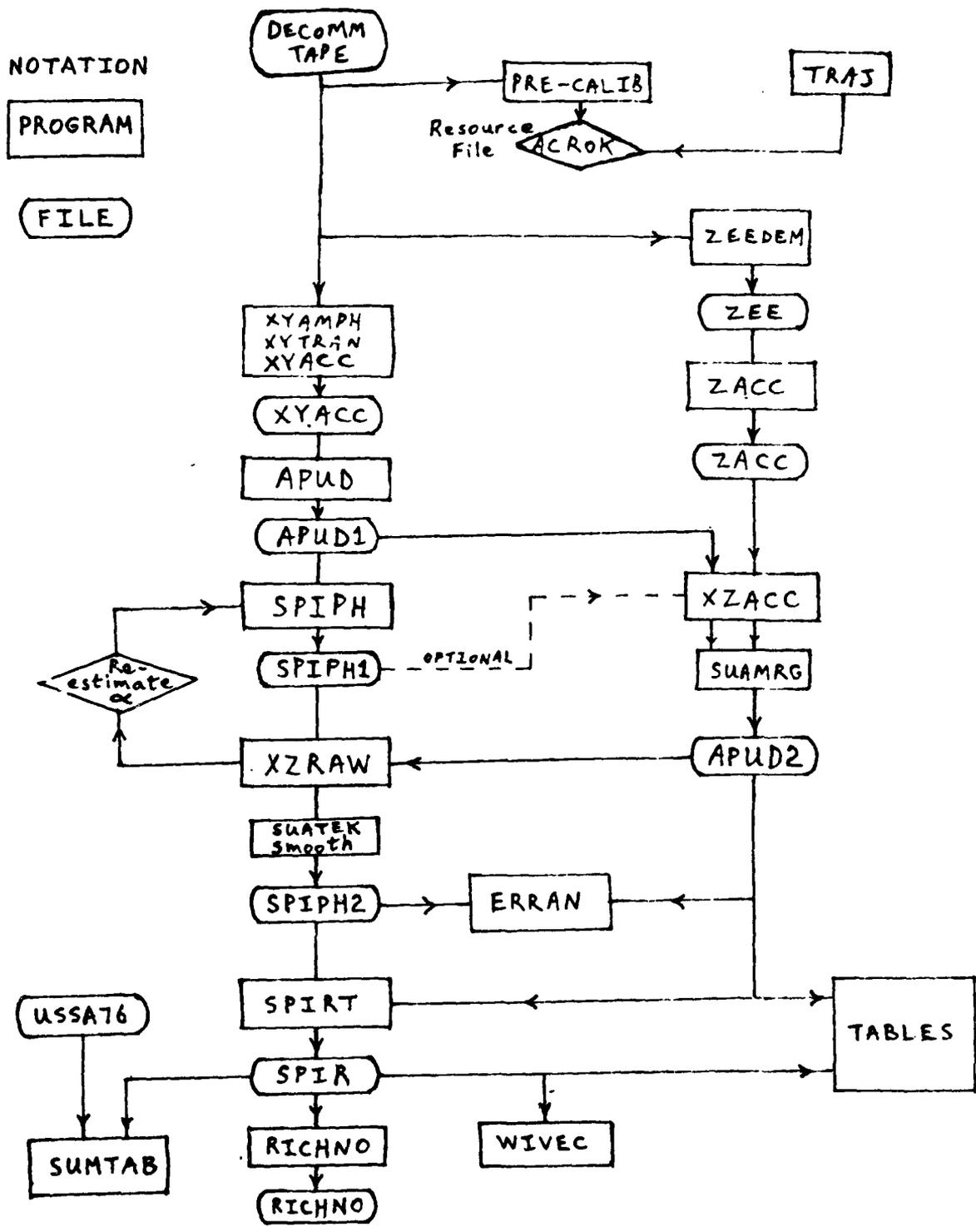
Figure 4.2   Schematic of the Rocket Sphere Processing System

83

4.2 Sensor Calibrations

Uncaging of the sensors after sphere release initiates a damped
resonant response in all the accelerometer bimorphs.   These
resonant frequencies are invaluable in fixing the calibrations,
because the vibrations are produced within the centrifugal force
field being experienced by the sensors, and the resultant
stiffness and sensitivity calibration estimates improve on the
values obtained during lab tests.   Correction factors are
applied by the researcher, based on the ratio of in-flight and
ground based resonant frequencies.   Optimized function fitting
techniques are used to converge on a best fit solution for each
damped oscillation frequency.   The Z-axis cases, where the
resonance is superposed on the precession modulated signal, have
also been implemented and solved using the appropriate extended
expressions.   A different type of procedure is necessary to
determine a calibration correction that accounts for the
attenuated slow time constant response of the Z-sensors as the
sphere experiences exponentially higher densities on re-entry.
Z-signal time constants are determined from log plots, and are
applied to lab tests that were performed using various
exponential driving functions.   A pre-calibration package of
results and supporting plots have been provided for each sphere
flight.

4.3 Trajectory Evaluation and Integration

In general the trajectory velocity is the greatest contributor to
the drag forces experienced by the sphere.   Since drag is given
by $\frac{1}{2} \, \rho \, C_d \, \frac{Area}{2m} \, V_R^2$ where V_R is the velocity of the sphere
relative to the atmosphere, it can be seen that inaccuracies in

V_R are amplified. A simplified sphere trajectory calculating routine was installed, a) to create good quality quick look trajectory velocities before refined results become available, and b) to evaluate initial trajectories provided by the range. Launcher referenced trajectory velocity components are formatted and entered at 2 to 5 second intervals in the experiment Resource File. Velocities at any time or altitude upleg or downleg are obtained by cubic interpolation.

4.4 Evolving Resource and Profile Files

In addition to trajectory information, the concept of the Resource File is to collect all initial parameters and intermediate results that are required for processing of subsequent stages of the analysis. Thus, sphere mass, cross-section area, original sensor calibrations, etc. are initially entered. The nominal spin rate is established early and is entered manually. Calibration adjustments to give continuity and consistency are determined later, and are then entered and called by subsequent programs. Figure 4.3 shows a sample segment of the Resource File for the AC13 flight. This presentation provides the investigator and the program user with an up-to-date status of the investigation for each experiment. Profile wind, density, and related solutions per altitude step form a much larger data base, and are not stored on the Resource File, but on successively augmented binary files for ready processing and plotting. Since many rocket sphere flights continue to be studied through improved multi-stages of processing which generate intermediate profiles, a logistics control procedure must be maintained. Figure 4.4 shows a recent chart which, using established input from the Resource File, permits any of the program modules to be rerun with minimum effort.

```
AC13
      12/01/80          540.00 SEC.       ESRANGE
SMASS,SAREA  (KG, M**2)
10.262, 0.05199
ALAT,FLAZ (LATITUDE, FLIGHT AZIM.)
68., -10.5
FRATE       (FRAME RATE PER SEC.)
.008
CALV        (CALIB. VOLTS PER COUNT)
.009775
RPS         (SPIN RATE, OFFSET, DRIFT   REVS. PER SEC.)
5.93340, -.0008, .20E-4
ALPHA,BETA  (AXIS TILTS  DEG.)
14., 0.
MXY         (1=USE X-SENSOR  2=USE Y-SENSOR)
2
TXY         (3-2, 2-1, 1-2, 2-3, 3-4  CROSS-OVER TIMES   X AND Y)
82.,94.,285.,312.,331.5, 80.,93.5,286.,313.5,333.5
CALXY       (ORIG. CAL.  M/S**2 PER VOLT FOR X1,X2,X3,X4,  Y1,Y2,Y3,Y4)
6.8375E-6,1.8071E-4,4.7216E-3,.1451
9.233E-6,2.489E-4,6.4410E-3,.1926
CRXY        (EST. SENS. RATIOS  X1/X2/X3/X4/Y4, Y1/Y2/Y3/Y4/Y4)
26.45,25.90,31.16,1.23, 30.25,24.75,29.92,1.00
CPXY        (EST. PHASE DIFFS  X1-X2-X3-X4-X4, Y1-Y2-Y3-Y4-X4)
-7.,45.,-56.,0.0, -3.,42.2,-60.5,-88.2
PHC         (PHASE BIAS  X-SENSOR  AND  Y-SENSOR)
270.,270.
PHS         (PHASE ADJUSTMENTS  X1,X2,X3,X4,  Y1,Y2,Y3,Y4)
18.,11.,56.,0., -66.8,-69.8,-27.5,-88.
CPH         (LOW ALT. SPIN-DOWN PHASE ADJ. = B*(A-ALT)**2)
85., .045
CAL         (REV. CAL.  M/S**2 PER VOLT FOR X1,X2,X3,X4,  Y1,Y2,Y3,Y4)
7.190E-6,1.902E-4,4.926E-3,.1535
8.425E-6,2.550E-4,6.3100E-3,.1888
PREF        (PRECESSION FREQUENCY)
.7248
TTST        (START TIMES FOR  Z1,Z2,Z3,NUT  SENSORS)
300.,310.,325.,340.
TTND        (END TIMES FOR  Z1,Z2,Z3,NUT  SENSORS)
322.,335.,350.,359.9
TRANS       (Z1-Z2, Z2-Z3, Z3-NUT  TRANSITION TIMES)
318.,322.,331.,335.,350.,350.
TCROSS      (Z1, Z2, Z3, NUT  CROSS-OVER TIMES)
320.,333.,350.,350.
BG          (BIAS-COUNTS  AND  GAIN-M/S**2/VOLT  FOR Z1,Z2,Z3,NUT)
510.,5.942E-3, 510.71,.05808, 510.36,.7012, 512.,0.
BIAS        (REV. BIAS COUNTS)
510.,510.41,510.22,512.
ZCAL        (REV. CALS.  M/S**2/VOLT  FOR Z1,Z2,Z3,NUT)
5.838E-3,5.721E-2,.6996,0.
ZTST,ZTND (START,END OF Z-NUT-SENSOR PROCESSING)
300., 345.
BOT,HND     (BOTTOM ALT. FOR XYUP,  END ALT. FOR PROCESSING)
85., 55.
ENDROK     ********************    END OF ROCKET RECORD
```

Figure 4.3 Evolving Resource File (sample segment)

PROCEDURE	PROGRAM	FILES	
		INPUT	OUTPUT
DEMODULATE Z-SENSOR SIGNALS USING KNOWN PRECESSION FREQ. TO GIVE COUNTS/SENSOR	ZEEDEM	AC??TAP	ZEEDEM
DETERMINE OPTIMUM BIAS AND GAIN RATIOS BETWEEN Z-NUT CHANNELS, USING Z2 BIAS ESTIMATE FROM INSPECTION OF PLOTS. ADJUST Z-CALS LEAVING Z2*Z3*Z4 PRODUCT UNCHANGED. APPLY Z-CALS AND BIASES TO CREATE ZACC FILE FROM ZEEDEM COUNTS	ZACC	ZEEDEM	ZACC
ESTABLISH REVISED CALS AND PHASE ADJUST TO GIVE CONTINUITY OF XYACC AND PHASE BETWEEN X-SENSORS, Y-SENSORS, AND X-Y	XYAMPH FOLLOWED BY XYTRAN	AC??TAP AC??TAP	NONE XYTRAN
COMPLETE XYACC RUN USING FINAL GAIN AND PHASE CALS WITH ZERO PHASE ADJUST	XYACC	AC??TAP	XYACC
SMOOTHING AND 1/4 KM. INTERVAL DATA GENERATION FROM FULL XYACC FILE. THIS IS THE ZERO PHASE ADJUST FILE	XYAPUD	XYACC	APUD1
INTERACTIVE SOLUTION FOR RPS, PHC, BETA, ALPHA, SPIND, SALT, DELRPS TO MATCH UPLEG-DOWNLEG CROSSWINDS (UPDATE SPIPH1 AFTER FIXING ALPHA USING XZACC, XZRAW, AND ERRAN)	SPIPH	APUD1	SPIPH1
GENERATE 1/4 KM. INTERVAL XZACC FILE FROM ORIGINAL ZACC FILE, USING APUD1 AND OPTIONAL SPIPH1 FILE	XZACC	ZACC APUD1 (SPIPH1)	XZACC
USE SUAMRG TO MERGE XZACC FILE WITH APUD1 FILE GIVING COMMON DATA FILE	SUAMRG	XZACC	APUD2
USE OVERLAPPING XY AND Z DATA TO SOLVE FOR FURTHER DOWNLEG WIND PROFILE, AND TO RE-ESTIMATE ALPHA	XZRAW	SPIPH1 APUD2	XZRAW
SMOOTH UP-DOWN PHASE AND DOWNLEG WIND SOLUTIONS BEFORE DENSITY-TEMPERATURE CALCULATIONS, AND FOR FINAL PLOTS	SUATEK	XZRAW	SPIPH2
ERROR ESTIMATION PROGRAM MAY BE RUN HERE TO OBTAIN SENSITIVITY ESTIMATES FOR EFFECTS OF CALS, TRAJ VELS, ALPHA, AND PHASE ON RHOCD, VXW, VYW	ERRAN	SPIPH2 APUD2	NONE
ITERATIVE RUN TO SIMULTANEOUSLY SOLVE FOR RHO, TEMP, CD CREATING THE FINAL SOLUTION FILE FOR DENSITY, TEMPERATURE, AND WINDS (N-S AND E-W USING FLT.AZ.)	SPIRT	SPIPH2 APUD2	SPIR
DETERMINE RICHARDSON NUMBER VS. ALT. (TURBULENCE)	RICHNO	SPIR	RICHNO
WIND VECTOR PROFILE PRESENTATION	WIVEC	SPIR	WIVEC

Figure 4.4 Processing System for Density, Temperature, Winds
(programs to calibrate, plot, tabulate not shown)

87

4.5 Signal Demodulation and Conditioning

The equatorial plane (X-Y) sensors are spin frequency modulated,
with the amplitude of the signal a direct measure of the lateral
drag forces experienced by the sphere.   Sine wave function
fitting is employed to determine the modulating lateral force
amplitude and phase.   Calibration sensitivities between sensor
channels usually turn out to be somewhat inconsistent, so that
sensed acceleration values between, say, X3 and X4, exhibit a
jump discontinuity.   A program package was developed to adjust
all initial calibration sensivities so that the net percent
change for all sensors is minimized, while imposing continuity
in the transition regions, and overlap between X and Y sensors.
Care is needed in this trimming operation, to avoid interpreting
transition discontinuities as density profile features.

The Z-axis sensors are not sensitive to the sphere spin, but the
signals are modulated at the precession frequency, which here
must be rejected and not demodulated.   The resulting signal for
each channel starts from near zero and builds up exponentially,
with the channel gains set to overlap while providing maximum
dynamic range, as for the X-Y sensors above.   Gain optimization
is again employed for continuity, but special attention is
required to estimate and subtract a built-in non-zero bias.
Figure 4.5 is a composite plot of the final clean accelerations
sensed by the Z-sensor downleg, and the X-Y sensors upleg and
downleg.   For the X-Y sensors in particular, the high frequency
spin modulated acceleration signal ($\approx$ 6Hz) results in excellent
bias free data.   Demodulation is performed at $\frac{1}{2}$ spin cycle, or
at less than 0.1 sec steps.   At the lower altitudes where the
sphere fall velocity exceeds 1 km/sec, this still allows solu-
tions about 100 m apart.   Analyses to date have been conducted
conservatively at 1/4 km intervals, but this extension to higher
resolution can be readily implemented, for more detailed studies
of atmospheric wave and structure patterns.

88
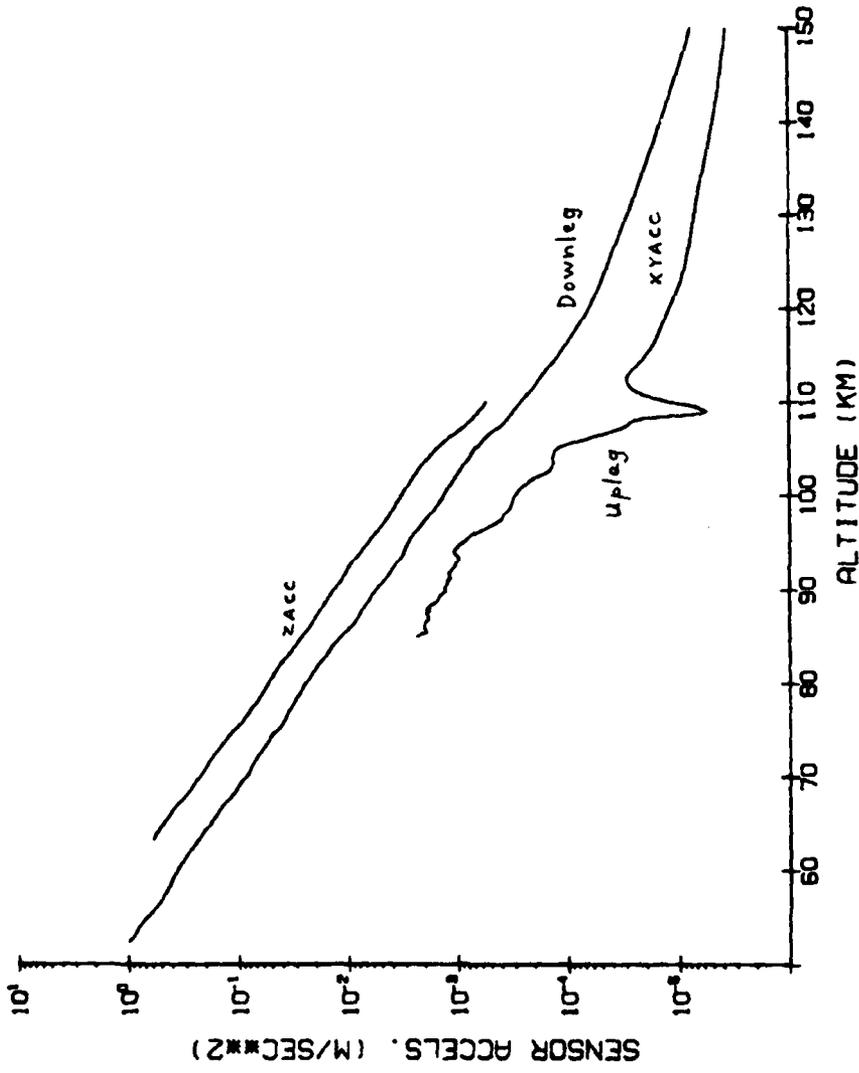
Figure 4.5 Z-sensor and XY-sensor Accelerations

4.6 Sensor Orientation and Winds

Use of a nominal sphere spin rate results in a stable solution
for acceleration as a function of altitude.   The phase or
apparent direction of the acceleration force on the spinning
sphere is, however, extremely sensitive to any offset between
true and nominal spin rate.   The difference is evident as a
runaway condition where the apparent peak of the acceleration
does not remain locked in the general direction of the trajec-
tory.   An effective procedure has been devised to optimize for
true spin rate and reference phase, so as to result in transverse
wind velocity solutions that are as close as possible on upleg
and downleg.   The transverse wind is given by

$$V_{yw} = \frac{1}{R(h)} \text{ EACC } \sin\theta \qquad (4.1)$$

where

$$R(h) = V_R \, \rho \, C_d \, \frac{Area}{2m} \qquad (4.2)$$

EACC is the X-Y or equatorial sensed acceleration,

θ is the phase to be optimized,

V_R is roughly the trajectory velocity, and

ρ approximates the true density profile after a few iterations.

The phase θ obtained originally using the nominal spin rate
becomes modified according to

$$\theta' = \theta - \epsilon T + \phi \qquad (4.3)$$

where ϵ is the spin rate vernier offset, T is trajectory time, ϕ
is the reference phase adjustment, and θ' is the corrected phase.

Upleg and downleg transverse wind sensitivities

$$\frac{\delta V_{yw}}{\delta \epsilon} \quad \text{and} \quad \frac{\delta V_{yw}}{\delta \phi}$$

are then used to adjust ϵ and θ for closest upleg-downleg match.

Low altitude spin down is also estimated in this manner by
optimizing an altitude dependent polynomial, and in fact
introduces the possibility of investigating spin deceleration
models.   A significant achievement was the identification and
quantification of an internal damping spin deceleration for AC13,
showing up as a parabolic phase deviation.

Figure 4.6 shows the development steps at this stage.   Figure
4.6(a) shows typical upleg-downleg phase solutions for a good
fixed nominal spin rate.   Figure 4.6(b) shows the final revised
spin-phase after the optimization process, which gives the
crosswind match of Figure 4.6(c).

A crucial part of the atmospheric profile analysis is the
determination of the forward tilt α of the sphere axis in the
trajectory plane.   The basic sensed acceleration equations in
the non-rotating coordinate system of the sphere fixed in the
trajectory plane are

$$XYZ_{acc} = [\vec{V}_t + \vec{V}_w] \; \vec{B}(\beta) \; \vec{A}(\alpha) \; [V_R \; P \; C_d \; \frac{Area}{2m}] \qquad (4.4)$$

where subscripts t and w refer to the trajectory and wind
respectively, $A(\alpha)$, $B(\beta)$ are spherical coordinate transformations
corresponding to sphere axis tilt in-, across- the trajectory
plane.

The cross tilt β is almost indistinguishable from a small
difference in spin rate, in its effect on the sensed accel-
erations.   When sun sensors are installed on daytime flights,
this parameter can be further studied along with spin-down.
The procedure for establishing α consists of assuming low winds
in the 60-80 km region where X-Y as well as Z sensor accelera-
tions are available, and then applying Eq. 4.4.   Once α is
fixed, the above equation is also applied as follows:

91

a) Phase obtained using fixed spin rate. With spin orientation not established, upleg-downleg wind solutions differ.
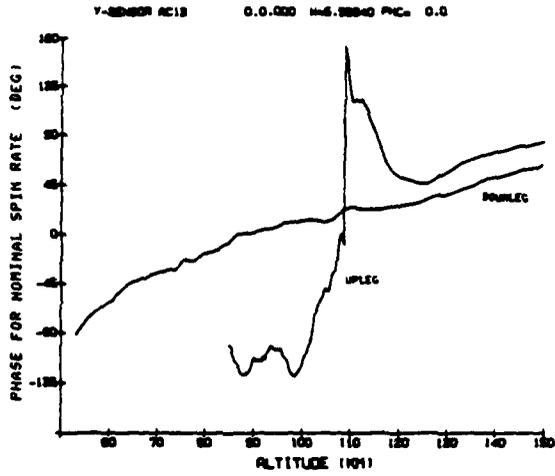
b) Phase obtained with spin rate, damping and drag spin-down, and reference phase optimized for closest cross-wind match.
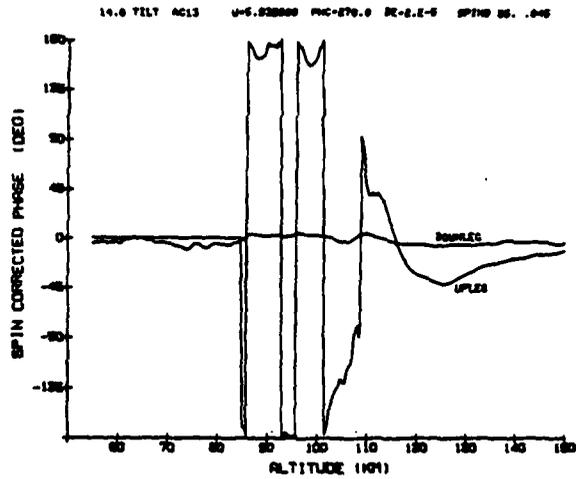
c) Upleg & downleg cross-winds obtained from phase optimization of (b) above. Downleg values below 85 km. were set to approach Robin sphere test results.
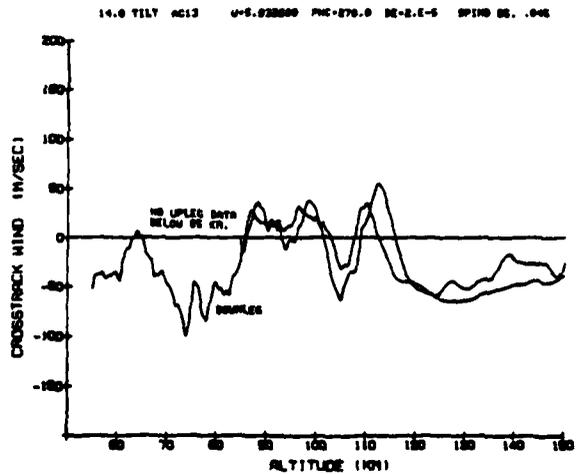
Figure 4.6   Determination of Spin Phase and Crosstrack Wind (AC13)

92

a) In the region above 80 km, in-track winds and density are
   solved simultaneously using upleg-downleg X-Y data.

b) In the 80 km and lower region, in-track winds are solved
   using downleg X and Z data for the fixed α, and then with
   winds known, density is solved using downleg X data alone.

Figure 4.7 shows the final estimated in-track wind profile.
Problems of reliability of Z-sensor calibration and filter time
response, and therefore uncertainty in the 80 km transition
region have been encountered.   Overlapping upleg X-Y and downleg
Z data are usually available in the 80-100 km region, but
unfortunately the Z data are least reliable here.   Improved
recovery of the true Z-accelerations should be feasible by a
procedure that inverts the sensor response transfer function.

4.7   Resolution of Density-Temperature Profiles

Equation 4.4 shows that once trajectory, wind velocity vectors,
and the sphere orientation are known, PC_d is also solved
simultaneously and forms the next stage irreducible data base.
C_d is a function of Reynolds number(R_e) and Mach number(M), which
in turn depend on temperature and the density profile.   Given
PC_d and V_R profiles, this interrelationship necessitates an
iterative solution procedure as shown in Figure 4.8.

The temperature profile T_m is obtained by integrating along the
density profile under the assumptions of the ideal gas law and
hydrostatic equilibrium.   The drag coefficient C_d is obtained
using Whitfield's model for low R_e,[6] and provides smooth
transition between the free molecular flow and the continuum
regions.[1]   Figure 4.9 profiles the density ratio to the US
Standard Atmosphere (1976), and the associated temperature, that
was obtained for AC13.

93
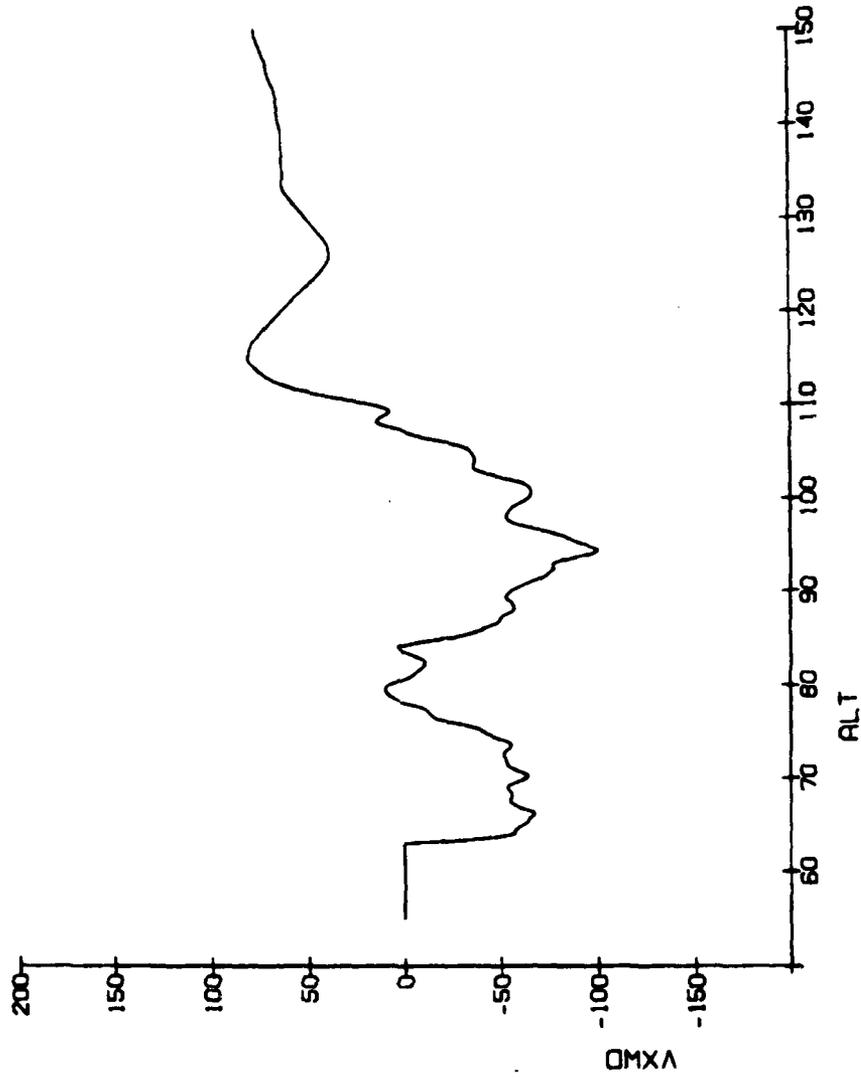
Figure 4.7 Composite Estimate for In-track Wind Profile
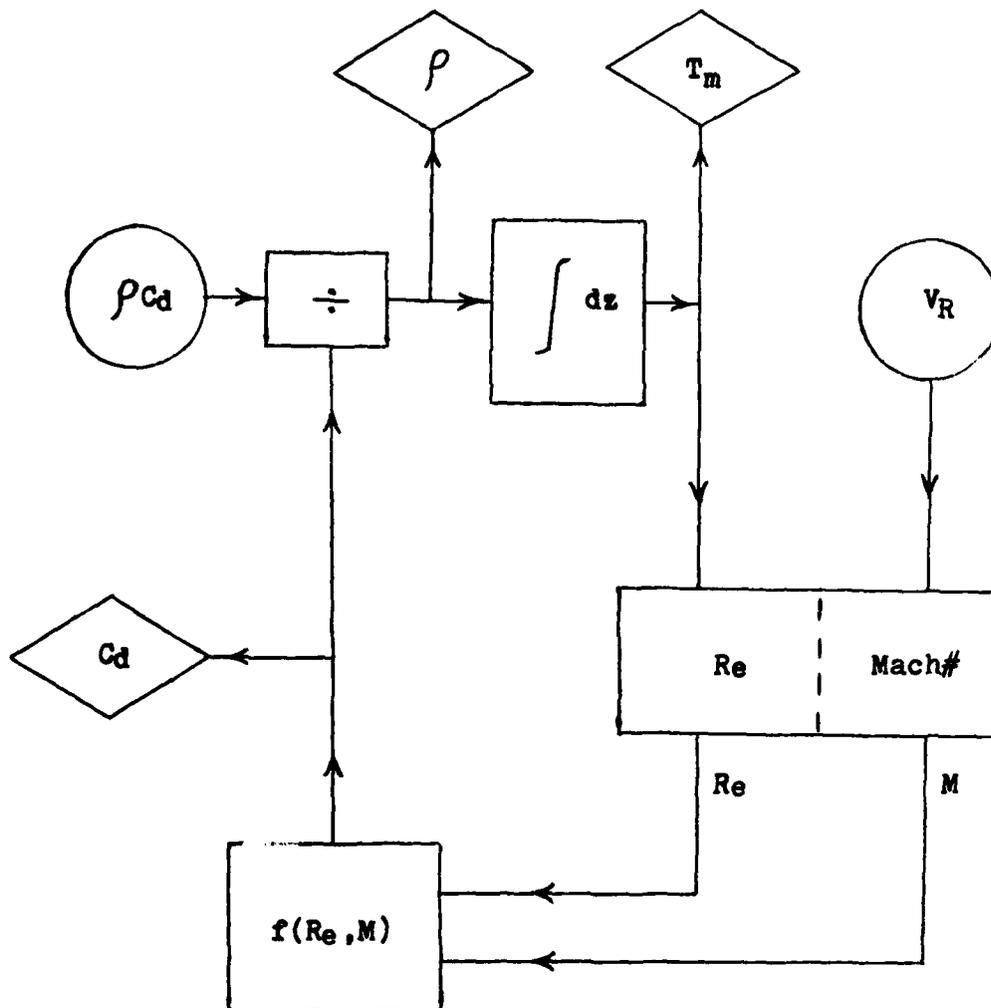
Figure 4.8   Density-Temperature Profiles from ρC_d and V_R
(the nonlinear dependence of C_d on these parameters
necessitates an iterative solution procedure)
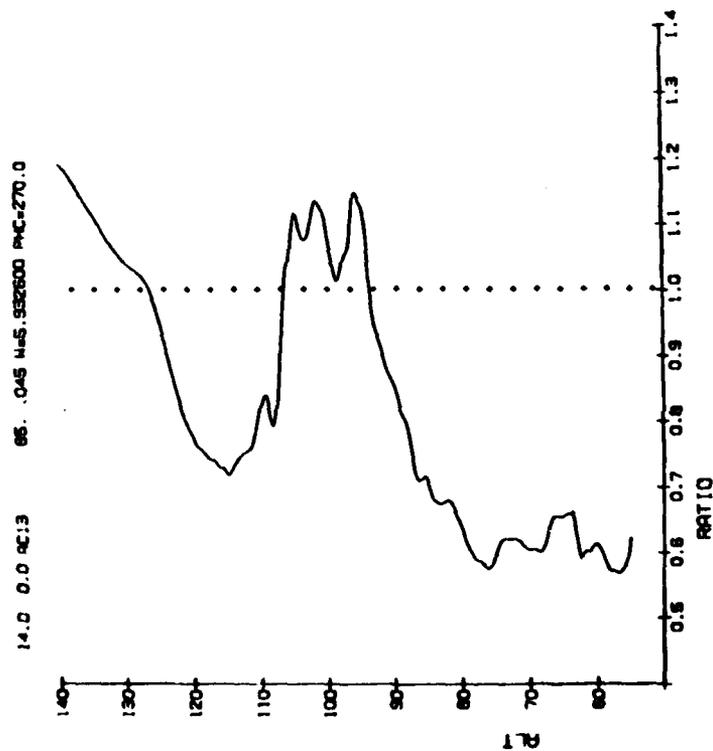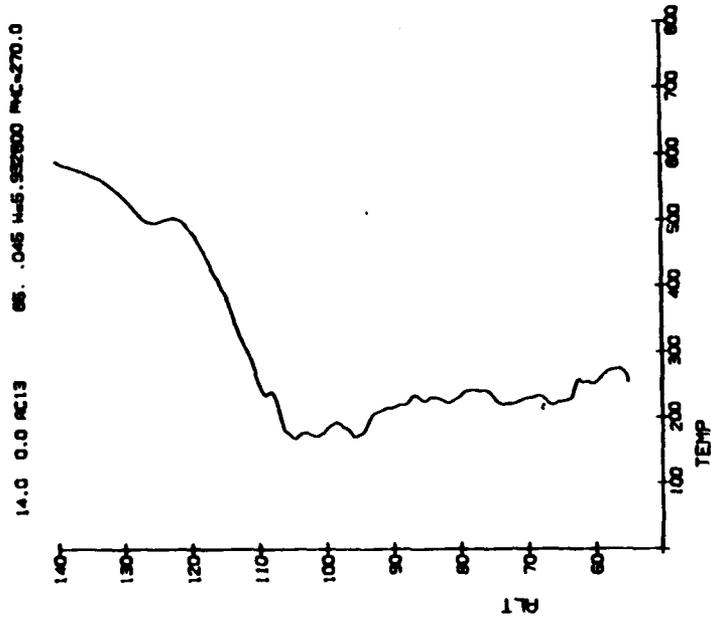
Figure 4.9 Solved Density Ratio (to USSA76), and Temperature Profiles (AC13)
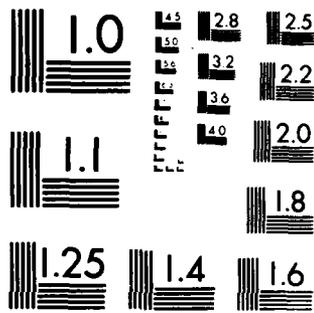
MICROCOPY RESOLUTION TEST CHART

NATIONAL BUREAU OF STANDARDS-1963-A

4.8 Tabular and Graphical Presentations

The processing system propagates augmented profile solution
results in SUATEK binary format, and tabulations of desired
results are accomplished by simple print-out programs. The
Tektronix plotting capability inherent with the files permits
intensive interactive operation and evaluation of results of
successive processing programs. This capability has permitted
the incorporation of many of the analytical features described
before, which otherwise would be extremely tedious in a batch
processing mode. The present system allows for repeated
refining passes after the investigator evaluates results, e.g.
revised axis tilt, calibration modification, spin-down model
adjustment, consideration of improved drag coefficient model, or
installation of other processing modules.

We include here a tabular summary (Table 4.1) of atmosphere and
wind profiles. The latter is also depicted in a specialized
plot (Figure 4.10) which combines altitude and wind vector data.

4.9 Comparison with Other Concurrent Experiments

Robin sphere and chemical release experiment results become
available as the final results for all aspects of a test or
campaign are collected for coordination. Good density and wind
profile estimates are usually provided from Robin sphere analyses
performed around 60-70 km. altitude, which is where the rocket
sphere spin deceleration and therefore the wind and density
profile is least reliable. Improvement of the spin deceleration
model, and even the sphere axis tilt may be warranted if the
consensus from the other tests so dictates. These test wind
velocities are provided in geographic coordinates, and are
converted to the sphere trajectory system for direct comparison.

97

Table 4.1 Summary of Atmosphere and Wind Profile (AC13)

ALTITUDE (KM)	S-N WIND (M/S)	W-E WIND (M/S)	TEMP (DEG K)	TEMP-US76 (DEG K)	DENSITY (KG/M**3)	DENSITY RATIO TO USSA76
140.	-58.4	34.1	590.4	30.7	4.570E-09	1.193
139.	-58.3	28.8	584.5	33.1	4.855E-09	1.184
138.	-57.9	30.1	581.2	38.3	5.135E-09	1.168
137.	-56.8	30.0	577.0	43.6	5.437E-09	1.163
136.	-54.4	48.0	574.1	48.5	5.764E-09	1.136
135.	-53.3	52.9	569.8	53.1	6.121E-09	1.120
134.	-53.3	52.9	565.2	57.7	6.504E-09	1.103
133.	-52.0	64.5	560.6	62.6	6.911E-09	1.094
132.	-49.5	57.3	553.6	64.9	7.360E-09	1.070
131.	-44.9	60.3	545.8	66.7	7.918E-09	1.057
130.	-40.8	60.4	537.2	67.9	8.510E-09	1.044
129.	-37.3	57.4	526.2	67.0	9.197E-09	1.035
128.	-34.1	52.8	513.8	64.8	9.865E-09	1.028
127.	-30.8	51.1	503.1	64.5	1.083E-08	1.016
126.	-28.4	55.0	497.0	69.0	1.165E-08	.995
125.	-29.0	61.5	496.1	78.9	1.241E-08	.962
124.	-30.7	65.9	499.3	93.1	1.312E-08	.919
123.	-35.6	64.9	502.3	107.4	1.388E-08	.875
122.	-41.4	61.9	502.5	119.0	1.475E-08	.835
121.	-47.2	58.9	497.2	125.3	1.587E-08	.803
120.	-52.0	57.1	484.8	124.8	1.734E-08	.780
119.	-57.1	56.7	470.4	122.4	1.909E-08	.761
118.	-61.7	57.1	450.5	114.5	2.134E-08	.750
117.	-66.0	58.9	428.8	104.8	2.410E-08	.742
116.	-69.9	53.2	409.8	97.8	2.719E-08	.731
115.	-72.8	43.0	389.6	89.6	3.096E-08	.722
114.	-73.7	31.8	361.8	73.8	3.631E-08	.730
113.	-70.1	19.0	332.8	56.5	4.332E-08	.746
112.	-63.2	5.0	308.2	44.8	5.161E-08	.755
111.	-49.0	-14.4	284.3	32.3	6.342E-08	.770
110.	-26.9	-29.0	262.9	12.9	7.815E-08	.819
109.	-12.8	-27.4	235.1	4.7	9.729E-08	.838
108.	-15.0	-9.4	239.0	15.7	1.096E-07	.794
107.	2.0	14.7	207.8	-9.8	1.453E-07	.880
106.	21.6	26.2	178.3	-34.8	2.014E-07	1.031
105.	39.2	24.0	168.8	-40.0	2.563E-07	1.103
104.	39.8	10.9	174.1	-31.2	3.011E-07	1.068
103.	35.9	-5.2	177.3	-24.9	3.558E-07	1.078
102.	50.3	-16.6	172.4	-27.1	4.411E-07	1.121
101.	61.9	-25.0	174.0	-23.2	5.290E-07	1.127
100.	61.0	-28.7	181.9	-13.2	6.097E-07	1.088
99.	52.9	-29.2	190.7	-2.5	6.936E-07	1.031
98.	48.4	-32.1	190.0	-1.7	8.272E-07	1.025
97.	53.8	-38.6	183.4	-7.0	1.024E-06	1.057
96.	72.9	-42.5	171.2	-18.1	1.333E-06	1.138
95.	87.6	-29.8	174.2	-14.2	1.576E-06	1.131
94.	94.9	-27.2	186.8	-1.0	1.769E-06	1.059
93.	76.1	-23.3	206.2	19.0	1.896E-06	.948
92.	72.2	-29.3	210.0	23.0	2.185E-06	.913
91.	83.4	-28.0	214.3	27.5	2.504E-06	.878
90.	53.4	-22.2	215.5	28.6	2.908E-06	.851
89.	50.1	-24.6	218.5	32.7	3.325E-06	.815
88.	52.9	-28.4	221.1	34.2	3.841E-06	.788
87.	44.2	-35.7	233.2	46.3	4.216E-06	.724
86.	38.7	-21.2	226.6	41.8	4.963E-06	.713
85.	28.0	10.8	226.4	37.5	5.807E-06	.706
84.	3.3	35.3	230.6	39.8	6.589E-06	.680
83.	13.9	42.9	227.9	35.1	7.708E-06	.676
82.	19.6	51.3	222.7	28.0	9.143E-06	.681
81.	11.5	51.5	226.8	30.1	1.042E-05	.661
80.	2.3	49.0	232.9	34.3	1.172E-05	.635
79.	6.1	57.0	240.5	40.0	1.306E-05	.609
78.	19.4	81.3	242.2	39.6	1.480E-05	.590
77.	25.9	71.8	240.7	38.2	1.720E-05	.594
76.	30.9	42.1	240.5	34.1	1.977E-05	.578
75.	51.2	46.8	238.5	20.1	2.307E-05	.601
74.	66.1	75.8	220.7	10.4	2.881E-05	.621
73.	64.5	82.1	221.3	9.0	3.343E-05	.621
72.	62.3	51.6	222.1	7.8	3.872E-05	.621
71.	62.7	40.8	227.2	10.4	4.393E-05	.610
70.	72.5	29.0	230.2	10.6	5.016E-05	.606
69.	58.8	21.2	232.2	9.9	5.745E-05	.604
68.	59.8	24.2	231.7	8.7	6.845E-05	.609
67.	58.1	13.3	221.8	-6.0	8.046E-05	.644
66.	69.6	3.4	221.2	-9.3	9.386E-05	.656
65.	61.1	-11.5	225.1	-8.2	1.071E-04	.657
64.	49.8	-14.1	227.7	-8.4	1.228E-04	.660
63.	.3	1.4	248.0	10.3	1.29?E-04	.611
62.	2.0	10.6	254.3	12.8	1.446E-04	.601
61.	5.2	28.1	254.0	9.8	1.651E-04	.604
60.	7.4	39.9	252.8	5.8	1.895E-04	.612
59.	8.7	38.2	263.5	13.8	2.070E-04	.591
58.	7.8	40.4	272.3	19.8	2.270E-04	.573
57.	8.8	36.9	274.1	16.6	2.549E-04	.570
56.	8.8	36.7	271.6	13.5	2.908E-04	.576
55.	8.8	81.3	283.4	-7.4	3.838E-04	.623
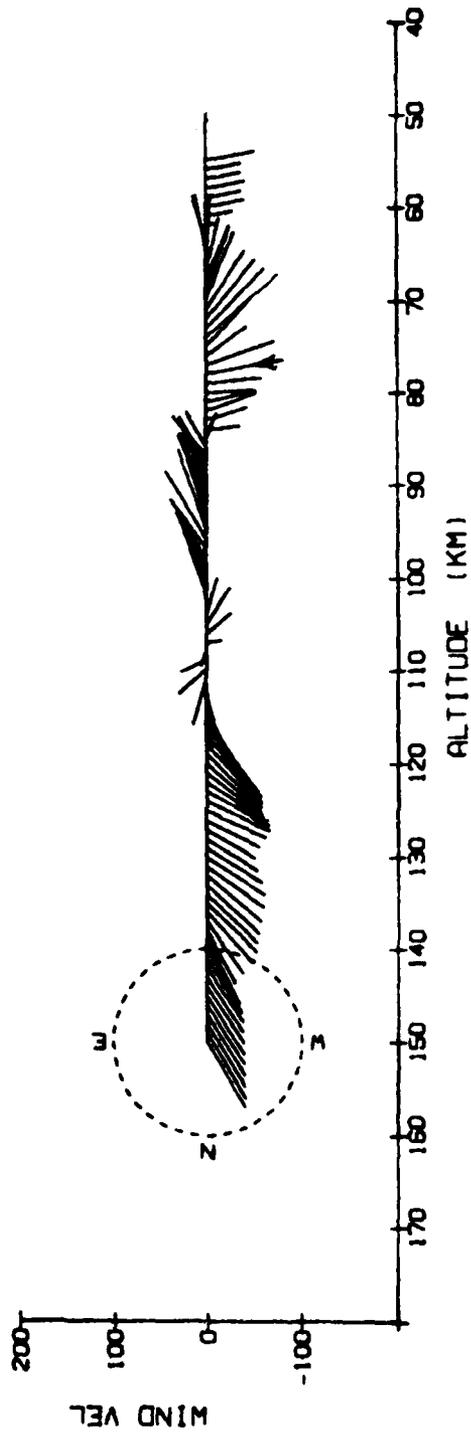
Figure 4.10 Plot of Geographic Wind Vector Profile (AC13)

99

In this manner it was concluded that the AC12 and AC13 Z-acceleration values were about 15% low, and the revised calibrations jointly improved in-track wind and low altitude densities. Chemical release measurements provide good wind velocity estimates at the higher altitudes, with greatest confidence placed on these tests under conditions of uniform winds, particularly in directions transverse to the lines of sight. Refinement of the rocket sphere spin rate, suggesting a cross-track axis tilt, would be possible using these data.

4.10   Evaluation of Reliability of Results

Uncertainties in the density and wind solutions arise as discussed above, primarily from

      a) Calibration coefficients

      b) Trajectory velocity provided

      c) Spin axis tilt estimate

      d) Spin phase orientation estimate

The equations that have been described in Section 4.6 for the inversion of Eq. 4.4 are also directly useable for determining the sensitivity of the solutions to variations in the above four parameters.   An error analysis program has evolved in parallel with the complete solution algorithm, and turns out to be most useful, not only to establish error-bars, but also to determine whether any combination of adjustments of the parameters would bring results closer to values from other sources. (Table 4.2) Further advances in these sensitivity estimating programs are possible in order to include other variables such as cross-track tilt, and for implementation of alternate solution procedures in the 80 km transition region.

100

Table 4.2 Solution Sensitivity Error Analysis (AC13)

14.0 0.0 AC13   86. .045 U=0.938600 PHC=270.0

ERROR ANALYSIS FOR RCD, VXW, VYW, DUE TO
1% ERROR IN CAL, 1 R/S ERROR IN VXT, VZT,
AND 1 DEG. ERROR IN ALPHA, PHASE.

ALT	CAL	RCD % UXT	UZT	ALF	PHI	CAL	VXW R/S UXT	UZT	ALF	PHI	CAL	VYW R/S UXT	UZT	ALF	PHI
150.0	1.00	-.56	-.26	-9.64	-.13	0.00	.91	.23	23.61	.89	0.00	-.12	-.03	-1.94	7.07
149.0	1.00	-.53	-.26	-9.48	-.04	0.00	.85	.21	23.59	.79	0.00	-.12	-.03	-1.94	7.17
148.0	1.00	-.51	-.25	-9.34	-.07	0.00	.79	.20	23.45	.88	0.00	-.11	-.03	-1.94	7.21
147.0	1.00	-.49	-.25	-9.21	-.14	0.00	.73	.18	23.32	1.01	0.00	-.11	-.03	-1.94	7.25
146.0	1.00	-.47	-.24	-9.09	-.18	0.00	.68	.17	23.18	1.08	0.00	-.10	-.03	-1.94	7.28
145.0	1.00	-.45	-.23	-8.99	-.15	0.00	.64	.16	23.12	.99	0.00	-.10	-.03	-1.92	7.34
144.0	1.00	-.44	-.23	-8.89	-.13	0.00	.60	.15	22.94	.97	0.00	-.10	-.02	-1.84	7.38
143.0	1.00	-.42	-.23	-8.80	-.15	0.00	.56	.14	22.82	1.01	0.00	-.10	-.02	-1.94	7.41
142.0	1.00	-.41	-.22	-8.73	-.18	0.00	.53	.13	22.75	1.06	0.00	-.09	-.02	-1.92	7.46
141.0	1.00	-.40	-.22	-8.66	-.16	0.00	.50	.13	22.72	1.06	0.00	-.08	-.02	-1.81	7.52
140.0	1.00	-.39	-.21	-8.59	-.18	0.00	.48	.12	22.66	1.07	0.00	-.08	-.02	-1.44	7.57
139.0	1.00	-.38	-.21	-8.53	-.23	0.00	.45	.11	22.59	1.15	0.00	-.06	-.01	-1.27	7.64
138.0	1.00	-.37	-.21	-8.47	-.22	0.00	.43	.11	22.68	1.16	0.00	-.06	-.01	-1.17	7.68
137.0	1.00	-.36	-.20	-8.43	-.16	0.00	.41	.10	22.56	1.12	0.00	-.08	-.02	-1.95	7.71
136.0	1.00	-.35	-.20	-8.39	-.09	0.00	.39	.10	22.53	1.08	0.00	-.11	-.03	-2.68	7.78
135.0	1.00	-.36	-.20	-8.36	-.07	0.00	.37	.09	22.52	1.09	0.00	-.12	-.03	-3.04	7.84
134.0	1.00	-.34	-.19	-8.32	-.07	0.00	.35	.09	22.68	1.18	0.00	-.12	-.03	-3.04	7.90
133.0	1.00	-.33	-.19	-8.29	-.06	0.00	.34	.08	22.61	1.12	0.00	-.12	-.03	-3.16	7.95
132.0	1.00	-.32	-.19	-8.24	-.06	0.00	.32	.08	22.29	1.17	0.00	-.13	-.03	-3.41	7.95
131.0	1.00	-.32	-.18	-8.19	-.05	0.00	.29	.07	21.98	1.19	0.00	-.14	-.03	-3.68	7.94
130.0	1.00	-.31	-.18	-8.14	-.00	0.00	.27	.07	21.67	1.20	0.00	-.14	-.03	-3.74	7.90
129.0	1.00	-.31	-.18	-8.09	-.00	0.00	.24	.06	21.37	1.21	0.00	-.13	-.03	-3.67	7.90
128.0	1.00	-.30	-.18	-8.03	-.00	0.00	.22	.06	21.06	1.27	0.00	-.15	-.03	-3.44	7.87
127.0	1.00	-.30	-.18	-8.00	-.09	0.00	.20	.05	20.79	1.24	0.00	-.18	-.03	-3.21	7.86
126.0	1.00	-.29	-.17	-7.97	-.06	0.00	.19	.05	20.65	1.21	0.00	-.18	-.03	-3.52	7.89
125.0	1.00	-.29	-.17	-7.96	-.02	0.00	.18	.04	20.78	1.16	0.00	-.14	-.03	-3.98	7.96
124.0	1.00	-.28	-.17	-7.96	.02	0.00	.18	.04	20.97	1.09	0.00	-.15	-.04	-4.26	8.08
123.0	1.00	-.28	-.17	-7.96	.02	0.00	.18	.04	21.31	1.04	0.00	-.14	-.03	-4.12	8.21
122.0	1.00	-.27	-.17	-7.96	.01	0.00	.18	.05	21.70	1.01	0.00	-.13	-.03	-3.87	8.34
121.0	1.00	-.27	-.16	-7.97	-.00	0.00	.19	.06	22.10	.98	0.00	-.12	-.03	-3.55	8.47
120.0	1.00	-.27	-.16	-7.97	-.00	0.00	.19	.05	22.43	.93	0.00	-.11	-.03	-3.36	8.58
119.0	1.00	-.26	-.16	-7.98	.02	0.00	.19	.06	22.82	.82	0.00	-.10	-.03	-3.26	8.72
118.0	1.00	-.26	-.16	-7.98	.06	0.09	.19	.06	23.17	.60	0.00	-.10	-.03	-3.23	8.86
117.0	1.00	-.26	-.16	-7.98	.12	0.00	.20	.05	23.49	.30	0.00	-.10	-.02	-3.16	9.00
116.0	1.00	-.26	-.15	-7.98	.10	0.00	.20	.06	23.70	-.08	0.00	-.09	-.02	-3.05	9.12
115.0	1.00	-.26	-.15	-7.96	.23	0.00	.19	.05	23.81	-.44	0.00	-.07	-.02	-2.15	9.17
114.0	1.00	-.25	-.15	-7.93	.26	0.00	.18	.04	23.68	-.84	0.00	-.04	-.01	-1.29	9.17
113.0	1.00	-.25	-.15	-7.89	.26	0.00	.16	.04	23.18	-1.09	0.00	-.01	-.00	-.48	9.10
112.0	1.00	-.24	-.15	-7.84	.20	0.00	.13	.03	22.67	-1.02	0.00	.01	.00	.44	8.95
111.0	1.00	-.24	-.15	-7.76	.06	0.00	.09	.02	21.16	-.64	0.00	.05	.01	1.66	8.68
110.0	1.00	-.23	-.15	-7.66	-.08	0.00	.03	.01	19.27	-.36	0.00	.07	.02	2.39	8.37
109.0	1.00	-.23	-.15	-7.61	-.10	0.00	-.00	.00	18.17	-.15	0.00	.06	.02	2.11	8.16
108.0	1.00	-.23	-.15	-7.62	-.17	0.00	-.01	.00	18.18	.11	0.00	.06	.02	.84	8.14
107.0	1.00	-.23	-.14	-7.57	-.08	0.00	-.03	-.01	17.69	.61	0.00	-.03	-.01	-1.07	8.04
106.0	1.00	-.22	-.14	-7.52	-.06	0.00	-.06	-.02	16.61	.80	0.00	-.06	-.01	-2.07	7.84
105.0	1.00	-.22	-.14	-7.46	-.11	0.00	-.10	-.03	15.10	1.07	0.00	-.06	-.02	-2.21	7.55
104.0	1.00	-.22	-.14	-7.45	-.13	0.00	-.12	-.03	14.77	.88	0.00	-.04	-.01	-1.29	7.52
103.0	1.00	-.21	-.14	-7.45	-.13	0.00	-.11	-.03	14.94	.60	0.00	-.00	-.00	-.11	7.62
102.0	1.00	-.21	-.14	-7.40	-.08	0.00	-.15	-.04	13.63	.18	0.00	.01	.00	.51	7.77
101.0	1.00	-.21	-.14	-7.37	-.03	0.00	-.18	-.04	12.70	-.14	0.00	.03	.01	.96	7.70
100.0	1.00	-.21	-.14	-7.37	.05	0.00	-.18	-.04	12.72	-.41	0.00	.03	.01	1.23	7.23
99.0	1.00	-.20	-.14	-7.39	.05	0.00	-.17	-.04	13.36	-.58	0.00	.04	.01	1.37	7.41
98.0	1.00	-.20	-.14	-7.39	.04	0.00	-.17	-.04	13.62	-.60	0.00	.04	.01	1.64	7.48
97.0	1.00	-.20	-.14	-7.38	-.06	0.00	-.18	-.04	13.06	-.32	0.00	.05	.01	2.02	7.43
96.0	1.00	-.20	-.13	-7.33	-.09	0.00	-.22	-.05	11.58	-.18	0.00	.05	.01	8.06	7.16
95.0	1.00	-.19	-.13	-7.31	-.06	0.00	-.24	-.06	10.72	-.02	0.00	.02	.01	.96	6.98
94.0	1.00	-.19	-.13	-7.29	-.07	0.00	-.26	-.07	9.91	.08	0.00	.02	.00	.68	6.84
93.0	1.00	-.19	-.13	-7.32	-.04	0.00	-.22	-.06	11.61	-.01	0.00	.02	.00	.65	7.25
92.0	1.00	-.19	-.13	-7.32	-.04	0.00	-.22	-.06	11.69	-.16	0.00	.03	.01	1.12	7.30
91.0	1.00	-.19	-.13	-7.34	-.02	0.00	-.21	-.05	12.46	-.23	0.00	.03	.01	1.15	7.51
90.0	1.00	-.19	-.13	-7.35	-.01	0.00	-.19	-.05	13.34	-.15	0.00	.02	.01	.87	7.71
89.0	1.00	-.19	-.13	-7.36	.04	0.00	-.19	-.05	13.63	-.48	0.00	.03	.01	1.08	7.80
88.0	1.00	-.19	-.13	-7.35	.06	0.00	-.20	-.05	13.00	-.57	0.00	.01	.01	1.13	7.72
87.0	1.00	-.19	-.13	-7.36	-.04	0.00	-.18	-.05	13.92	-.36	0.00	.04	.01	1.24	7.57
86.0	1.00	-.19	-.13	-7.37	-.04	0.00	-.18	-.04	14.70	-.10	0.00	.02	.01	1.00	8.00
85.0	1.00	-.18	-.12	-7.38	-.00	0.00	-.17	-.04	14.82	.20	0.00	-.03	-.01	-1.11	8.21
84.0	1.00	-.01	-.17	.74	.14	0.00	-1.00	.19	-21.81	0.00	0.00	.00	-.03	.16	8.92
83.0	1.00	-.01	-.17	.73	.18	0.00	-1.00	.18	-21.89	0.00	0.00	.00	-.04	.20	8.88
82.0	1.00	-.01	-.16	.72	.22	0.00	-1.00	.18	-22.00	0.00	0.00	.00	-.05	.25	9.05
81.0	1.00	-.01	-.16	.72	.21	0.00	-1.00	.18	-22.18	0.00	0.00	.00	-.05	.24	9.07
80.0	1.00	-.01	-.16	.73	.19	0.00	-1.00	.19	-22.36	0.00	0.00	.00	-.04	.22	9.08
79.0	1.00	-.01	-.16	.72	.23	0.00	-1.00	.18	-22.48	0.00	0.00	.00	-.05	.25	9.15
78.0	1.00	-.01	-.16	.71	.12	0.00	-1.00	.17	-22.63	0.00	0.00	.00	-.07	.34	9.20
77.0	1.00	-.01	-.16	.70	.20	0.00	-1.00	.16	-22.70	0.00	0.00	.00	-.06	.31	9.28
76.0	1.00	-.01	-.16	.68	.19	0.00	-1.00	.16	-22.70	0.00	0.00	.00	-.04	.19	9.20
75.0	1.00	-.01	-.16	.66	.03	0.00	-1.00	.14	-22.73	0.00	0.00	.00	-.04	.08	9.47
74.0	1.00	-.01	-.15	.64	.37	0.00	-1.00	.13	-22.80	0.00	0.00	.01	-.06	.31	9.46
73.0	1.00	-.01	-.15	.64	.31	0.00	-1.00	.13	-22.93	0.00	0.00	.00	-.05	.28	9.39
72.0	1.00	-.01	-.15	.64	.26	0.00	-1.00	.13	-23.06	0.00	0.00	.00	-.05	.23	9.37
71.0	1.00	-.01	-.15	.63	.22	0.00	-1.00	.13	-23.18	0.00	0.00	.00	-.04	.19	9.37
70.0	1.00	-.01	-.14	.62	.10	0.00	-1.00	.12	-23.25	0.00	0.00	.00	-.03	.15	9.37
69.0	1.00	-.01	-.14	.63	.13	0.00	-1.00	.13	-23.42	0.00	0.00	.00	-.02	.12	9.37
68.0	1.00	-.01	-.14	.63	.13	0.00	-1.00	.13	-23.54	0.00	0.00	.00	-.03	.13	9.40
67.0	1.00	-.01	-.14	.62	.10	0.00	-1.00	.12	-23.66	0.00	0.00	.00	-.02	.10	9.41
66.0	1.00	-.00	-.14	.61	.07	0.00	-1.00	.11	-23.73	0.00	0.00	.00	-.01	.06	9.43
65.0	1.00	-.00	-.14	.61	.04	0.00	-1.00	.12	-23.87	0.00	0.00	-.00	-.00	.01	9.44
64.0	1.00	-.00	-.14	.62	-.02	0.00	-1.00	.13	-24.04	0.00	0.00	-.00	.00	-.01	9.47

101

4.11 Auxiliary Associated Phenomena

As described in the previous sections, studies of AC10, AC12 and
AC13 have been completed; and initial processing for flights AC14
thru AC16 has begun.   Results and procedures as now implemented
have been of sufficient resolution quality to lead to the
reporting of basic phenomena,[2,3] the identification of gravity
waves,[4] and the association of density gradient reversals with
supersonic auroral fronts.[5]   The experiment also provides a
fertile source for other unscheduled but important measurements
in the lower thermosphere, such as estimating the drag and spin
down processes.   A special study of the telemetry AGC signal was
conducted for the sphere's spinning antenna, in order to fix spin
orientation.   It was shown that the antenna side-lobes
introduced unexpected non-uniform spin modulation, rendering
phase analysis unreliable.   Future daytime flights will include
a sun-sensor, and accurate spin down phase determination should
be possible.

Atmospheric turbulence studies were also performed through
calculation of Richardson number profiles from the solved
atmospheric density-temperature profiles.   This parameter
indicates where the gradient becomes too steep to sustain a
stable density profile.

102

References

1. Philbrick, C.R., Faire, A.C., and Fryklund, D.H., "Measurements of Atmospheric Density at Kwajalein Atoll, 18 May 1977", AFGL-TR-78-0058, January 1978.

2. Philbrick, C.R., McIsaac, J.P., and Bhavnani, K.H., "Atmospheric Structure Associated with Dynamical Processes in the Mesosphere and Lower Thermosphere", IAGA Symposium, Edinburgh, Aug 81

3. Philbrick, C.R. et al, "Vertical Density and Temperature Structure over Northern Europe", Adv. Space Res., 1983, Vol. 2, No. 10.

4. Philbrick, C.R. et al, "Mid-Latitude Measurements of Atmospheric Waves and Structure", EOS Vol 63, 45, Nov 1982.

5. Philbrick, C.R. et al, "Density and Temperature Structure over Northern Europe", JATP (to be published).

6. Whitfield, D.L., "Mean Free Path of Molecules from a Surface in Rarefied Flow with Application to Correlating Drag Data", AIAA Paper No. 73-198, January 1973.

5.0 Interactive Graphics Systems for AFGL Applications

5.1 Graphical Functions

Plotting capabilities very similar to those for conventional
static plotters such as Calcomp or microfiche are valuable to a
broad range of investigators, for interactive use on the CDC-6600
system at AFGL.   This includes

- a) Stacked or overlaid X-Y plotting i.e. more than one plot
  displayed.
- b) Linear or logarithmic axes scales.
- c) Symbol and connected line plotting to distinguish the
  graphs.
- d) Additional X-axes for concurrent parameters.
- e) Range of data plotted controlled by record count or
  dependency variable limits.
- f) Flexible heading and axis labelling.
- g) Running average and other simple plot smoothing options.
- h) Compatability between off-line and on-line data base
  requirements and procedures.

These capabilities have been implemented for conventional X-Y
plots as well as for special pictorial presentations.   An
integrated interactive graphics package SUATEK[1,3] incorporates
the above and other useful specialized features.   Figures 5.1
and 5.2 show the range of options that are available to the
SUATEK user in menu form.   Figure 5.1 lists the items that may
be set by the user in order to select variables to be plotted,
or to lay out the plot frame, or to enable options.   Activated
options may work in extended combinations, and Figure 5.2
describes each one briefly.

BRIEF DESCRIPTION OF THE TERMS

NXV - NUMBER OF THE X-VARIABLE
NY1 - NUMBER OF THE FIRST Y-VARIABLE
     UPTO 4 Y VARIABLES NY1-NY4 PER PLOT
XL - LENGTH OF X-AXIS IN INCHES (TEKTRONIX COPY IS 50%)
Y1L - LENGTH OF Y1-AXIS
XMIN,XMAX - LEFTMOST, RIGHTMOST ENDS OF X-AXIS
Y1MN,Y1MX - BOTTOM, TOP END VALUES OF Y1-VARIABLE
XOFF - LEFT(-VE) OR RIGHT(+VE) X-AXIS OFFSET IN INCHES
Y1OF - DOWN(-VE) OR UP(+VE) Y1-AXIS OFFSET
IPLX - X-AXIS SCALE LINEAR(0) OR LOG(1)
       2 STARTS LINEAR SCALE FROM XMIN MARKED AS ZERO
IPL1 - Y1 SCALE AND PLOT OPTIONS LINEAR(0,2,4) OR LOG(1,3,5)
       0-1 PRODUCES SYMBOLS AT DATA POINTS
       2-3 PRODUCES A LINE THROUGH DATA POINTS (DEFAULT)
       4-5 PRODUCES CONNECTED SYMBOLS THROUGH DATA POINTS

NX1 - NUMBER OF FIRST EXTRA X-AXIS VARIABLE (UPTO 4 ALLOWED)
IST,ISP,IREP - START,STOP, AND REPEAT FACTOR FOR RECORDS
       IREP-1 RECORDS ARE SKIPPED (DEFAULT-1)
IPARM....NCHK - PLOT AND DATA HANDLING OPTIONS
       =0 DEACTIVATED, =1 ACTIVATED
NDPN - NUMBER OF DEPENDENCY PARAMETERS (UPTO 5 ALLOWED)
IDP1 - NUMBER OF THE FIRST DEPENDENCY VARIABLE
P1MN,P1MX - MIN-MAX ACCEPTANCE RANGE FOR VARIABLE IDP1
       BEFORE CORRESPONDING DATA IS PLOTTED

Figure 5.1 SUATEK Menu of Facilities

105

DESCRIPTION OF OPTIONS   IPARM.....NCHK

IPARM - OVERLAY PLOTS FOR SPECIFIED RANGES OF A PARAMETRIC VARIABLE. USE DEPENDENCY PARAMETERS OR PROMPTING TO FIX OTHER SIGNIFICANT VARIABLES.   INCLUDES OPTION TO

ISORT - SORT UPTO 512 DATA POINTS ON X(-1) OR Y(-2)

IRAV - RUNNING AVERAGE FOR WINDOW OF 'N' DATA POINTS VALUE OF 'N' WILL BE REQUESTED

IPOLF - MAKE N'TH ORDER POLYNOMIAL FIT TO DATA IN PLOT RANGE (N<20) VALUE OF 'N' WILL BE REQUESTED

ISING - SINGLE PLOT (1-4) FROM MULTIPLE PLOT SPEC

ILBL - REVISE PLOT AXES AND HEADER LABELS PROMPTING FOR REVISION WILL OCCUR

IRANGE - REVISE X AND Y PLOT MIN-MAX RANGES DEFAULT IS THE PLOT FRAME RANGES

ICOMB - PLOT LINEAR COMBINATION OF UP TO 4 VARIABLES (D(NU)*FACTOR + ...) PROMPTING FOR NU,FACTOR WILL OCCUR

ICON - Z-CONTOUR PLOT VS. X-Y VARIABLES (Z IS A NUMBER DEFINED BY A*U+B) PROMPTING FOR NU,A,B WILL OCCUR

ICURF - RUNNING CUBIC FIT FOR WINDOW OF 'N' DATA PLOINTS VALUE OF 'N' WILL BE REQUESTED

IEDIT - DELETE, REPLACE, INTERPOLATE, OR SMOOTH DATA (VALUE OF DELETE VARIABLE IS SET TO -9.E99) PRIOR TO EDITING, PROMPTING GUIDE WILL BE DISPLAYED

IMERG - REPLACE Y-VARIABLE DATA BY EDITED AND CURVE FIT RESULTS OPTION TO MERGE WILL BE OFFERED AFTER PLOTTING

NSPEC - UPDATE PLOT SPEC FROM 'NSPEC'TH RECORD ON SUSPEC RECORDS MUST BE SEPARATED BY / IN COLUMN 1 AFTER UPDATING NSPEC WILL BE RESET TO ZERO

NCHK - OPTION TO ABORT AFTER PLOTTING 'NCHK' POINTS PROMPTING TO ABORT OR CONTINUE WILL OCCUR

Figure 5.2 Description of Activatable SUATEK Otions

5.2 Analytical Functions

The following functions can be performed on the data base for
direct graphical evaluation and revision:

a) Data may be selectively edited, replaced, and filtered.

b) Data may be plotted conditionally, depending on its
range or that of some other significant concurrent
variable (dependency parameter).

c) Data may be sorted according to one or more variable
prior to viewing.

d) Functional combinations of variables may be formed as
the variable to be plotted.

e) Polynomial fits to segments of the data stream an be
applied and viewed.

f) Running polynomial fits over the whole data s   may
be applied and viewed.

g) Parameters determined during any of the above analysis
procedures may be presented for recording and
evaluation.

h) New data formed by any of the above procedures may
replace or augment the original data base.

5.3 Data Base Structure

The philosophy for a basic format for the data base for SUATEK
has been the capability of handling data streams of indeterminate
length, where each variable to be considered appears in each
record, in standard floating binary format.   The only other
information necessary on such a file is a header containing

a) Number of variables per record.

b) Alphanumeric (axis label) per variable.

An optional plot heading label may be added.   Figure 5.3 gives
the specification for SUATEK files.

DESCRIPTION OF SUATEK FORMAT FILES

SUATEK FORMAT FILES FOR USE ON THE CDC-6600 ARE BLOCK TYPE 'I' RECORD TYPE 'W' BINARY FILES. THEY CONSIST OF ONE TO THREE HEADER RECORDS DESCRIBING THE DATA, FOLLOWED BY UNIFORM DATA RECORDS EACH CONSISTING OF ONE REAL NUMBER PER VARIABLE. THESE DATA ARE GENERALLY THE RESULTS OF VARIOUS ANALYSIS AND PROCESSING PROCEDURES, AND MAY BE READILY MANIPULATED AND PLOTTED USING SUATEK WITH THE SYSTEM FACILITIES AT AFGL.

THESE FILES MAY BE ACCESSED AS FOLLOWS (ASSUMED TAPE1 HERE)

READ(1) NOV,MN,LAE,MMA,((LBL(I,J),I-1,3),J-1,NOV)
IF(LAE.NE.0) READ(1) (MLBL(I),I-1,5)
IF(MMA.NE.0) READ(1) ((DMNX(I,J),I-1,2),J-1,NOV)

READ(1) (D(J),J-1,NOV) ...... ALL SUBSEQUENT RECORDS

WHERE
NOV   – NUMBER OF VARIABLES
MN   – FLAG (PRESENTLY UNASSIGNED)
LAE   – -1 IF HEADER LABEL 'MLBL' FOLLOWS
MMA   – -1 IF PLOT MIN-MAX RANGES FOLLOW
LBL   – 3 WORD HOLLERITH DESCRIPTOR PER VARIABLE
MLBL – 5 WORD HOLLERITH LABEL (IF LAE-1)
DMNX – MIN AND MAX PLOT RANGE PER VARIABLE (IF MMA-1)

D   – ARRAY OF REAL NUMBERS
        NOTE :.:
        -9.9E99 REPRESENTS AN IGNORABLE VALUE
        E.G. SAMPLE NOT PRESENT WHEN MERGING DATA
        -8.0E99 INDICATES A DELIBERATELY DELETED VALUE,
        FOR POSSIBLE SUBSEQUENT REPLACEMENT

Figure 5.3   General Specification for a SUATEK File

108

This specification is the simplest possible, and places the
fewest constraints on the organization and development of new
functional options. The header records turn out to be self-
descriptive if the file needs to be examined. An important
aspect of this file design is that it frequently corresponds to
the sequence in which experimental data are telemetered and
stored on tape. A variable that might appear say once in 64
records is identified by another subcom frame number variable,
which is necessarily available in the transmission. Dependency
plotting with the appropriate subcom number then achieves the
desired separation.

The only additional restrictions placed on the file structure
relate to two special values for each variable. Since a
variable value may not exist in concurrence with others in a
record, a dummy fill or IGNORE value is required to which the
processing must be completely transparent. In other cases a
variable value may be absent or consciously removed, and where
the system is required to be aware of this break in the data.
Here a DELETE value is required, which causes a break while
plotting, and which may be automatically replaced during certain
curve fitting procedures. The numbers assigned to DELETE and
IGNORE are $-9.E99$ and $-9.9E99$ respectively, values which are
extremely unlikely to be encountered.

The main objection to the above data base structure may be the
inefficient use of disk file storage when a few bits worth of
information is floated and stored in a full 60-bit CDC word.
SUATEK could be modified to handle either the conventional or
a packed file format automatically through a flag bit in the
header. A packed file processing package available in the
SUNY library could be adapted for this implementation.

5.4 Implementation of the Internal File Processing

The processing functions outl..ned in Section 5.2 are generally
required to act on only two variables (X,Y), even though other
dependency variables may determine which records are accepted or
rejected.   Subsequent stages for any complex process, e.g. edit
followed by curve fit, are handled by two auxiliary files which
contain only the accepted X,Y values and their record number, and
which are used solely for internal reading, processing, and
plotting by SUATEK.   A processing pass on one of these files
creates the next stage data on the other file, and this see-saw
procedure is continued.   Details of each analytical procedure
will not be discussed, as they are extensions of conventional
techniques.   During a pass such as curve fitting, DELETE records
are skipped, additional data are read in order to form an
adequate window for the fit, and the DELETE records are replaced
to form a continuous plot.   Merging of the final reworked data
into the original file is readily accomplished using the record
number saved on the auxiliary files.

5.5 Implementation of the Interactive Modules

Acceptance of the graphics capabilities by researchers for their
own use is a significant consideration.   A self-prompting plot
specification is displayed and forms the initial menu.   The user
may enter a "?" for a short description of any parameter dis-
played.   Plot spec modification is accomplished by entries that
are nearly identical to the spec display.   This special input
section has the virtue of permitting gradual build up of each
plot specification, and of readily becoming habitual and
unnoticed by the typical SUATEK user.   Figure 5.4 is a summary
guide for interactive input.   This scheme has also been adopted
for the SUACON contour plotting system. (Section 5.6)

110

SUATEK INPUT GUIDE

TO ENTER OR CHANGE PARAMETER VALUES:

   MAKE ENTRIES EXACTLY AS DISPLAYED.
   FOR EXAMPLE: XMIN=80,XMAX=160.,NY1=3   ETC.
    EMBEDDED BLANKS ARE IGNORED

   SEPARATE ENTRIES BY ',' OR BY 'CR',
   WITH A MAXIMUM OF 80 CHARS/LINE,
   AND EACH ENTRY FULLY CONTAINED IN A LINE.

   TERMINATE ENTRY BY '/' IN ANY POSITION,
   OR BY '1' IN POSITION ONE.

CONTROL IS AS FOLLOWS:

/ IN POSITION ONE INITIATES PLOTTING.

/ IN ANY OTHER POSITION GIVES A SUMMARY
   'PLOT SPEC' STATUS PRINT-OUT, AND
   IN POSITION TWO ALSO PRESENTS ALL OPTIONS.

1 IN POSITION ONE INITIALIZES PLOT MIN-MAX VALUES
   FROM TAPE1 FOLLOWED BY 'PLOT SPEC' STATUS SUMMARY.

1/ ADDITIONALLY DISPLAYS ALL VARIABLES AND OPTIONS.

// IN POSITIONS ONE-TWO STOPS THE PROGRAM.

   AN OPTION IS ACTIVATED WHEN SET TO NON-ZERO.
   (SUBSEQUENT PROCEDURES ARE SELF-PROMPTING)

Figure 5.4 Summary Guide for SUATEK Interactive Input

111

Output prior to and after plotting freely uses prompting requests
to interact with the user, and calls for specific data or actions
as the function that has been activated progresses.   Cross hairs
adjustment for editing proceeds in a similar manner, with the
appearance of the cross hairs being the signal for user action.

Realization of some of the above functions requires interchange-
able use of list directed and formatted print statements, as well
as the PLOTLIB and TEKSIM libraries.   Compatibility of usage
between these utility packages was explored with the systems
group at AFGL, and a calibration pass that was originally
incorporated is now not required.

Realization of any of the interactive graphics packages must be
through the CDC-6600 INTERCOM system.   This system is limited to
$70K_8$ memory, and therefore calls for an Overlay or Segmented
organization of routines that need not be co-resident.   This is
optimized in SUATEK by branching into one of
    i) the input section
    ii) the analytical processing sections (which may have
        their own sub-branches)
    iii) the plot section
Data file handling and common blocks are resident at all times.
File buffer sizes are set at the 64 word size of the mass storage
PRU's.

The NOS/BE job control procedure language has been implemented,
and the user can begin to plot with minimal effort -- viz. one
command: BEGIN,SUA,TEK,M,HISFILE,ID=HISNAME.
where M is the Tektronix unit number and may also be PEN or MIC
for off-line plotting purposes.

112

As mentioned above, pen-and-ink or microfiche plots, identical to
those displayable on the Tektronix, may be initiated using SUATEK
files.   The data input plot requested is also identical to the
entries that are keyed in on-line.   Thus the user does not have
to learn a second plotting system.   Figure 5.5 gives the sample
deck set-up for initiating these plots.   Four cards for special
data and labelling precede the normal SUATEK type input.   Other
differences are that the off-line (SUAPEN) version does not allow
interactive input; values such as N for an N-point running
average must be input where the prompt would normally occur.
Off-line plotting is also likely to consist of multiple plots
from successive files, possibly with identical plot specifi-
cations.   These extra facilities are implemented in SUAPEN.

The requirement for versatile file extraction and merging capabi-
lities, arising out of the proliferation of SUATEK format files
for analyses or plots, has been supported specifically by program
SUAMRG.   Specific segments and variables may be selected,
relabelled, and merged with or without acceptance of special
variable control values such as DELETE.   Figure 5.6 summarizes
SUAMRG options, and shows a sample execution.

5.6   Three Dimensional Graphical Systems

Other graphical presentation capabilities are valuable for multi-
variable files, particularly

        i)   Contour plotting
        ii)   Isometric plotting

Employing different approaches, these plot forms permit introd-
uction of another dimension for viewing and interpreting data.

113

```
JOBNM,CM77777.       SUATEK OFFLINE PENPLOTS       ????     YOURNAME
BEGIN,SUA,TEK,PEN,YOURSUFILE,ID=YOURID.
EOR
SCALE FAC(DEF=1.)              1  IN COL. 30 USES PLOT SPEC SET REPEATEDLY
  YOURNAME    TEL NO
                        (BLANK CARD)
                        (BLANK CARD)
XL=180.,XMIN=240,XMAX=420                     (PLOT SPECS
NY1=2,Y1MN=0.,Y1MX=8.,Y1L=1.                   IN STANDARD
NY2=3,Y2MN=0,Y2MX=.8,Y2L=4,Y2OF=1.25          INTERACTIVE
NY3=4,Y3MN=0,Y3MX=.8,Y3L=4,Y3OF=5.5/          SUATEK FORMAT)
/
           (SIMILAR ENTRIES FOR
            FURTHER PLOTS)
//
EOR
```

Figure 5.5a   Sample Deck Set-up for Pen-and-Ink Plots

PENPLOT OR MICROFICHE PLOTS MAY BE MADE FROM
SUATEK FILES.   NO NEW INSTRUCTION REPERTOIRE
NEEDS TO BE LEARNED, SINCE PLOT SET-UP INPUT
IS IDENTICAL TO THAT FOR ON-LINE SUATEK.

```
JOBNM,CM77777.     SUATEK MICROFICHE PLOTS       ????     YOURNAME
BEGIN,SUA,TEK,MIC,YOURSUFILE,ID=YOURID.
EOR
SCALE FAC(DEF=1.)              1  IN COL. 30 USES PLOT SPEC SET REPEATEDLY
  YOURNAME    TEL NO
MICROFICHE TITLE1 (42 CHARACTERS)
MICROFICHE TITLE2 (42 CHARACTERS)       1  IN COL. 50 FOR MODULO 7 FRAMES
XL=10.,XMIN=240,XMAX=260                     (PLOT SPECS
NY1=2,Y1MN=0.,Y1MX=8.,Y1L=1.                  IN STANDARD
NY2=3,Y2MN=0,Y2MX=.8,Y2L=4,Y2OF=1.25         INTERACTIVE
NY3=4,Y3MN=0,Y3MX=.8,Y3L=4,Y3OF=5.5/         SUATEK FORMAT)
/
           (SIMILAR ENTRIES FOR
            FURTHER PLOTS)
//
EOR
```

Figure 5.5b   Sample Deck Set-up for Microfiche Plots

```
        SUAMRG OPTIONS FOR MERGING TAPEA AND TAPEB

OPTION 1 -- INTERLEAVE BASED ON MUTUAL VARIABLE
            EQUIVALENCE RECORDS WITHIN TOLERANCE
OPTION 2 -- INTERLEAVE BASED ON MUTUAL VARIABLE
            INCLUDE ALL RECORDS
OPTION 3 -- STACK WRITE TAPEA RECORDS
            FOLLOWED BY TAPEB RECORDS
OPTION 4 -- STACK SEPARATED BY 'DELETE' RECORD

   SELECT OPTION (DEFAULT 0=1) *** 0


 TAPEA VARIABLES    FILTER 0   DOWN LEG
1   TIME
2   ALTITUDE
3   IG
4   FILTER
5   COUNTS


 TAPEB VARIABLES    FILTER 3   DOWN LEG
1   TIME
2   ALTITUDE
3   IG
4   FILTER
5   COUNTS


     TO MERGE ENTER  NOVA, NOVB   (0,0  TO EXIT)
ONE COMMON VARIABLE (NOVA.NE.0 AND NOVB.NE.0) ALLOWED


 ENTER  NOVA, NOVB 1,1
 ENTER TOLERANCE AND RANGE (DEFAULT=0,0,0) 0.,0.,0.
 ENTER  NOVA, NOVB 2,0
 ENTER  NOVA, NOVB 5,0
 ENTER  NOVA, NOVB 0,5.
 ENTER  NOVA, NOVB 0,0
 TOLERANCE FOR EQUIVALENCING RECORDS SET AT  .05


 ENTER  ALPHANUMERIC LABEL
  MERGED R0D AND R3D FILES


 REVISE VARIABLE LABELS? (0=NO) 0
 REVISE PLOT MIN-MAX RANGES? (0=NO) 0


1   TIME
2   ALTITUDE
3   COUNTS
4   COUNTS


502 RECORDS WRITTEN TO TAPEI
      END  SUAMRG
```

Figure 5.6   SUAMRG Options and Sample Execution

115

5.6.1 Contour Plotting

Characteristics of the interrelationship between measurements and causal parameters can be highlighted through these presentations. NCAR (Boulder, CO) has developed a comprehensive package that offers many versions of these capabilities which are suitable for off-line use but, due to their computer memory requirements and large range of options, cannot be operated in on-line ($70K_8$) mode. Contour plotting is, however, a presentation that offers valuable insight in many applications, and the CONREC routines as adapted by Aiken (AFGL), were implemented for on-line Tektronix plotting. This system, SUACON, allows interactive adjustment of simple options such as frame size, axes scales and labels, and selection of contour levels to be plotted. Figure 5.7(a), (b) are two pages from the current user's guide. The binary data file must consist of a header and successive records of a fixed number of X,Z data pairs:

Record 1 - MLBL(5),LBL(3,2)
    where, MLBL is a 50 character alphanumeric plot label
           LBL contains 30 char X and Y axes labels

Record 2 ... NX,(X(I),Z(I),I=1,NX)
    where, NX = number of X,Y pairs in each record
           X(I) = X values, must be equally spaced
           Z(I) = function of X,Y being contoured
    Successive records represent equally spaced Y values.

A maximum of 50 records with NX < 50 is presently allowed. This format is compatible with program ISOTEK which produces isometric plots of the same data.

SUACON — INTERACTIVE CONTOURING

Following an audit of the input data file, SUACON
offers the user a number of default or activatable
options for generating contour plots of the data.
The options and the interaction are described using a
sample session, as reproduced on the following pages.

Audit and Initial Presentation

X and Z min-max values are as encountered on the input file.
Y values corresponding to each record do not occur on the file
and may therefore be redefined during the plotting session.
Default Y min-max values are set to the X min-max values.
Entering $\angle$ directly produces the default plot of Example 1.

Options default values may be retained, or changes may
be keyed in as shown underlined in the examples.

XL,YL specify the plot frame i.e. the length of the
X- and Y- axes in inches (default = 8 inches)

XMIN,XMAX are the minimum and maximum for the frame range and
YMIN,YMAX establish the plot scale, given the axes lengths

XOFF,YOFF are the offsets for positioning the plot frame

Options below are off(=0) but may be selectively activated(=1)

ILABC labels the contour levels
IDASHN draws negative level contours dashed
IMXMN labels local maxima-minima levels
ILBL allows modification of header and axes labels

IPICK,NCONT are used for Contour Level Specification as follows:

Desired contour levels to be drawn must always be identified,
and may also be interactively revised after viewing the plot.

With IPICK off, NCONT evenly spaced contour levels may be
automatically selected as in Example 2.
With IPICK on, contour levels may be individually specified
as in Example 3,
or, previously set contour levels may be listed
and selectively revised as in Example 4.

Figure 5.7(a) Excerpt from SUACON User's Guide

EXAMPLE 4.   ENTRIES TO PLOT WITH REVISED CONTOUR LEVELS
             (LEVELS 1 & 10 DELETED)

```
???/
REPEAT PREVIOUS PLOT? (1=YES)0
REVISE CONTOUR LEVELS AS FOLLOWS
EACH CURRENT LEVEL WILL BE DISPLAYED
ENTER  -1  TO DELETE A LEVEL
        0  TO RETAIN A LEVEL
        1  TO REVISE THE LEVEL

LEVEL    1 CONTOUR VALUE        .9500E+00 ?-1
LEVEL    2 CONTOUR VALUE        .9000E+00 ?0
LEVEL    3 CONTOUR VALUE        .7500E+00 ?0
LEVEL    4 CONTOUR VALUE        .5000E+00 ?0
LEVEL    5 CONTOUR VALUE        .2500E+00 ?0
LEVEL    6 CONTOUR VALUE       -.2500E+00 ?0
LEVEL    7 CONTOUR VALUE       -.5000E+00 ?0
LEVEL    8 CONTOUR VALUE       -.7500E+00 ?0
LEVEL    9 CONTOUR VALUE       -.9000E+00 ?0
LEVEL   10 CONTOUR VALUE       -.9500E+00 ?-1
DO YOU WISH TO ADD ANY LEVELS? (1=YES)?0
```
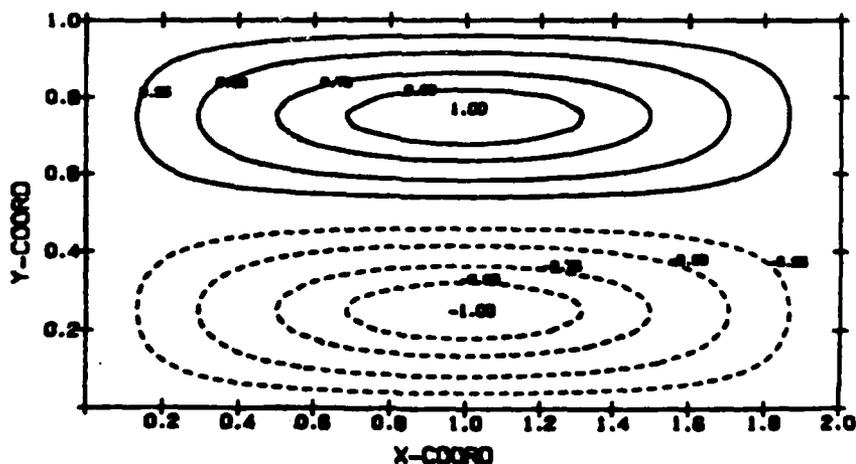

Figure 5.7(b)   Excerpt from SUACON User's Guide

118

The Procedure

After ETL,??? for extended interactive sessions, SUACON may be
set up and activated for Tektronix and associated Pen and Ink or
Microfiche plotting with a single command as follows:

BEGIN,CON,TOUR,MODE,pfn,ID=pfid.

where   MODE = 1 or 2 (Tektronix #) for Interactive use,
                PEN or MIC (off-line not implemented)
         If ID is omitted a local file "pfn" is assumed,
                and a local file TAPE1 is created.
   If pfn is also omitted, the default lfn is TAPE1.

5.6.2   Isometric Plotting

Another package (ISOTEK) developed from basic principles of
hidden line removal, and using an identical data base format to
the one for SUACON, was developed for isometric presentations of
three-dimensional data.   The system simplifies the basic
approach of Wray[2] by allowing interactive selection of block
min-max ranges and therefore the viewing orientation and scale.
Block depiction, tick marks, cross-hatching, and other simple
options are implemented.   Figure 5.8 shows sample usage.

```
COMMAND- ISOTEK

 ENTER START AND END RECORD NUMBERS (DEF=0,0)   >0,0

 ENTER PLOT BLOCK LIMITS (DEF=0,0)
 XMIN,XMAX  >-2.5,7.5
 YMIN,YMAX  >-4,12

TO HIDE LINES INTERPOLATE WITH EVENLY SPACES POINTS
 ENTER NUMBER OF POINTS PER LINE (0=PLOT RAW DATA) >250

 ENTER NUMBER OF CROSS LINES WANTED (DEF=0) >50
50 GRID LINES HAVE BEEN COPIED
     WITH SUATEK FORMAT ON TAPE 1
     STOP
     060000 MAXIMUM EXECUTION FL.
     7.703 CP SECONDS EXECUTION TIME.
COMMAND- SUATEK2
```
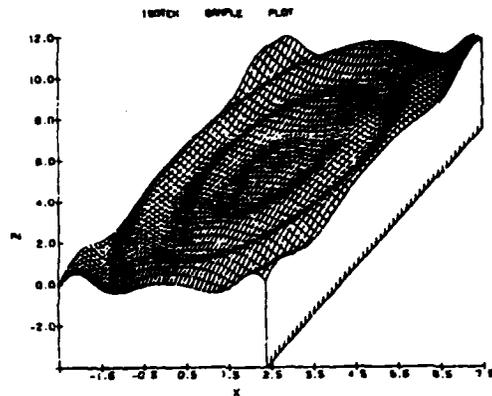


```
COMMAND- ISOTEK

 ENTER START AND END RECORD NUMBERS (DEF=0,0)   >25,48

 ENTER PLOT BLOCK LIMITS (DEF=0,0)
 XMIN,XMAX  >-5.5,2.5
 YMIN,YMAX  >-2,6

TO HIDE LINES INTERPOLATE WITH EVENLY SPACES POINTS
 ENTER NUMBER OF POINTS PER LINE (0=PLOT RAW DATA) >200

 ENTER NUMBER OF CROSS LINES WANTED (DEF=0) >0
24 GRID LINES HAVE BEEN COPIED
     WITH SUATEK FORMAT ON TAPE 1
     STOP
     060000 MAXIMUM EXECUTION FL.
     3.368 CP SECONDS EXECUTION TIME.
COMMAND- SUATEK2
```
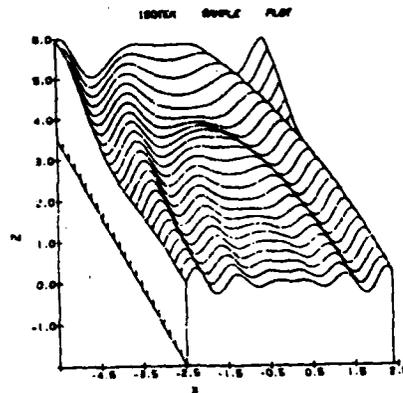

Figure 5.8   ISOTEK - Interactive Isometric Sample Plots
             (An intermediate file is created for SUATEK)

120

References

1. Bhavnani, K.H. and McInerney, R.E., "SUATEK Interactive
   Graphics User's Guide", (periodically updated guide to
   latest features and usage).

2. Wray, Jr., W.B., "Fortran IV CDC 6400 Computer Program for
   Constructing Isometric Diagrams", Univ. of Calif., Berkeley.

3. Ziemba, E.J. and McInerney, R.E., "SUATEK - An Interactive
   Graphics Program", AFGL-TM #22, August 1979.